

# **Post-Modification on Micro- and Macroscopic Polymer Surfaces and their Corresponding Applications**

Dissertation

with the aim of achieving the doctoral degree at the Faculty of  
Mathematics, Informatics and Natural Science

Submitted to the  
Department of Chemistry  
University of Hamburg

**Xiaoxiao Zhang**

Hamburg, 2019



Date of approval for publication: 15. August 2019



The following evaluators recommend the admission of the dissertation:

1. Evaluator: Prof. Dr. Patrick Théato
2. Evaluator: Prof. Dr. Hans-Ulrich Moritz

Date of the disputation: 15. August 2019

Members of the examination committee:

1. Prof. Dr. Patrick Théato
2. Prof. Dr. Wolfgang Maison
3. Dr. Werner Pauer



The experimental work described in this thesis has been carried out between October 2015 and January 2019 at the Institute for Technical and Macromolecular Chemistry, University of Hamburg in the research group of Prof. Dr. Patrick Théato.



## List of Publications

1. **X.X. Zhang**, Z.W. Li, S.J. Lin, P. Théato, Fibrous materials based on polymeric salicyl active esters as efficient adsorbents for selective removal of anionic dye, submitted manuscript.

This study is part of the discussion in Chapter 5.1

2. **X.X. Zhang**, P. Théato, Free-standing fibrous membranes based on polymeric salicyl active esters for highly efficient adsorption and selective adsorption of anionic or cationic dyes from water, submitted manuscript.

This study is part of the discussion in Chapter 5.2

3. **X.X. Zhang**, S.J. Lin, P. Théato, A universal surface post-modification method based on active ester functional benzophenone, in preparation.

This study is part of the discussion in Chapter 5.3

4. S.J. Lin, J.J. Shang, **X.X. Zhang**, P. Théato, “Breathing” CO<sub>2</sub>-, O<sub>2</sub>- and light-responsive vesicles from a triblock copolymer for rate-tunable controlled release, *Macromolecular Rapid Communication* 39 (2018) 1700313.



# Table of Contents

<b>List of Publications.....</b>	<b>I</b>
<b>List of Abbreviations.....</b>	<b>VI</b>
<b>1. Zusammenfassung.....</b>	<b>1</b>
<b>2. Abstract.....</b>	<b>5</b>
<b>3. Introduction.....</b>	<b>7</b>
3.1 Post-polymerization modification .....	7
3.2 Polymeric active esters .....	8
3.2.1 NHS-based active ester polymers .....	8
3.2.2 PFP-based active ester polymers .....	10
3.2.3 Salicyl-based active ester polymers .....	12
3.3 Water pollution.....	13
3.3.1 Shortage of fresh water .....	13
3.3.2 Various water purification methods.....	14
3.4 Electrospinning.....	16
3.4.1 Electrospinning technique.....	16
3.4.2 Electrospun fibrous membranes for water purification .....	18
3.5 UV-initiated cross-linking .....	21
3.6 Spin coating technique.....	24
<b>4. Concept and Motivation.....</b>	<b>27</b>
<b>5. Results and Discussion.....</b>	<b>29</b>

5.1 Preparation, characterization and adsorption performance study of PMSAE-based fibrous adsorbents.....	29
5.1.1 Characterizations of the fibrous membrane precursor PMSAE and of the fibrous adsorbents .....	30
5.1.2 Adsorption performance .....	32
5.1.3 Adsorption kinetics .....	36
5.1.4 Adsorption isotherms .....	41
5.1.5 Recyclability of the adsorbents .....	43
5.1.6 Comparison with other adsorbents reported in the literature.....	44
5.1.7 Mechanism exploration.....	47
5.1.8 Conclusions.....	48
5.2 Preparation, characterization and adsorption performance study of PMAM-based fibrous adsorbents.....	49
5.2.1 Characterizations of the fibrous membrane precursor PMAM and of the fibrous adsorbents .....	50
5.2.2 Adsorption performance of the fibrous adsorbents for different dyes.....	52
5.2.3 Selective adsorption performance of the fibrous adsorbents .....	53
5.2.4 The effect of pH on the adsorption performance of the fibrous adsorbents .....	55
5.2.5 Adsorption kinetics .....	57
5.2.6 Adsorption isotherms .....	61
5.2.7 Investigation of the Mechanism.....	63
5.2.8 Conclusions.....	65

5.3 A universal surface post-modification method based on active ester functional benzophenone .....	67
5.3.1 Synthesis and characterization of active ester BBPE.....	67
5.3.2 Application of this surface modification method.....	69
5.3.2.1 Modification of chemically inert polyolefins surfaces.....	70
5.3.2.2 Control of grafting density .....	74
5.3.2.3 Surface chemical patterns generation using UV-lithography.....	77
5.3.2.4 Other applications .....	79
5.3.3 Conclusions.....	82
<b>6. Conclusions and Outlook.....</b>	<b>83</b>
<b>7. Experimental Part .....</b>	<b>87</b>
7.1 Materials .....	87
7.2 Characterization.....	87
7.3 Synthesis.....	88
7.4 Preparation of electrospun fibrous membrane precursors .....	90
7.5 Post-modification of electrospun fibrous membrane precursors .....	91
7.6 Adsorption experiments.....	92
<b>8. References .....</b>	<b>95</b>
<b>9. Appendix .....</b>	<b>113</b>
A. List of chemicals.....	113
B. Supporting information.....	117

**10. Acknowledgement ..... 121**

**11. Declaration on oath ..... 123**

## List of Abbreviations

ABP	4-Acryloyloxybenzophenone
AFM	Atomic force microscopy
AIBN	Azobisisobutyronitrile
APD	(±)-3-Amino-1,2-propanediol
AR	Azorubine
BBA	4-Benzoylbenzoic acid
BBPE	Benzoic acid, 4-benzoyl-,2,3,4,5,6-pentafluorophenyl ester
BP-QAS	Benzophenone group terminated quaternary ammonium salt
BY	Bismarck brown Y
CA	Contact angle
Cal	Calcein
CV	Crystal violet
DCC	<i>N,N'</i> -Dicyclohexylcarbodiimide
DMAP	4-(Dimethylamino)pyridine
DMF	Dimethyl formamide
D–R	Dubinin–Radushkevich
ETA	Ethanolamine
Et <sub>3</sub> N	Triethylamine
GPC	Gel permeation chromatography
KIT	Karlsruhe Institute of Technology

MB	Methyl blue
MeB	Methylene blue
MO	Methyl orange
MOPs	Microporous organic polymers
MSAE	Methyl salicylate acrylic ester
Mt/IPS2	Polyaspartate-montmorillonite composite with quaternary phosphonium salt
NHS	N-hydroxysuccinimide
NR	Neutral red
OG	Orange G
PABP	Poly(4-acryloyloxybenzophenone)
PE	Polyethylene
PET	Polyethylene terephthalate
PFP	Pentafluorophenon
PMAM	Blend polymers (PMSAE, PABP, PMMA)
PMAM-APD	(±)-3-Amino-1,2-propanediol modified blend polymers (PMSAE, PABP, PMMA)
PMAM-TTDD	4,7,10-Trioxa-1,13-tridecanediamine modified blend polymers (PMSAE, PABP, PMMA)
PMMA	Poly(methyl methacrylate)
PMSAE	Poly(methyl salicylate acrylic ester)
PMSAE-TAD	3,6,9-Triazaundecan-1,11-diamin modified poly(methyl salicylate acrylic ester)

PMSAE-TTDD	4,7,10-Trioxa-1,13-tridecanediamine modified poly(methyl salicylate acrylic ester)
PNHSA	Poly( <i>N</i> -hydroxysuccinimide acrylate)
PNHSMA	Poly( <i>N</i> -hydroxysuccinimide methacrylate)
PP	Polypropylene
PPFPA	Poly(pentafluorophenyl acrylate)
PPFPMA	Poly(pentafluorophenyl methacrylate)
PS	Ponceau S
PZS	Poly(cyclotriphosphazene-co-4,4'- sulfonyldiphenol)
RhB	Rhodamine B
RMS	Root mean square
SEM	Scanning electron microscopy
TAD	3,6,9-Triazaundecan-1,11-diamin
THF	Tetrahydrofuran
TTDD	4,7,10-Trioxa-1,13-tridecanediamine
UHH	University of Hamburg
UV	Ultraviolet



## 1. Zusammenfassung

Die Oberflächeneigenschaften von Polymermaterialien sind äußerst wichtig, da sie die Funktionen der Polymermaterialien und ihre entsprechenden Anwendungen bestimmen. Die Entwicklung vielseitiger und kosteneffizienter Oberflächenmodifizierungsmethoden hat das Interesse sowohl der akademischen als auch der industriellen Forschung geweckt. In der vorliegenden Studie sind vielseitige und einfache Modifizierungsmethoden für mikro- und makroskopische Polymeroberflächen entwickelt worden, und ihre entsprechenden Anwendungen wurden systematisch untersucht. Die Vorteile von Aktivestern, Elektrofasern, UV-Bestrahlung und Nachmodifizierung wurden im Rahmen des Entwicklungsprozesses des Verfahrens miteinander kombiniert.

Im ersten Projekt wurden aus polymerem Aktivester Poly(methylsalicylatacrylester) (PMSAE) erstmals durch Elektrospinning Fasermembranen hergestellt. Nach weiterer Nachmodifizierung durch eine einfache und milde oberflächenanaloge Reaktion unter Verwendung von 4,7,10-Trioxa-1,13-tridecandiamin (TTDD) und 3,6,9-Triazaundecan-1,11-diamin (TAD) wurden zwei Arten von faserigen Adsorbentien, nämlich PMSAE-TTDD und PMSAE-TAD erhalten. Die Morphologie der hergestellten faserigen Adsorbentien wurde mittels REM charakterisiert und die Vollständigkeit des Nachmodifizierungsprozesses wurde durch FTIR ermittelt. Die Adsorbentien wurden des Weiteren auf ihre Adsorptions- und Selektivitätsleistung hinsichtlich verschiedener organischer Farbstoffe sowie auf ihre Wiederverwendbarkeit getestet. Um die Adsorptionsdaten zu analysieren und damit den Adsorptionsmechanismus zu untersuchen, wurden vier kinetische Modelle und drei Isothermenmodelle verwendet. Die Ergebnisse zeigten, dass die faserigen Adsorbentien eine extrem hohe Adsorptionskapazität gegenüber dem anionischen Farbstoff Methylblau (MB) (PMSAE-TTDD: 1652 mg / g; PMSAE-TAD: 1585 mg / g) aufwiesen sowie eine gute selektive Adsorptionskapazität von anionischen Farbstoffen aus kationischen Farbstoffen und

## ZUSAMMENFASSUNG

---

dass sie mindestens fünfmal wiederverwendet werden können. Der Adsorptionsmechanismus der faserigen Adsorber gegenüber organischen Farbstoffen beruht auf elektrostatischen Wechselwirkungen zwischen der Oberfläche der faserigen Adsorber und den organischen Farbstoffen.

Das zweite Projekt baut auf dem ersten Projekt auf und konzentriert sich auf die Verbesserung der Vielfalt der Nachmodifikationsprozesse. Für das Elektrosponning wurden Polymermischungen verwendet, die aus Poly(methylmethacrylat) (PMMA), Photovernetzer Poly(4-acryloyloxy-benzophenon) (PABP) und PMSAE anstelle des homogenen PMSAE zusammengesetzt waren, was zur Bildung der Fasermembranen aus PMAM führte. Nach der Modifikation mit TTDD und ( $\pm$ ) -3-Amino-1,2-propandiol (APD) wurden zwei verschiedene Arten von faserigen Adsorbentien, nämlich PMAM-TTDD und PMAM-APD erhalten. Ihre Adsorptionsleistungen wurden mit der gleichen Methode wie im ersten Projekt untersucht. Die Ergebnisse zeigten, dass die Vielfalt des Nachmodifikationsprozesses erfolgreich verbessert werden konnte. Der neu entwickelte faserige Adsorber, PMAM-TTDD, zeigte eine hohe Adsorptionskapazität von 1545 mg / g (nur geringfügig niedriger als die von PMSAE-TTDD) hinsichtlich des anionischen Farbstoffes MB und eine gute selektive Adsorptionskapazität von anionischen Farbstoffen aus einer Mischung mit kationischen Farbstoffen. PMAM-APD zeigte eine gute Adsorptionskapazität von 577 mg/g hinsichtlich des kationischen Farbstoffes CV und eine gute selektive Adsorptionskapazität von kationischen Farbstoffen aus anionischen Farbstoffen.

Im dritten Projekt wurde eine niedermolekulare Verbindung aus Benzoesäure und 4-Benzoyl-, 2,3,4,5,6-Pentafluorphenylester (BBPE), auf kostengünstige Weise synthetisiert. BBPE kombiniert aktive Ester mit photoreaktiven Gruppen und legt damit die Grundlage für eine vielversprechende, neue Methode zur Oberflächen-Nachmodifizierung mit mehreren neuen Anwendungsfeldern. In diesem Projekt wurde die Methode verwendet, um die Oberflächen von inerten Polyolefinen, porösen Batterieseparatoren und den Pflanzenblättern

## ZUSAMMENFASSUNG

---

zu modifizieren. Die Ergebnisse zeigten, dass dieses Verfahren die folgenden Vorteile aufweist: 1) es ermöglicht einen einfachen Zugang zum chemischen Anhaften von aktiven Beschichtungen auf praktisch jeder Oberfläche, die eine aliphatische C-H-Bindung enthält. Gewünschte funktionelle Gruppen können durch weitere oberflächenanaloge Reaktion leicht gebunden werden; 2) die Handhabung ist einfach, da sie keine Katalysatorzugabe und nur milde Reaktionsbedingungen erfordert; 3) es können chemische Muster in verschiedenen Formen und in unterschiedlichen Maßstäben erhalten werden, indem einfach verschiedene Fotomasken gegeneinander ausgetauscht werden, um den Bereich der UV-Bestrahlung zu steuern; 4) das Verfahren ist auch anwendbar, um die Oberflächeneigenschaften von natürlichen Substraten wie Pflanzenblättern zu verändern; 5) es kann auch verwendet werden, um poröse Materialien zu modifizieren, ohne den Grad an Porosität anpassen zu müssen.



## 2. Abstract

The surface properties of polymeric materials are extremely important as they determine the materials' functions and further decide their corresponding applications. Developing versatile and cost-efficient surface modification methods has been attracting the interest of both the academic and the industrial community. This study developed versatile and simple modification methods for micro- and macroscopic polymer surfaces and systematically investigated their corresponding applications. The advantages of active esters, electro-spun fibers, UV-irradiation and post-modification have been synergized during the method development process.

In the first project, the polymeric active ester poly(methyl salicylate acrylic ester) (PMSAE) was for the first time electro-spun into fibrous membranes. After further post-modification through a simple and mild surface-analogous reaction using 4,7,10-trioxa-1,13-tridecanediamine (TTDD) and 3,6,9-triazaundecan-1,11-diamin (TAD), two fibrous adsorbents, PMSAE-TTDD and PMSAE-TAD, were obtained. The morphology of the produced fibrous adsorbents was characterized utilizing SEM and the completeness of the post-modification process was determined using FTIR. The adsorbents were further tested for their adsorption and selectivity performance of different organic dyes as well as for their reusability. To analyze the adsorption data and thus explore the adsorption mechanism, four kinetic models and three isotherm models were used. The results indicated that the fibrous adsorbents show an extremely high adsorption capacity towards the anionic dye methyl blue (MB) (PMSAE-TTDD: 1652 mg/g; PMSAE-TAD: 1585 mg/g), a good selective adsorption capacity of anionic dyes from a mixture with cationic dyes and that they can be reused at least 5 times. The adsorption mechanism of the fibrous adsorbents towards organic dyes is based on electrostatic interactions between the surface of the fibrous adsorbents and the organic dyes.

## ABSTRACT

---

Based on the first project, the second project focuses on improving the diversity of the post-modification process. Polymer blends which were composed of poly(methyl methacrylate) (PMMA), the photo-crosslinker poly(4-acryloyloxybenzophenone) (PABP) and PMSAE instead of the homogeneous PMSAE were used for electrospinning, which resulted in the fibrous membrane PMAM. After post-modification with TTDD and ( $\pm$ )-3-amino-1,2-propanediol (APD), two different types of fibrous adsorbents PMAM-TTDD and PMAM-APD were obtained. Their adsorption performances were investigated using the same method as in the first project. The results show that the diversity of the post-modification process was successfully improved. The newly developed fibrous adsorbent PMAM-TTDD exhibit a high adsorption capacity of 1545 mg/g (just slightly lower than that of PMSAE-TTDD) towards the anionic dye MB and a good selective adsorption capacity of anionic dyes from cationic dyes. PMAM-APD shows a good adsorption capacity of 577 mg/g towards the cationic dye CV and a good selective adsorption capacity of cationic dyes from anionic dyes.

In the third project, a small molecule compound benzoic acid, 4-benzoyl-2,3,4,5,6-pentafluorophenyl ester (BBPE) was synthesized in a cost-efficient way. BBPE combines an active ester with a photo-reactive group, thus laying the foundation for a promising, new surface post-modification method with several possible application fields. In this study, it was used to modify the inert polyolefins surfaces, porous battery separators and plant leaves. The results showed that this method features the following advantages: 1) it provides an easy and simple way to chemically attach active coatings on any surface that contains aliphatic C-H bonds. Desired functional groups could be easily attached through further surface-analogous reaction; 2) the process is easy to control, requires no catalyst addition and takes place under mild reaction conditions; 3) chemical patterns of different shapes and scales can be obtained easily via a simple change of photomasks which control the UV-irradiation area; 4) it also allows to change the surface properties of natural substrates such as plant leaves; 5) it can be used to modify porous materials without changing the porosity degree.

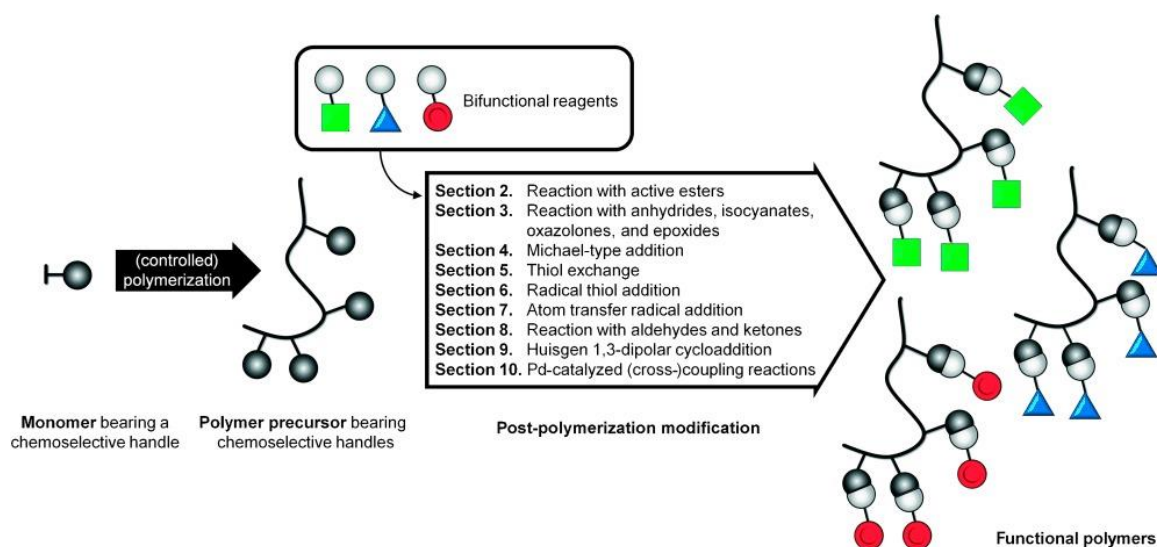
## 3. Introduction

### 3.1 Post-polymerization modification

Post-polymerization modification is a popular synthetic method to prepare functional polymer materials.<sup>1</sup> The general concept is to directly polymerize or copolymerize monomers that bear chemoselective handles and are inert towards the polymerization conditions, resulting in reactive precursor polymers. And subsequently, these precursor polymers can be quantitatively converted into various functional groups.<sup>2</sup>

One of the most prominent advantages of post-polymerization modification is the way it introduces multiple functional groups in a controlled fashion and it can efficiently avoid cumbersome synthesis processes.<sup>3</sup> The introduction of functional groups that are not compatible with common polymerization conditions is another of the most pronounced advantages of this method,<sup>4</sup> making post-polymerization modification the first choice when it comes to the synthesis of systematic polymer libraries.

Popular precursor polymers that are reported in the literature include polymeric active esters, polymeric anhydrides, isocyanates, oxazolones, and epoxides, polymers that can carry out Michael-Type addition reactions, polymers bearing aldehydes and ketones, etc.<sup>2</sup> The general concept of post-polymerization modification is schematically shown in Scheme 3-1.



**Scheme 3-1** Synthesis of polymers by post-polymerization modification. (Reproduced with permission.<sup>2</sup>

Copyright © 2009 WILEY - VCH Verlag GmbH & Co. KGaA, Weinheim)

## 3.2 Polymeric active esters

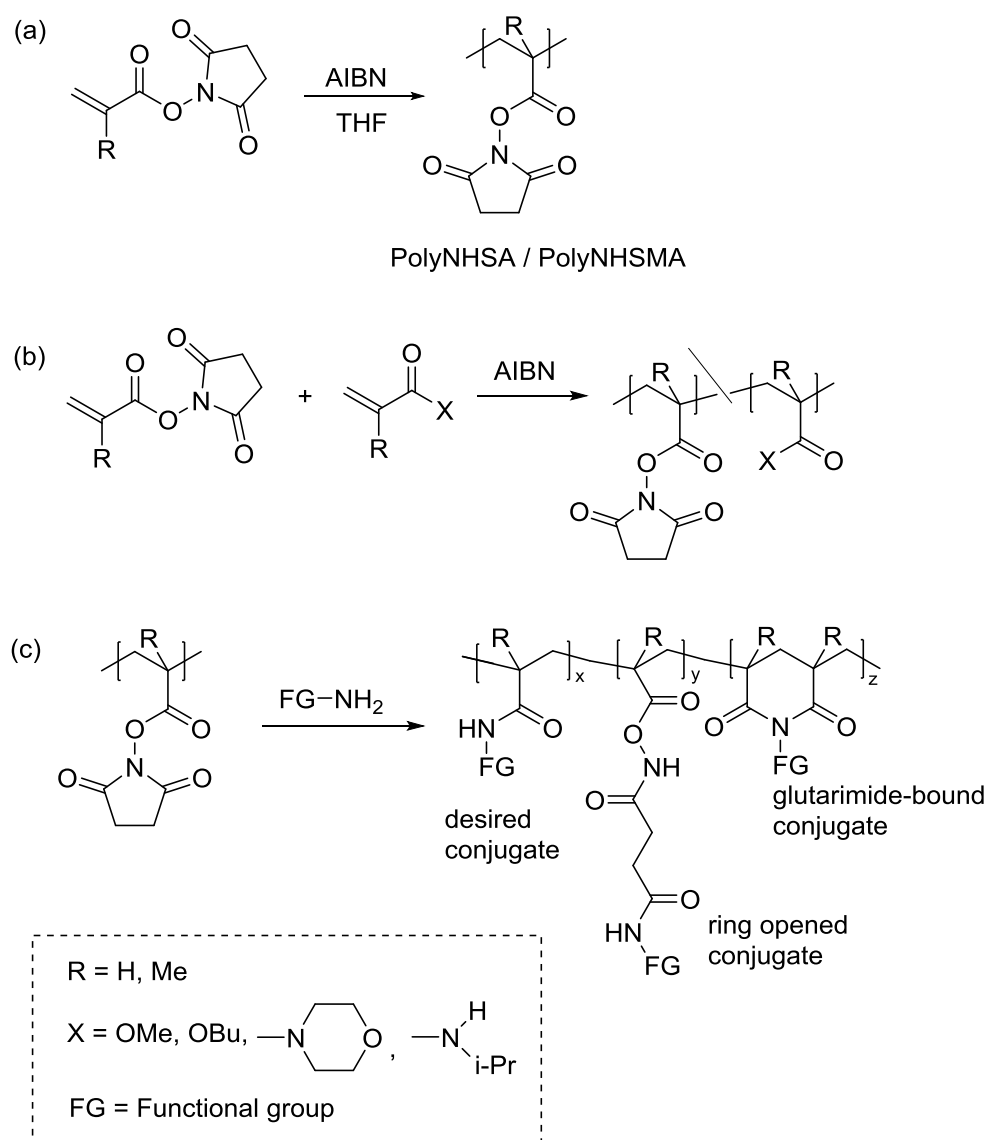
As mentioned in the above section 3.1, polymeric active esters are one type of the popular precursor polymers for preparing functional polymer materials. Polymeric active esters have been considered promising for the preparation of reactive precursor polymers as they are free of metal and have mild reaction conditions since reported by Ferruti et al<sup>5</sup> and Ringsdorf et al in 20 Century 70s.<sup>2, 6</sup> The most popular and explicitly explored polymeric active esters are *N*-hydroxysuccinimide (NHS) based active ester polymers<sup>7-10</sup> and pentafluorophenyl (PFP) based active ester polymers<sup>11-15</sup>.

### 3.2.1 NHS-based active ester polymers

NHS-based active ester polymers are the oldest polymeric active esters.<sup>3</sup> They exhibit a twofold advantage. On the one hand, they are quite (yet not fully) resistant to hydrolysis.<sup>16</sup> On the other hand, nucleophilic aminolysis with primary and secondary amines can easily take place under mild reaction conditions to generate functionalized polyacrylamide derivatives.<sup>3</sup> Poly(*N*-hydroxysuccinimide acrylate) (PNHSA) and poly(*N*-hydroxysuccinimide methacrylate) (PNHSMA) synthesized by free radical polymerization were first reported by

## INTRODUCTION

Ringsdorf and Ferruti.<sup>5, 7</sup> The reaction is shown in Scheme 3-2 (a). Murata and coworkers<sup>9</sup> reported the synthesis of polymer brushes containing succinimide active ester groups. The polymer brushes were attached to the surface of silicon oxide substrates. In the subsequent step, amines that carry additional desired functional groups such as amino acids, dyes, crown ethers etc. can be attached to the polymer brushes via aminolysis. The resulting functional polymer brushes have the potential to be useful for a wide range of different applications especially in the field of biosensors.



**Scheme 3-2** (a) Free radical homopolymerization of NHSA/NHSMA. (b) Free radical copolymerization of NHSA/NHSMA. (c) Side reactions during aminolysis of polyNHSA/polyNHSMA. (Reproduced with permission.<sup>3</sup> Copyright © 2015 American Chemical Society)

## INTRODUCTION

---

However, the disadvantages of NHS-based active ester polymers are not negligible. One major disadvantage is the poor solubility of NHS-based active ester homopolymers in most organic solvents (except for DMF and DMSO).<sup>3</sup> Therefore NHSA and NHSMA are commonly copolymerized with other monomers as shown in Scheme 3-2 (b).<sup>3</sup> This method can solve the solubility problem. However, it also results in a decrease of reactive sites. Another drawback are the unexpected ring-opening and glutarimide-forming side reactions during the aminolysis step as shown in Scheme 3-2 (c).<sup>3, 17</sup> Although Wong and Putnam<sup>10</sup> established a protocol to overcome this drawback, it requires to carry out the aminolysis process using an excess of primary amine-containing nucleophile and at a high temperature of 75°C. Due to the drawbacks mentioned above, the utilization of NHS-based active ester polymers is limited.

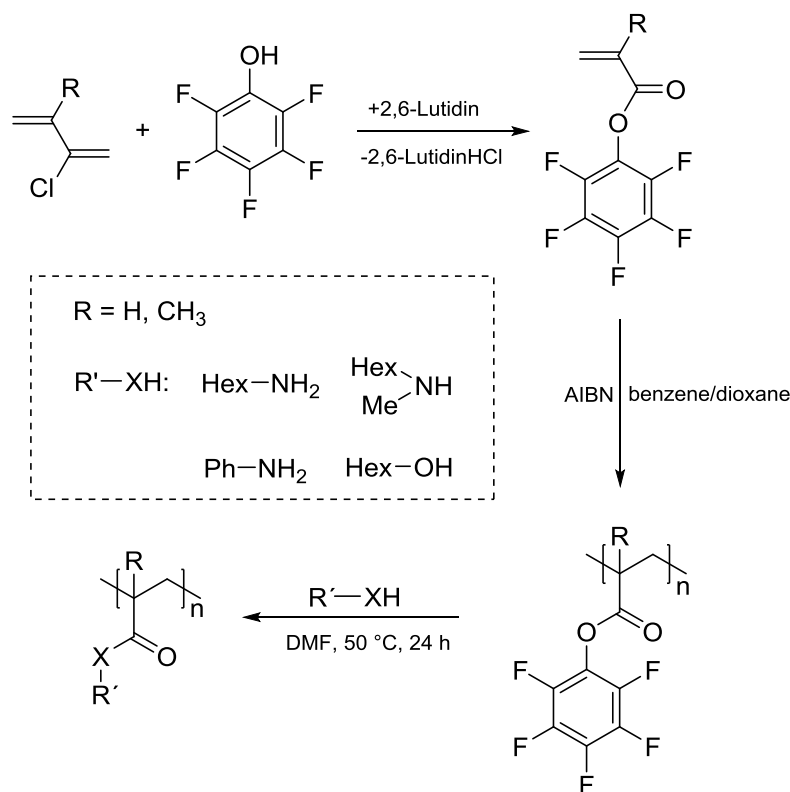
### 3.2.2 PFP-based active ester polymers

The synthesis of the PFP-based active ester polymers poly(pentafluorophenyl acrylate) (PPFPA) via bulk polymerization was first reported by Blazejewski et al<sup>11</sup> in 1999. However, due to the crosslinking during the bulk polymerization process, the obtained polymers cannot dissolve in the solvents THF, 1,2,4-trichlorobenzene, *N,N*-dimethylacetamide, hexafluoroisopropanol or cresol. This flaw made it impossible to use size exclusion chromatography analysis or another characterization method, thus eliminating the chance for further research or application.

However, this situation changed since Eberhardt and coworkers reported the synthesis of PPFPA and poly(pentafluorophenyl methacrylate) (PPFPMA) using AIBN as a thermal initiator.<sup>18</sup> They found that the obtained PFP-based active ester polymers exhibited an excellent solubility in most organic solvents and better reactivities in the subsequent substitution step than the commonly used NHS-based active ester polymers. This report provides new precursor polymers for the preparation of multifunctional materials. The

## INTRODUCTION

preparation of PFPA/PFPMA, their polymerization to PPFPA/PPFPMA and their substitution with various nucleophiles are shown in Scheme 3-3.



**Scheme 3-3** The preparation of PFPA/PFPMA, their polymerization to PPFPA/PPFPMA and their substitution with various nucleophiles. (Reproduced with permission.<sup>3, 18</sup> Copyright © 2015 American Chemical Society © 2005 Elsevier Ltd.)

Since then, PFP-based active ester polymers caught a lot of attention and have been explicitly explored. Park and coworkers prepared transparent conductive multilayered films using active PFP ester modified multiwalled carbon nanotubes.<sup>19</sup> Their work was meaningful in two aspects. Firstly, it made it possible to fabricate nanoscale electronic components using carbon nanotubes. Secondly, it contributed to the application in bionanoelectronics by providing the possibility of introducing bioactive compounds or biological complexes onto multiwalled carbon nanotubes. Schattling et al.<sup>20</sup> reported that PFP-based active ester polymers provide easy access to prepare temperature-, light- and redox triple-responsive polymers. The obtained triple-responsive polymers have a promising potential for molecular

## INTRODUCTION

---

information processing. Gaballa and Théato<sup>21</sup> reported the successful preparation of glucose-responsive polymeric micelles from a precursor PPFPA block copolymer. They also pointed out that the glucose-responsive micelles have the potential to be used in a self-regulated insulin delivery system.

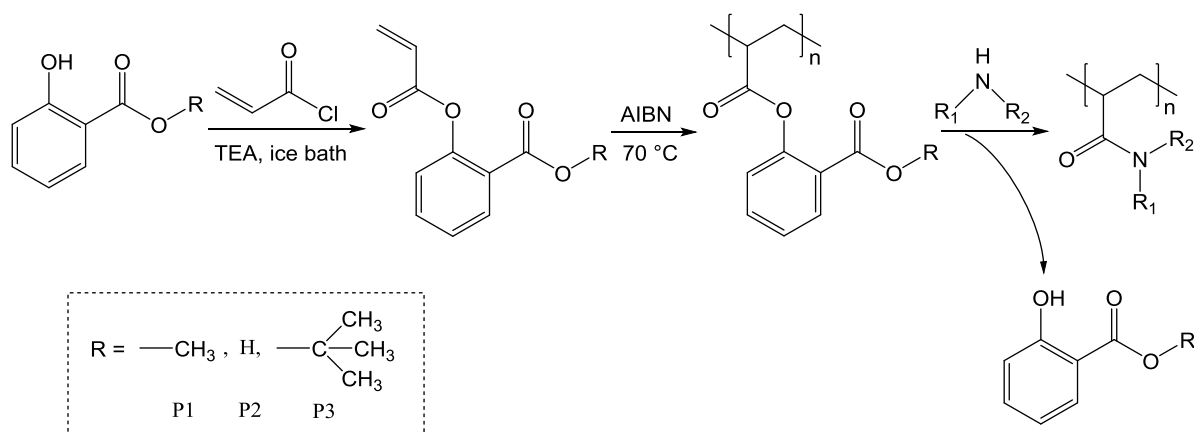
PFPA-based active ester polymers feature a series of advantages such as a simple synthesis and purification process, an excellent solubility in most organic solvents, an outstanding reactivity towards amines in the subsequent aminolysis process, a convenient characterization of the aminolysis process by <sup>19</sup>F NMR and FTIR spectroscopy etc.<sup>1, 18, 22</sup> However, the disadvantage of the toxicity of the pentafluorophenol group is not negligible. The release of pentafluorophenol groups during the subsequent post-modification aminolysis process and the possibly remaining PFPA-ester groups in the polymers render their application in the biological area controversial.<sup>1</sup>

### 3.2.3 Salicyl-based active ester polymers

Salicyl-based ester monomers were first synthesized by Boudreaux et al in 1997.<sup>23</sup> They were copolymerized with acrylic acid to investigate the release of phenolic compounds via hydrolysis, making them potentially useful as plant growth regulators.<sup>23</sup> He and coworkers first reported salicyl-based esters as polymeric active esters.<sup>1</sup> The post-polymerization modification property was explored with different amines, the active ester reactivity was compared with the established PPFPA and the cell cytotoxicity of the released group during the post-modification step was investigated using HeLa cells. They found that salicyl-based ester polymers enable an almost quantitative functionalization with primary amines even though the reactivity of salicyl-based ester polymers is not as high as that of PFPA-based active ester polymers in terms of secondary amines.<sup>1</sup> Furthermore, the significantly reduced cytotoxicity and the cost-effectiveness makes them ideal candidates for the preparation of bio-

# INTRODUCTION

related functional materials. The synthesis of salicyl-based ester polymers and their subsequent aminolysis process is shown in Scheme 3-4.



**Scheme 3-4** Synthesis of Poly(methyl-salicylate acrylate) (P1), Poly(salicyl acrylate) (P2), and Poly(tert-butyl-salicylate acrylate) (P3) and Their Post-Polymerization Modification with Amines. (Reproduced with permission.<sup>1</sup> Copyright © 2014 American Chemical Society)

## 3.3 Water pollution

### 3.3.1 Shortage of fresh water

The availability of fresh water is one of the big challenges of modern civilization. In the twenty-first century different socio-economic factors like population explosion, industrialization, urbanization and rapid development of economy have resulted in an extensive pollution of water, endangering humans and other organisms alike.<sup>24</sup> Although 70% of the surface of the earth is covered by water, the supply of fresh water is limited: only 2.7% of the water on earth is considered fresh, of which only 0.3% is accessible to human beings. That means only around 0.007% of the water on earth is available to human beings.<sup>25</sup> This makes water a scarce resource in many parts of the world and its pollution a big problem. In numbers, nowadays, 1 billion people have no access to safe drinking water<sup>26</sup> and the number might reach up to 4 billion by 2050<sup>27</sup> according to the reports of the World Health

Organization.<sup>24</sup> Various industry effluents make up a large portion of wastewater. A large amount of those can be contributes to effluents containing dyes and their intermediates from the textile, leather, paper, plastic and paint industries, mainly from cleaning processes.<sup>24, 28</sup> Once poured into clean water, industry effluents cause adverse effect on aquatic plants, photosynthetic bacteria and the ecology of the surrounding water.<sup>24</sup> Since fresh water is a scarce resource and many of the mentioned industries contributing to waste water pollution are often located in developing countries, which suffer from overpopulation and fresh water shortages, it is of vital importance to develop not only efficient but also cost-effective methods of cleaning contaminated water.

### **3.3.2 Various water purification methods**

Water contamination of especially organic dyes has been receiving increasing attention from academic as well as industrial research and from environmental policy makers.<sup>28</sup> Various water purification materials and methods have been reported, including coagulation, biological methods, ozone treatment and adsorption. Conventional methods normally have some disadvantages such as being time-consuming, having poor recyclability or releasing of secondary pollutants.<sup>24</sup>

Among these methods, adsorption has been regarded as particularly promising because it is safe, facile, economic, efficient, requires low-energy input and does not release or produce any by-products during the purification processes.<sup>29, 30</sup> Many different materials like activated carbon,<sup>31-33</sup> zeolites,<sup>34, 35</sup> clays,<sup>36, 37</sup> agricultural residues<sup>38, 39</sup> and so on have been investigated as adsorbents.<sup>40</sup> However, the utilization of these materials turned out to be either expensive, having low adsorption capacities or a low selectivity, or there were difficulties of separation or regeneration. Polymer-based adsorbents (including pure polymers and organic-inorganic hybrid polymers) exhibit important advantages over other adsorption materials in terms of being easy to functionalize.

## INTRODUCTION

For example, Wang and coworkers reported two pure polymer-based adsorbents, the bakelite-type anionic microporous organic polymers (MOPs) MOP-1 and MOP-2.<sup>41</sup> The materials feature the anionic skeleton, microporous properties and abundant hydroxyl groups. And they show a good adsorption performance: the maximum adsorption capacities toward the cationic dyes malachite green and methylene blue are 712.2 mg/g and 593.6 mg/g, respectively. In addition, the materials exhibit charge and size-selectivity: little adsorption was observed for the anionic dye methyl orange and the large-size cationic dye basic blue 7. Furthermore, the materials can be recycled at least four times with less than 5% loss of adsorption capacities. The structure of the MOPs and the adsorption-desorption mechanism are shown in Fig. 3-1.

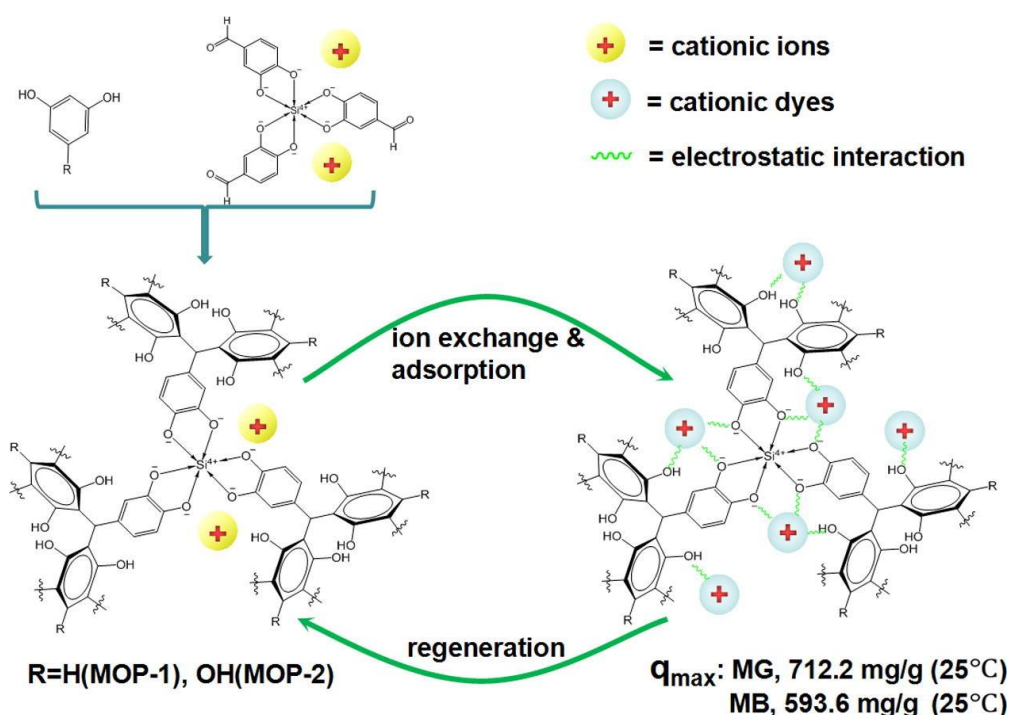


**Fig.3-1** The structure of the MOPs and the adsorption-desorption mechanism. (Reproduced with permission.<sup>41</sup> Copyright © 2019 Elsevier B.V.)

Wei et al. developed poly(cyclotriphosphazene-*co*-4,4'-sulfonyldiphenol) (PZS) based organic-inorganic hybrid polymer submicro-spheres (PZS submicro-spheres) via a one-step

# INTRODUCTION

precipitation copolymerization route.<sup>42</sup> They found that the equilibrium adsorption capacities of PZS submicro-spheres toward the guest dyes methylene blue, Bismarck brown Y (BY), neutral red (NR), rhodamine B (RhB), and calcein (Cal) are 142.46, 133.99, 116.73, 47.37, and 30.20 mg/g, respectively. For orange G (OG), ponceau S (PS) and methyl orange (MO), a little or no adsorption was exhibited. The mechanism of the selective adsorption is the host-guest interaction between adsorbents and adsorbates. The structure of the adsorbents PZS submicro-spheres and the corresponding selective adsorption performance are shown in Fig. 3-2.

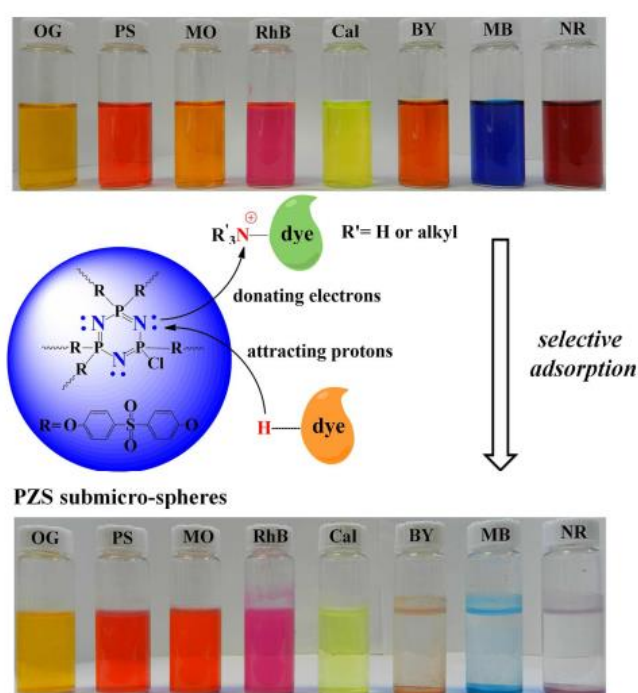


**Fig. 3-2** The structure of the adsorbents PZS submicro-spheres and the corresponding selective adsorption performance. (Reproduced with permission.<sup>42</sup> Copyright © 2015 The Royal Society of Chemistry)

## 3.4 Electrospinning

### 3.4.1 Electrospinning technique

Electrospinning is a practical technique for the production of polymer nanofibers with diameters within a range of 40-2000 nm.<sup>43, 44</sup> The genesis of electrospinning dates back to the year 1600 when William Gilbert first recorded the electrostatic attraction of a liquid.<sup>45</sup> Since

## INTRODUCTION

then related discovery and theory were constantly supplemented and improved. In the early 1990s electrospun nanofibers were reported by several research groups. Especially Reneker's research group popularized the term electrospinning. Since 1995, the electrospinning technology gained increasing interest both from academic and industrial research and correspondingly, the number of published papers has been exponentially increasing from year to year.<sup>45</sup> The typical set-up of the electrospinning technology is shown in Fig. 3-3. Its working principle is as follows:<sup>24, 46-48</sup> a polymer solution in a syringe is pressed out at a defined flow rate by a syringe pump. A high voltage is applied between the tip of the blunt needle and the grounded collector. A force will be generated due to the repulsion between charges in the polymer solution and attraction towards the grounded collector which is oppositely charged. When the force overcomes the surface tension of the polymer solution, a conical shape, which is known as the Taylor cone, will appear on the tip of the blunt needle. When the applied voltage is high enough, a charged jet of fluid will be ejected from the tip of the Taylor cone. The discharged jet undergoes an elongation process while the solvent evaporates. As a result, fibers are obtained.

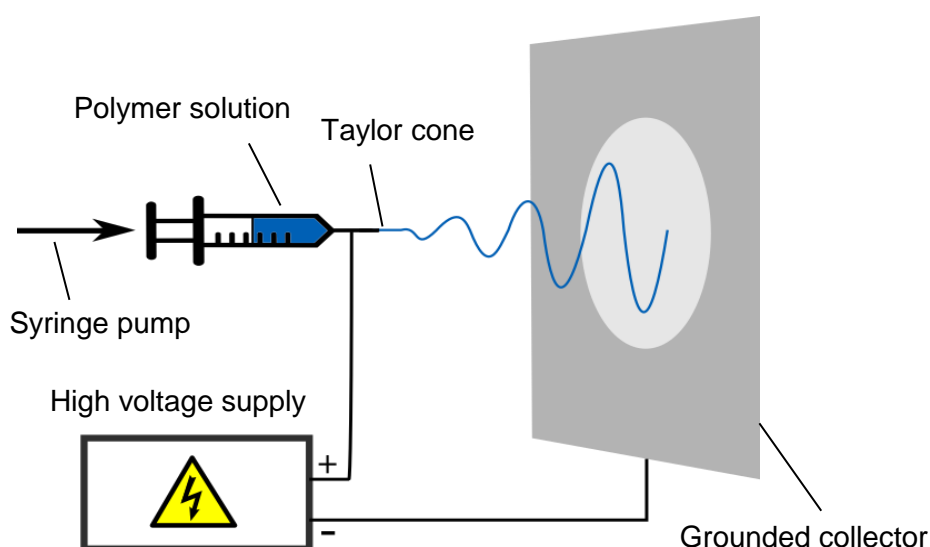


**Fig. 3-3** Schematic representation of an electrospinning apparatus with horizontal arrangement of the electrodes.

# INTRODUCTION

---

By adjusting the applied electrospinning parameters, changing the solvents used to dissolve polymers or using different polymer solution concentrations, it is possible to obtain fibers with different morphologies and orientation and surfaces with different topography. Other parameters such as ambient conditions can also affect the final obtained fiber properties obtained. The detailed effecting parameters are listed in Table 3-1.<sup>27, 49</sup> The produced fibers feature many interesting properties such as outstanding mechanical properties, a high surface area to volume ratio and the diameters of fibers in nanoscale.<sup>27, 46</sup> Several other techniques are available to generate nanofibers, for example, drawing,<sup>50</sup> template synthesis<sup>51, 52</sup> and phase separation<sup>53</sup>. However, electrospinning is highly preferred over other techniques as it is simple and reliable for the preparation of smooth nanofibers with controllable morphology from various polymers.<sup>27, 54</sup>

**Table 3-1** Effecting parameters for electrospinning (Reproduced with permission.<sup>27</sup> Copyright © 2014 Elsevier B.V.)

Solution parameters	Process parameters	Environmental conditions
Concentration	Electrostatic potential	Temperature
Viscosity	Electric field strength	Humidity
Surface tension	Electrostatic field shape	Local atmosphere flow
Conductivity	Working distance	Atmospheric composition
Dielectric constant	Feed rate	Pressure
Solvent volatility	Orifice diameter	

---

## 3.4.2 Electrospun fibrous membranes for water purification

Recent years have witnessed a growing interest in the emerging research area of water purification materials based on electrospun polymeric membranes. The growing interest can be attributed to their outstanding properties, e.g. a high porosity, a large specific surface area,

## INTRODUCTION

an easily tunable surface functionalities and an excellent mechanical behavior.<sup>24, 55</sup> The work principle of electrospun polymeric membranes for water purification comprises two aspects: adsorption and size exclusion as shown in Fig. 3-4. The performance of electrospun polymeric membranes is to a high extent determined by the surface properties. A hydrophobic membrane surface can easily cause membrane fouling. A membrane surface with chelating agents is efficient for organic impurities and heavy metal ions. Fortunately, the properties of the surface of an electrospun fibrous membrane can easily be changed by using blend polymers for electrospinning or post-surface modification.<sup>24</sup>

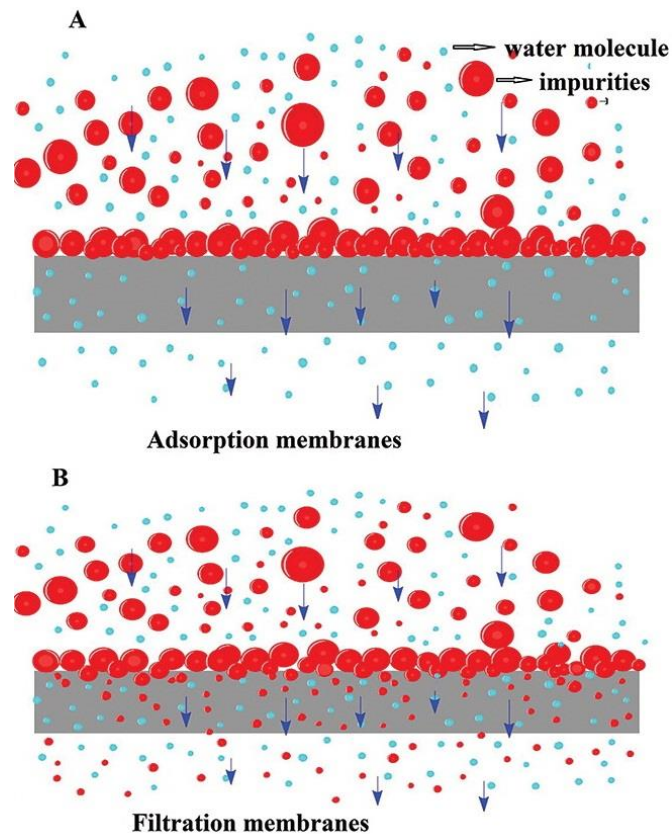


**Fig. 3-4** Schematic representation of (A) adsorption membrane; (B) filtration membrane. (Reproduced with permission.<sup>24</sup> Copyright © 2017 Taylor & Francis)

Various polymers such as polyacrylonitrile,<sup>56-58</sup> polyethersulfone,<sup>59, 60</sup> polysulfone,<sup>61, 62</sup> poly(vinylidene fluoride),<sup>63-66</sup> polyurethane,<sup>67-69</sup> polyester,<sup>70, 71</sup> cellulose acetate,<sup>72-74</sup> polyvinyl alcohol<sup>75-77</sup> and chitosan<sup>78-80</sup> have been used to prepare electrospun fibrous membranes for

## INTRODUCTION

---

water purification.<sup>24</sup> Among these polymers, some are hydrophobic and some are hydrophilic. The obtained hydrophobic electrospun fibrous membranes are prone to the mentioned fouling problem, while the hydrophilic ones normally suffer from poor mechanical strength.<sup>24</sup> Both of them need to be modified to overcome their respective limitations.

Ma and coworkers prepared novel composite nanofibers by depositing polypyrrole particles on electrospun poly(vinylidene fluoride) nanofibers with the assistance of polydopamine.<sup>81</sup> The homogeneous polypyrrole particle coating increased the hydrophilicity and roughness of the fibrous membrane surface. The adsorption abilities of the novel composite nanofibers were investigated with the cationic dye Methylene Blue, the anionic dye Congo Red and the heavy-metal ion Cr(VI). The results showed that the maximum adsorption capacities were 370.4, 384.6 and 126.7 mg/g, respectively. And the novel composite nanofibers showed a good regeneration ability. After using them for 12 cycles, the adsorption capacities were still at 76.8% and 75.7% of the initial adsorption capacities of Methylene Blue and Congo Red, respectively.

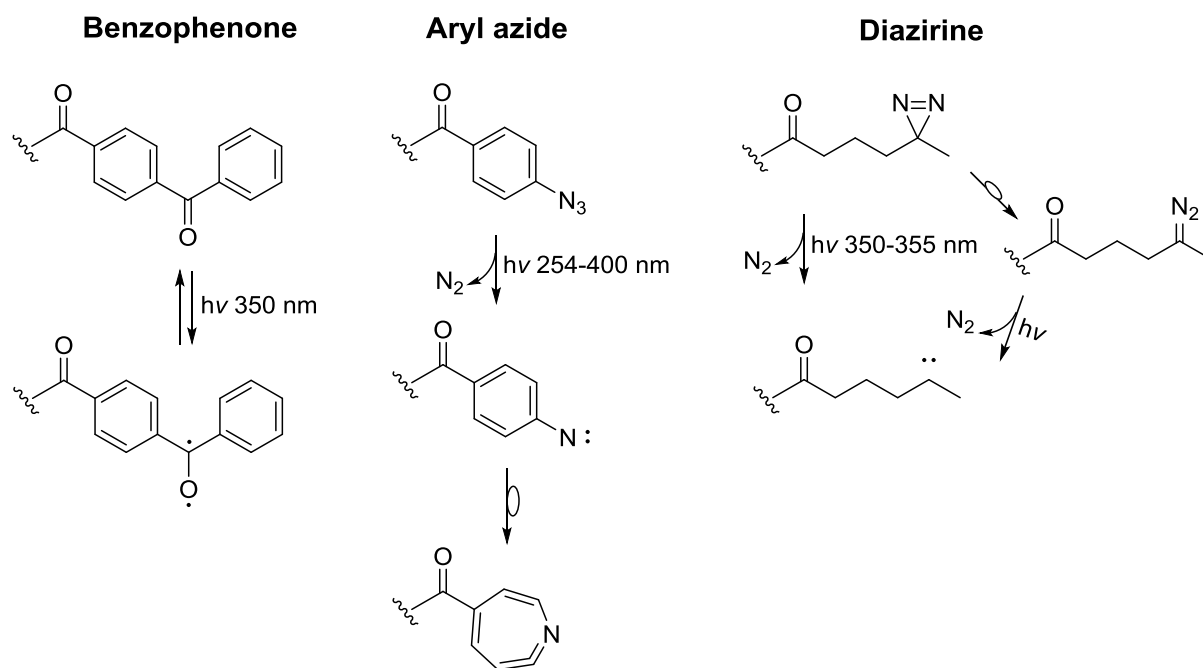
Sharma et al. reported that electrospun chitosan-poly(vinyl alcohol) composite nanofibers loaded with cerium could efficiently remove arsenic from contaminated water.<sup>82</sup> Chitosan was chosen as the electrospun polymer due to its film-forming capacity, its metal-binding capacity, its biodegradability and its antimicrobial activity.<sup>82, 83</sup> However, the high viscosity of the chitosan solution has an adverse effect on the electrospinning process of fibers. Therefore, water soluble and non-toxic poly(vinyl alcohol) was added to reduce the viscosity. Cerium(III) was added to the polymer blend because of its small ionic radius, high electric charge and higher potential energy. And the adding of Cerium(III) improved the adsorption capacity and decreased the adsorption time. The results showed that the maximum adsorption capacity of the obtained composite nanofibers toward As(III) adsorption is 18.0 mg/g. And As(III) can be selectively adsorbed in the presence of several other ionic species.

### 3.5 UV-initiated cross-linking

Ultraviolet (UV)-initiated cross-linking has been known since the 1950s.<sup>84</sup> The general concept is that upon UV-radiation, a photo-crosslinking group of the starting material is activated. The starting material becomes a highly reactive intermediate that can react with a neighboring functional group and form a new covalent bond.<sup>84</sup> The new covalent bond is termed a “cross-link”.<sup>84</sup> The main advantages of this technique are: (a) radiation can be conducted at room temperature; (b) it is solvent-free; (c) it is a low-cost and simple method. Mostly, three major photo-reactive groups are employed, such as benzophenones, aryl azides and diazirines.<sup>85</sup> The corresponding reactive intermediates are ketyl diradical, nitrene and carbene under UV-radiation.<sup>86</sup> The three photo-reactive groups and their corresponding reactive intermediates are shown in Scheme 3-5.

Benzophenone-derived ketyl diradicals can insert into C-H bonds. They can react with almost any neighboring alkyl-group via H-abstraction.<sup>87</sup> Aryl azide-derived nitrene groups can insert into neighboring X-H bonds (X=C, N, O, S) of amino acid residues. However, they can also quickly rearrange to the more stable electrophile 1,2-didehydroazepine as shown in Scheme 3-5, resulting in a reduction of the crosslinking efficiency and selectivity.<sup>86, 88</sup> Diazirine-derived carbene groups can also insert into neighboring X-H bonds (X=C, N, O, S) of amino acid residues. However, as illustrated in Scheme 3-5 they can also quickly rearrange to relatively inert diazo intermediates in a side-reaction, causing a decrease of the crosslinking efficiency.<sup>86, 89-91</sup> Based on the above analysis, we know that benzophenone-derived ketyl diradicals exhibit a higher chemoselectivity compared to the other two photo-reactive groups.<sup>86, 92</sup>

## INTRODUCTION

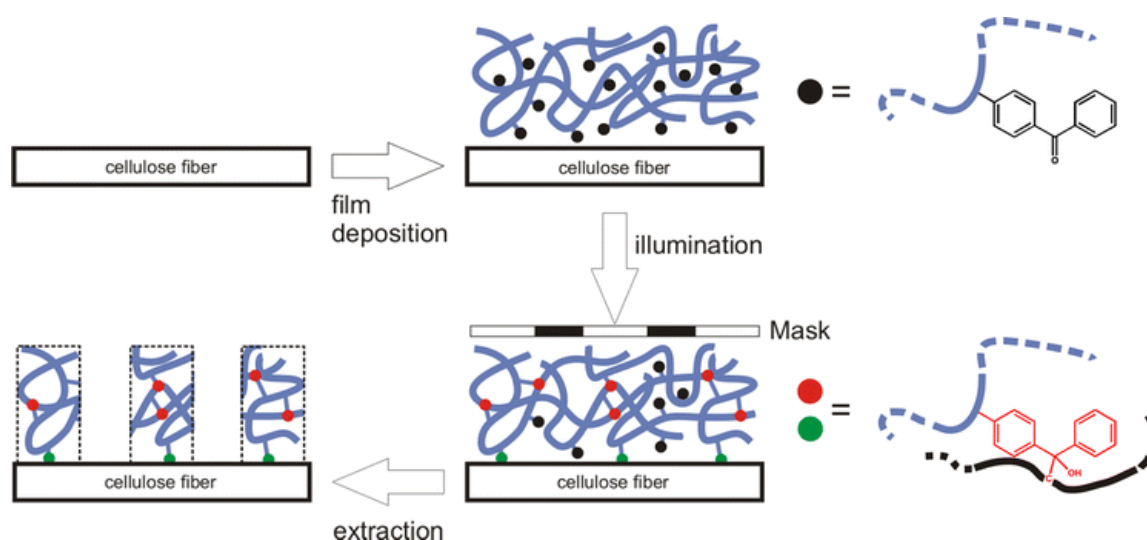


**Scheme 3-5** Three different types of photo-reactive groups. (Reproduced with permission.<sup>86</sup> Copyright © 2014 WILEY - VCH Verlag GmbH & Co. KGaA, Weinheim)

UV-irradiation can be used as one surface modification technique based on photografting polymerization.<sup>93</sup> As it needs light illumination, this surface modification technique allows UV-lithography to design chemical patterns on a substrate surface.<sup>87</sup> Benzophenone-containing polymers have experienced a renaissance in application because through a simple, one-step photo-reaction, they can be attached to and cross-linked on almost any kind of organic surface.<sup>87</sup> Böhm and coworkers reported using benzophenone-containing functional polymers to modify model filter papers.<sup>87</sup> They prepared poly(methyl methacrylate) copolymers that contain benzophenone photo-reactive groups. The copolymers were deposited on the model filter paper via dip-coating. After UV-irradiation, the copolymers were chemically linked to the paper substrates. And the linked copolymer amount can be controlled by adjustment of the copolymers concentration during the coating process. With the aid of lithographic masks, a millimeter-sized Y-shaped channel that can guide fluid penetration by capillary actions was obtained. In addition, the surface properties of the model

## INTRODUCTION

filter paper can be easily changed by embedding the desired functional groups in the benzophenone-containing copolymers. This method provides a guideline for the further design of “lab-on-paper devices”.<sup>94</sup> The UV-lithographic process for the creation of chemical patterns is shown in Scheme 3-6.



**Scheme 3-6** Schematic illustration of the lithographic process for the creation of chemical micropatterns. During the illumination step a mask is brought into contact with the substrate. No light passes through sections blocked by the mask, and non-bound polymer in shaded areas can be removed by solvent extraction. (Reproduced with permission.<sup>87</sup> Copyright © 2012 Springer Science Business Media Dordrecht)

Benzophenone can also be applied in the modification of a membrane for water purification.<sup>95-98</sup> Chen and coworkers reported a one-step eco-friendly method to modify poly(ethylene terephthalate) (PET) fabrics via a photochemical reaction with a benzophenone group terminated quaternary ammonium salt (BP-QAS).<sup>99</sup> Upon UV-irradiation, the small molecule compound BP-QAS was chemically attached to the PET surfaces like ribbons fixed at only one end. After modification, the PET fiber structure remained intact and the water permeability was not affected. The resulting PET fabrics exhibit a series of features: 1) an improved tearing strength resulting from the increased cohesive force between the fibers, 2) a

significantly improved hydrophilicity with an observable antistatic property, 3) excellent and durable broad-spectrum antimicrobial activity.

### 3.6 Spin coating technique

Spin coating is an important uniform film-forming technique.<sup>100</sup> Its study and application can be dated back to the beginning of the 20<sup>th</sup> century.<sup>101</sup> It has attracted great interest in academic and applied science due to its easy handling, reproducibility and applicability to various materials.<sup>102</sup> The schematic illustration of the spin coating technique is shown in Fig. 3-5. Its working principle is as follows.<sup>102, 103</sup> During the spin coating process, a substrate covered with coating solution is rotated. A strong shearing of the coating solution is induced by centrifugal forces. This results in most of the coating solution being ejected and the film becoming thinner until equilibrium is reached. Equilibrium can be determined by the applied spin speed and the coating solution viscosity. Once the solvent is evaporated, the final film thickness is reached. The concentration of the coating solution and the applied spin speed has a significant effect on the obtained film coating thickness. Normally, a higher solution concentration and a lower spin speed result in a thicker film coating.<sup>102</sup> The solvent volatility affects the film coating thickness as well. Norrman et al. found that when the same concentration of coating solution is used, a solvent with higher volatility can increase the film coating thickness.<sup>101</sup> Spin coating is applied in various fields such as in organic field-effect transistors,<sup>104</sup> sensors,<sup>105</sup> protective coatings,<sup>106</sup> optical coatings,<sup>107</sup> membranes<sup>108</sup> and others.<sup>101</sup>

## INTRODUCTION

---

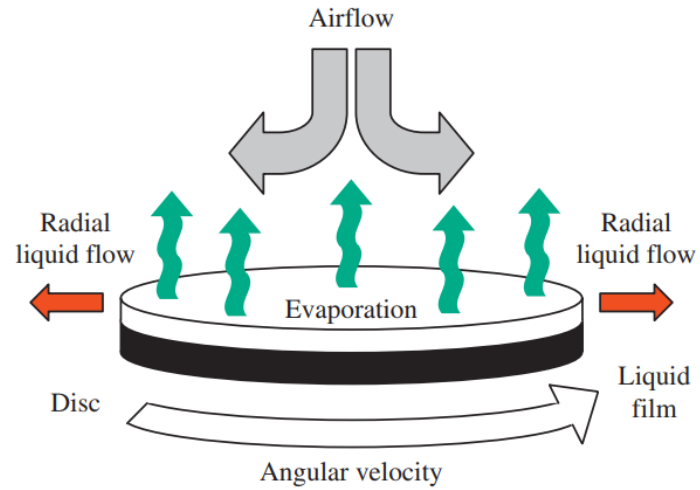


**Fig. 3-5** Schematic illustration of the spin coating technique. (Reproduced with permission.<sup>100</sup> Copyright © 2008 Elsevier B.V.)



### 4. Concept and Motivation

It is well known that the surface properties of polymeric materials are of vital importance as they determine the functions of polymeric materials and further decide their corresponding applications. Developing surface modification methods that are versatile and efficient is of significant interest for both academic and industrial research. The objective of this thesis is to develop versatile and simple modification methods for micro- and macroscopic polymeric material surfaces and to investigate their corresponding applications. The advantages of active esters, electro-spun fibers, UV-irradiation and post-modification are synergized to obtain the desired surface properties. As mentioned in section 3.1, polymeric active esters are one type of the popular precursor polymers for the preparation of functional polymer materials. However, to the best of our knowledge, electro-spinning of polymeric active ester into fiber membranes and their application for water purification has never been reported. Large quantity literature has been published about combining active ester polymers with photo-reactive polymers. However, combining a small molecule active ester with a photo-reactive group and its application of the resulting compound for the modification of material surfaces has never been investigated before. This study will fill in the above knowledge gap. The content of this study includes three parts and the detailed objective of each part is as follows:

The first part focuses on combining the advantages of polymer-based adsorbents and active esters by electro-spinning the polymeric active ester poly(methyl salicylate acrylic ester) (PMSAE) into fibrous membranes. Subsequently, the PMSAE fiber membranes will be post-modified under simple and mild reaction conditions. Finally, the application of the obtained fibrous adsorbents for the removal of organic dyes from water will be systematically investigated.

The second part focuses on increasing the diversity of the post-modification process by using polymer blends instead of the homogeneous polymer PMSAE for electrospinning.

## CONCEPT AND MOTIVATION

---

Consequently, the finally obtained fibrous adsorbents will be diverse in their application. The diversity will be measured and verified by how well the obtained fibrous adsorbents are able to remove organic dyes selectively.

The third part features a versatile post-modification method for surface modification which is possible by combining the advantages of an active ester and a photo-reactive group. The application of the resulting compound on various substrates, especially on inert polyolefins, and the creating of different chemical patterns and the changing of surface properties will be investigated. The unique advantage of the small molecule modification compound will be explored.

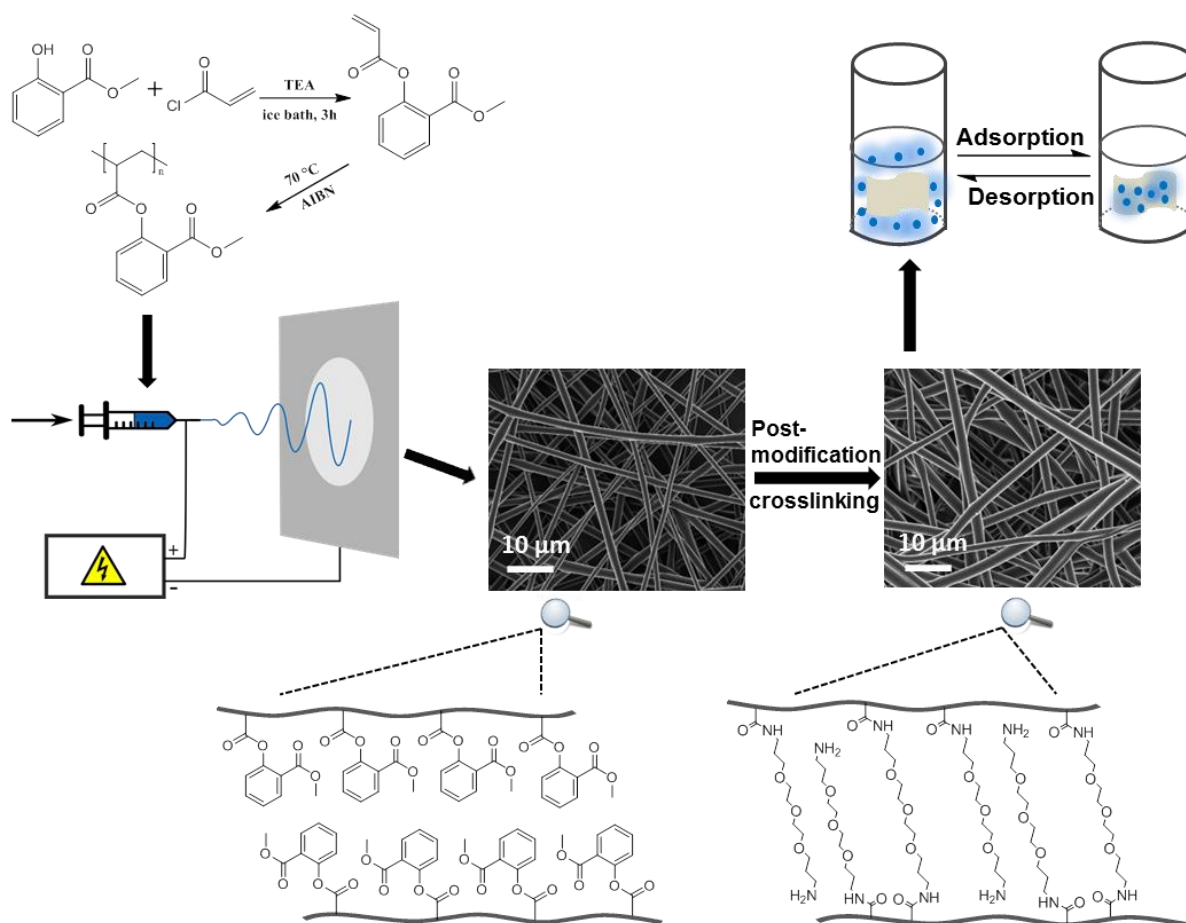
### 5. Results and Discussion

#### 5.1 Preparation, characterization and adsorption performance study of PMSAE-based fibrous adsorbents

This chapter is partially adapted from a submitted study.<sup>109</sup>

The focus in this chapter lies on combining the advantages of polymer-based adsorbents, post-polymerization modification, polymeric active esters and electrospinning to develop simple synthesized and cost-efficient materials for water purification. In this study, the salicyl-based polymeric active ester PMSAE was synthesized based on the method reported by Barbosa et al.,<sup>110</sup> but with some modification, which increased the yield significantly. For the first time, PMSAE was electrospun into polymer fibers and used for organic dyes wastewater treatment after a simple post-modification with desired functional groups. The morphology of the produced fibrous adsorbents was characterized utilizing SEM and the completeness of the post-modification process was determined using FTIR. The adsorbents were further tested for their adsorption and selectivity performance of different organic dyes as well as for their recyclability. To explore the adsorption mechanism, four kinetic models and three isotherm models were used to analyze the adsorption data. The process of the preparation of fibrous adsorbents and their application is presented as a schematic illustration in Scheme 5-1.

## RESULTS AND DISCUSSION



**Scheme 5-1** Schematic representation of the preparation of the adsorbents and their corresponding application.

### 5.1.1 Characterizations of the fibrous membrane precursor PMSAE and of the fibrous adsorbents

Active ester MSAE was synthesized according to the literature<sup>1, 110</sup> with some modification which significantly increased the yield from 77% to 92%. Subsequently, polymeric active ester PMSAE was obtained by free radical polymerization. In this work, I combined the advantages of polymer-based adsorbents and active esters by electro-spinning the polymeric active ester PMSAE into fiber membranes. Subsequently, the PMSAE fiber membranes were post-modified with 4,7,10-trioxa-1,13-tridecanediamine (TTDD) and 3,6,9-triazaundecan-1,11-diamin (TAD) under simple and mild reaction conditions. The final

## RESULTS AND DISCUSSION

---

products were two types of fibrous adsorbents, PMSAE-TTDD and PMSAE-TAD, respectively.

The corresponding morphologies of the adsorbents are shown in Fig. 5-1 (a-c). It can be observed from the images that the original PMSAE fibrous membrane and the post-modified PMSAE-TTDD, PMSAE-TAD fibrous membranes exhibit a very similar fiber morphology with a smooth and uniform surface and fiber diameters between 1-2  $\mu\text{m}$ .

FTIR-spectra were used to determine the conversion of the post-modification process. FTIR results of the fibers before post-modification, PMSAE, and after post-modification, PMSAE-TTDD and PMSAE-TAD, are shown in Fig. 5-1 (d). For the original PMSAE fiber, the bands at  $1754\text{ cm}^{-1}$  and  $1719\text{ cm}^{-1}$  are attributed to the C=O stretch of methyl salicylate ester and to the C=O stretch of methyl ester, respectively.<sup>1</sup> The band at  $1605\text{ cm}^{-1}$  is attributed to the C=C resonance vibrations in the aromatic ring of the methyl salicylate group. The successful post-modification of the PMSAE fibers with TTDD and TAD via aminolysis can be confirmed by the disappearance of the characteristic bands of the original PMSAE fiber and the appearance of new bands at  $1643\text{ cm}^{-1}$ ,  $1543\text{ cm}^{-1}$ , broad band around  $3284\text{ cm}^{-1}$ . These new bands correspond to the C=O stretching, the C-N bending and the N-H stretching of amide, respectively.

## RESULTS AND DISCUSSION

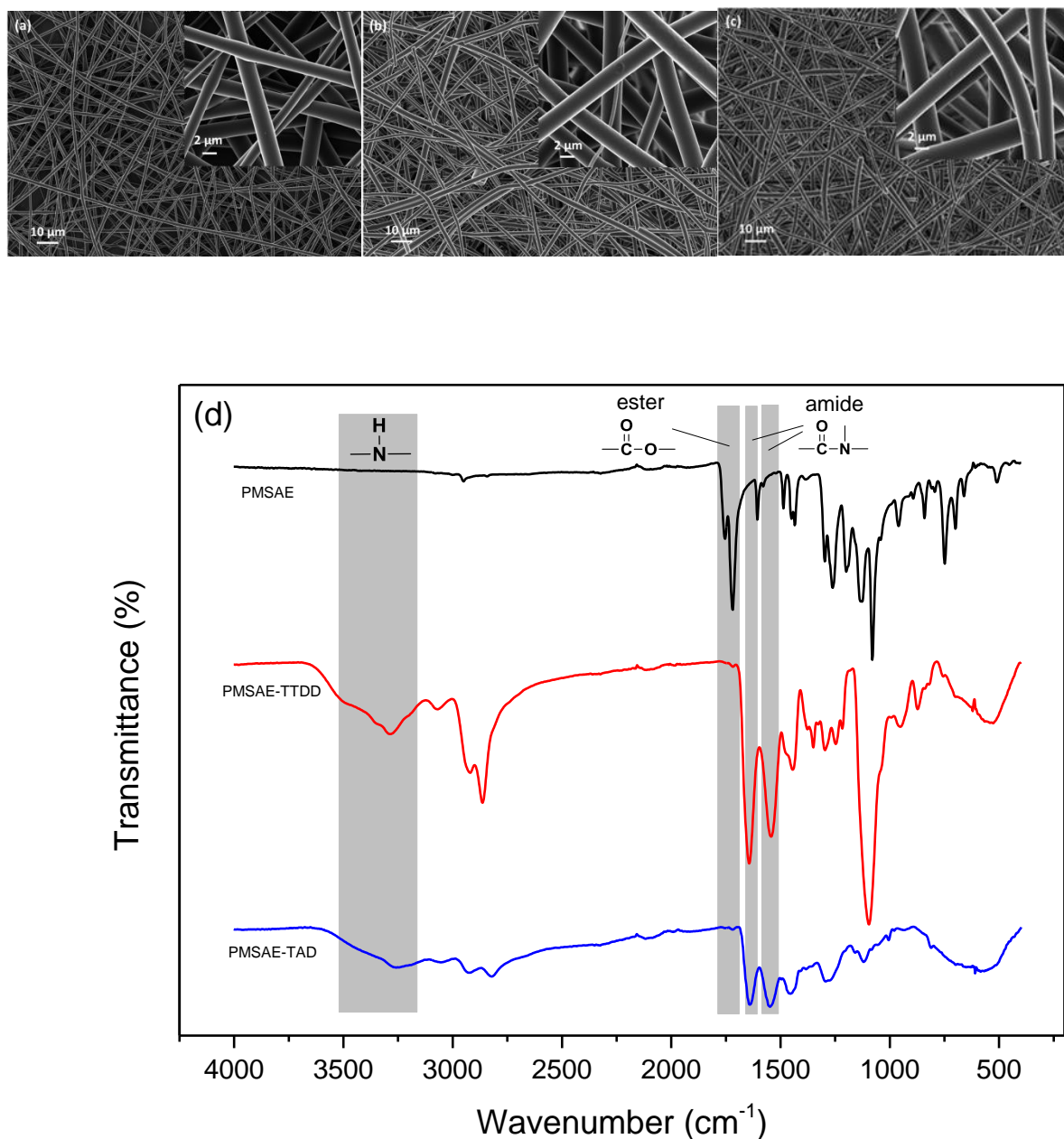


**Fig. 5-1** SEM images of (a) the original PMSAE fibers, (b) the PMSAE-TTDD fibers and (c) the PMSAE-TAD fibers. Insets show the high resolution SEM images. (d) IR of PMSAE before and after post-modification with TTDD and TAD.

### 5.1.2 Adsorption performance

The adsorption performance of the fibrous adsorbents PMSAE-TTDD and PMSAE-TAD were studied with two cationic dyes (methylene blue (MeB) and crystal violet (CV)) and three anionic dyes (azorubine (AR), orange G (OG) and methyl blue (MB)) (Fig. 5-2). 10 mg of

## RESULTS AND DISCUSSION

adsorbents were added to 40 mL dye solutions (1 mg/mL). After shaking at 240 RPM at ambient temperature for 4 h (predetermined), the concentrations of the dye solutions after adsorption were measured with an UV-Vis spectrophotometer and the adsorption capacities were calculated.

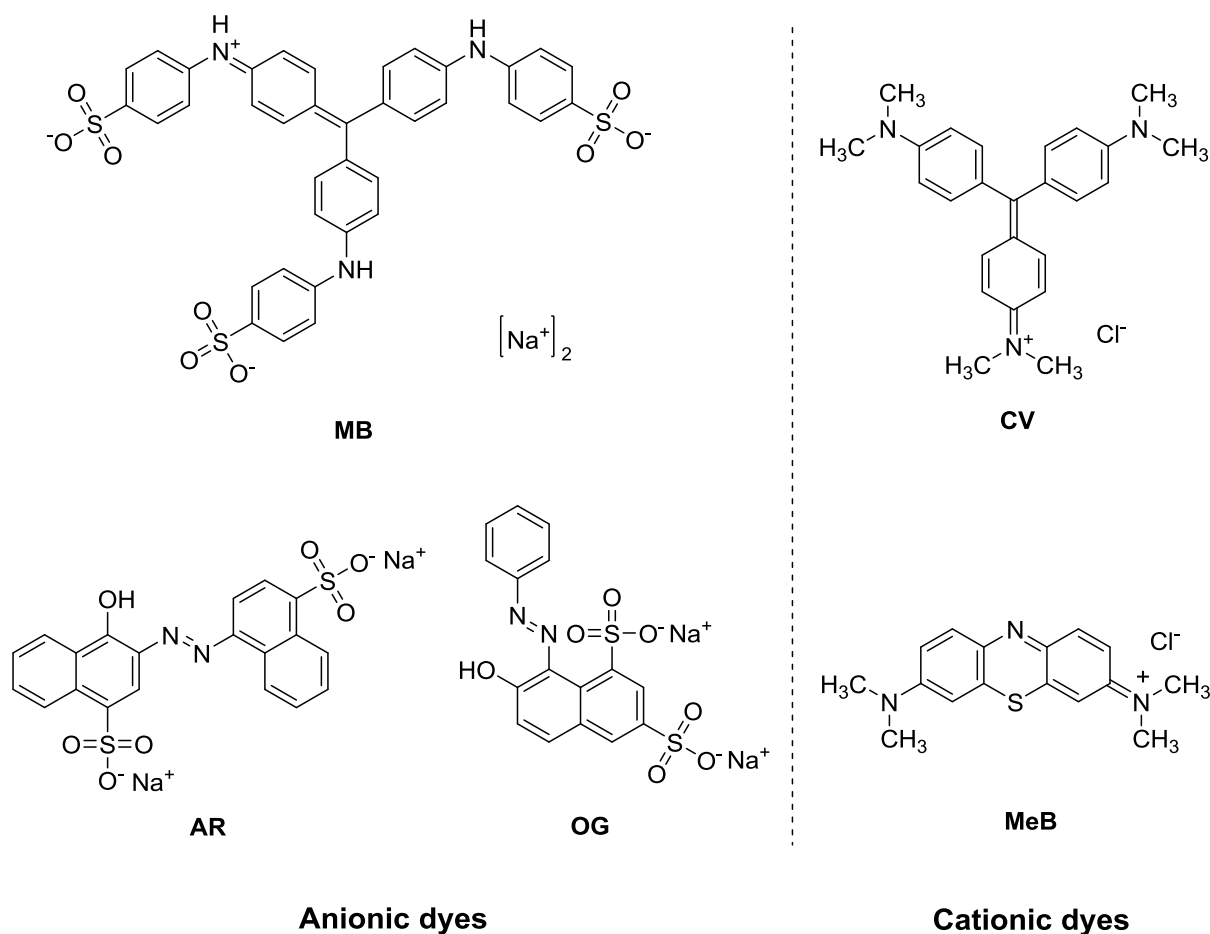


**Fig. 5-2** Molecular structures of the dyes used in the adsorption study, anionic dyes: MB, AR and OG; Cationic dyes: CV and MeB.

The results are shown in Fig. 5-3. It can be seen that there is no big difference in the adsorption capacity between these two adsorbents. Both adsorbents have a clear preference to adsorb anionic dyes. The adsorption capacity of anionic dyes was determined to be above 200 mg/g, and for the dye MB it was even above 1600 mg/g. However, for cationic dyes, the

## RESULTS AND DISCUSSION

adsorption capacity was below 200 mg/g or, as in case of the dye MeB, no adsorption could be observed at all.

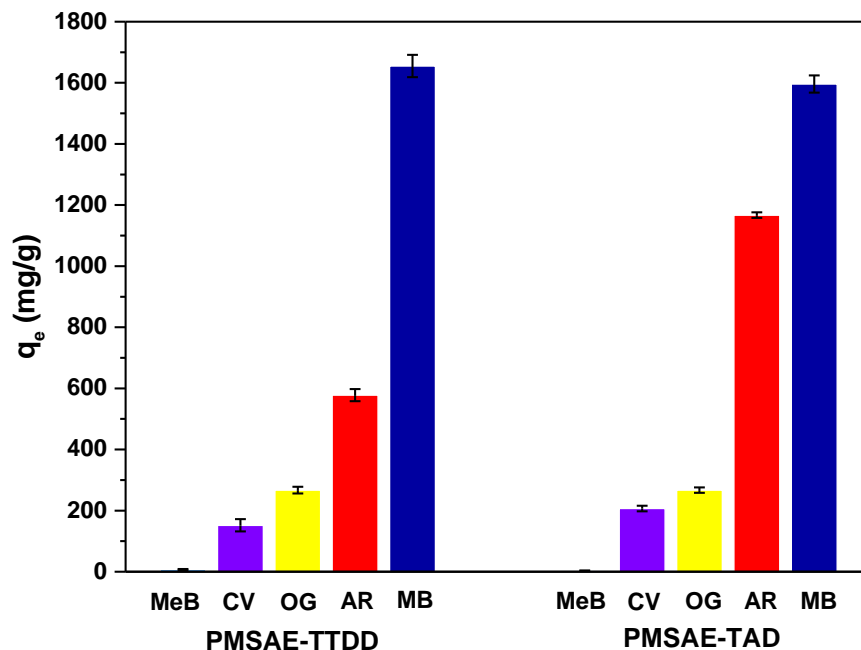


**Fig. 5-3** The adsorption capacity of different dyes on the fibrous adsorbents PMSAE-TTDD and PMSAE-TAD. Dye concentration: 1000 mg/L, adsorbent dosage: 10 mg.

Since the difference of the adsorption capacity between anionic and cationic dyes is so significant, I assume that the fibrous adsorbents feature a selective adsorption capacity. Therefore, the following experiment was carried out to verify this hypothesis. Mixed dye solutions of anionic and cationic dyes (AR and MeB as well as OG and MeB) with a mass ratio of 5:1 were prepared. The fibrous adsorbents PMSAE-TTDD and PMSAE-TAD were added to each mixture. After shaking for 4 h, the fibrous adsorbents could be pulled out of the solution as free standing membranes. UV-Vis spectra were measured of the mixed dye solutions before and after this adsorption process. The corresponding results are shown in Fig. 5-4. The optical photograph of Fig. 5-4 (a) and (b) clearly shows that the anionic dyes AR and OG can be selectively adsorbed from the mixture by both adsorbents and that the quantity is

## RESULTS AND DISCUSSION

even 5 times higher than that of the cationic dye MeB. The UV-Vis spectra in Fig. 5-4 (c) and (d) further verified this selective adsorption capacity. It can be seen in Fig. 5-4 (c) that before adsorption, 2 peaks appeared in the UV/Vis spectrum at 515 nm and 690 nm, corresponding to the dye AR and the dye MeB, respectively. The absorption peak of MeB was expected to appear at 660-665 nm, the slight shift might be due to the mixing of the dyes resulting in the change of the pH of the solution. Nevertheless, after adsorption, the peak at 515 nm disappeared almost completely, indicating that the adsorbents selectively adsorbed the anionic dye AR from the mixture. Fig. 5-4 (d) indicates that the adsorbents could selectively remove the anionic dye OG from the mixture.

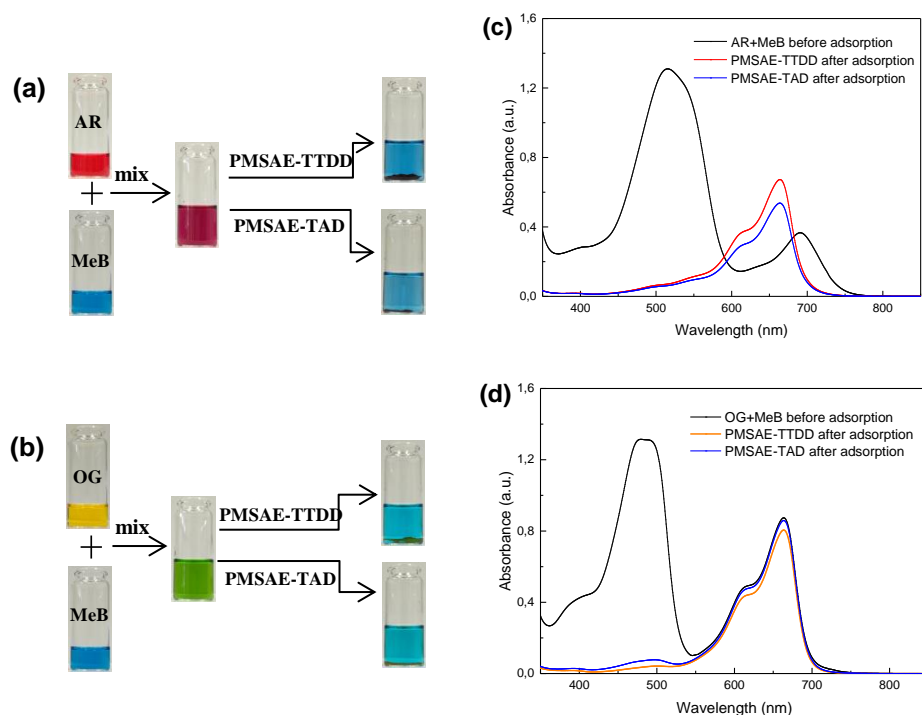


**Fig. 5-4** Optical photograph of the selective adsorption performance of PMSAE-TTDD and PMSAE-TAD (a) of the mixture AR-MeB (b) of the mixture OG-MeB; UV-Vis spectra (c) of the mixture AR-MeB (d) of the mixture OG-MeB before and after adsorption of PMSAE-TTDD and PMSAE-TAD.

There are abundant amides and ether (for PMSAE-TTDD) or imine (for PMSAE-TAD) groups in the fibrous adsorbents. Because of the surface charges of PMSAE-TTDD and

## RESULTS AND DISCUSSION

PMSAE-TAD, the adsorbents can be significantly affected by the pH of the solutions. These effects on the adsorption capacities of fibrous adsorbents toward the anionic dye MB were investigated. 40 mL of MB solutions (1 mg/mL) with different pH (3, 4, 6, 8, 9) were prepared. 10 mg of adsorbents were added to each solution. After shaking at room temperature for 4 h, the concentrations of the dye solutions were measured and the adsorption capacities were calculated. The results are shown in Fig. 5-5. It can be seen that increasing the pH resulted in a similar trend for both PMSAE-TTDD and PMSAE-TAD, namely that the adsorption capacity did not show any obvious changes in the range from pH 3 to pH 6. However, above pH 6, a significant decrease of the adsorption capacity was observed.

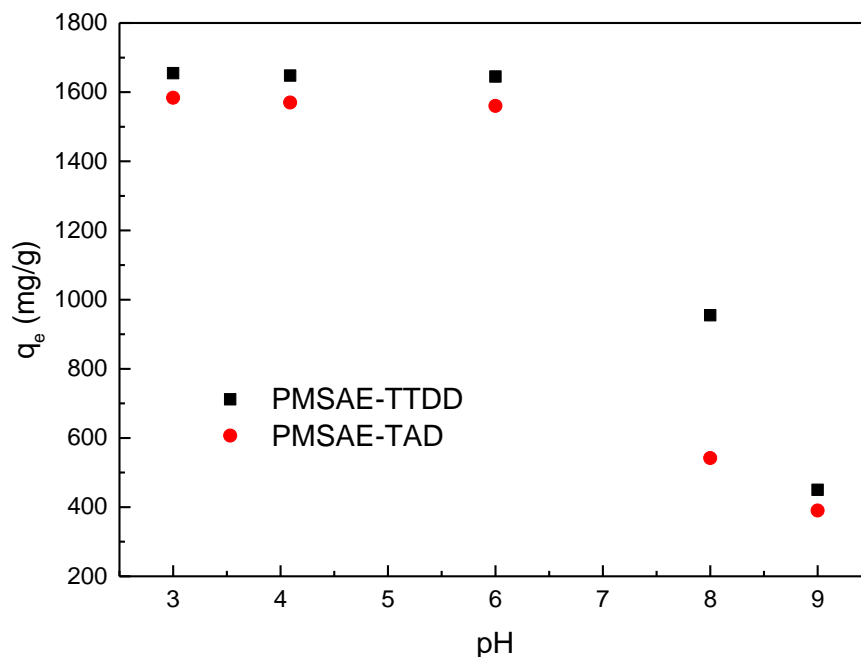


**Fig. 5-5** The effect of pH on the adsorption capacity of the adsorbents PMSAE-TTDD and PMSAE-TAD toward MB.

### 5.1.3 Adsorption kinetics

The study of the adsorption kinetics provides information on the adsorption rate and allows further exploration of the adsorption mechanism.<sup>111</sup> In this study, pseudo-first-order

## RESULTS AND DISCUSSION

---

and pseudo-second-order models were employed to analyze the adsorption data of MB onto the fibrous adsorbents PMSAE-TTDD and PMSAE-TAD. To further investigate the rate-controlling factor, intra-particle and liquid film diffusion models were also employed. The linearized form of these models is as follows:

(1) Pseudo-first-order model

$$\ln(q_e - q_t) = \ln q_e - k_1 t \quad (5-1)$$

where  $q_e$  (mg/g) and  $q_t$  (mg/g) are the adsorption capacities of MB on the adsorbents at equilibrium and time  $t$  (min), respectively;  $k_1$  ( $\text{min}^{-1}$ ) is the rate constant of the pseudo-first-order.

(2) Pseudo-second-order model

$$\frac{t}{q_t} = \frac{1}{k_2 q_e^2} + \frac{t}{q_e} \quad (5-2)$$

where  $k_2$  ( $\text{g}/(\text{mg min})$ ) is the equilibrium rate constant of the pseudo-second-order.

(3) Intra-particle diffusion model

$$q_t = k_p t^{0.5} + C \quad (5-3)$$

where  $C$  gives an idea about the thickness of the boundary layer,  $k_p$  ( $\text{g mg}^{-1} \text{min}^{-0.5}$ ) is the intra-particle diffusion rate constant.

(4) Liquid film diffusion model

$$\ln(1 - F) = -k_{fd} t \quad (5-4)$$

$$F = \frac{q_t}{q_e} \quad (5-5)$$

where  $F$  is the fractional achievement of equilibrium at time  $t$ ,  $k_{fd}$  ( $\text{min}^{-1}$ ) is the adsorption rate constant.

The adsorption kinetics data and the fitting results are shown in Fig. 5-6 and Table 5-1.

## RESULTS AND DISCUSSION

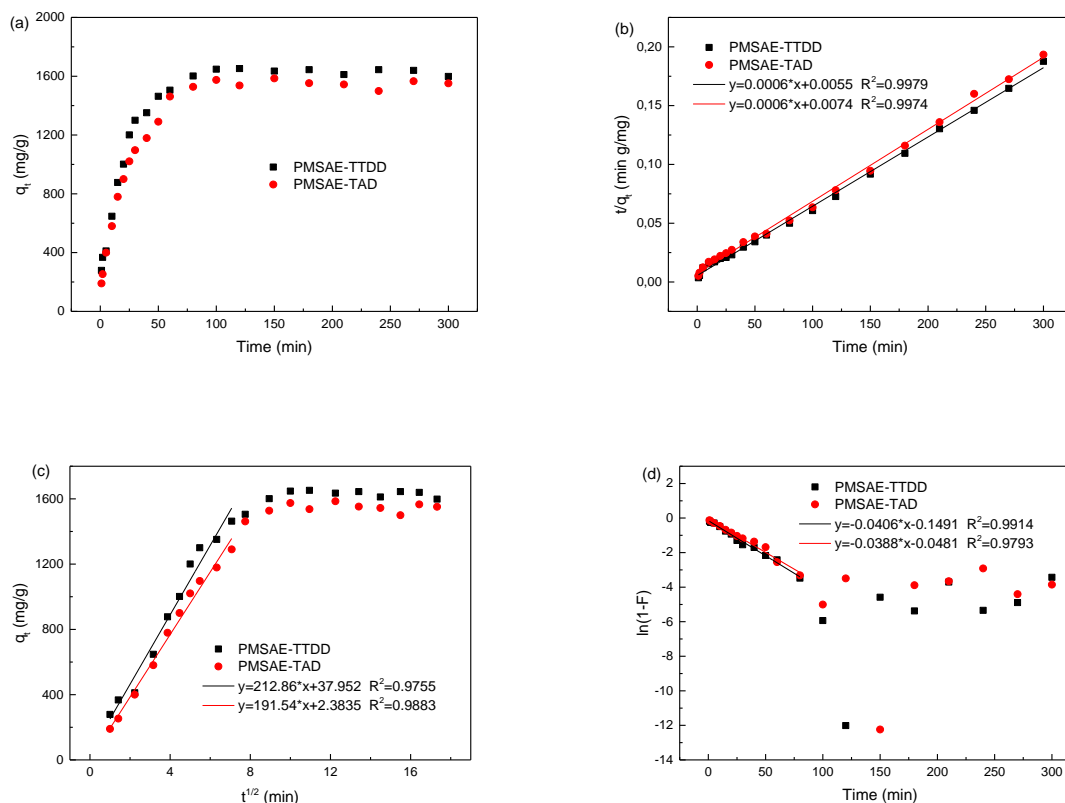


**Fig. 5-6** (a) Effect of contact time on MB adsorption by PMSAE-TTDD and PMSAE-TAD. (b) Linear fitting of pseudo-second-order kinetics, (c) Intra-particle diffusion and (d) Liquid film diffusion kinetics for adsorption of MB on PMSAE-TTDD and PMSAE-TAD.

It can be seen in Fig. 5-6 (a) that the adsorption of MB by PMSAE-TTDD and PMSAE-TAD showed similar adsorption trends with time. First, the adsorption capacity increased relatively fast during the initial stage within the first 50 minutes, then it slowed down and finally it approached an equilibrium after 90 min. Fig. 5-6 (b) shows that the fitting plots of the pseudo-second-order kinetic model exhibit a good linearity, which was also proven by the higher value of  $R^2$  ( $> 0.99$ ) compared to that of the pseudo-first-order (see Table 5-1). Meanwhile, the calculated  $q_e$  of each fibrous adsorbent could also be better fitted to a pseudo-second-order model, indicating that the adsorption process followed a pseudo-second order kinetic model. This indicates that the rate-limiting step in the adsorption process may be

## RESULTS AND DISCUSSION

---

chemical adsorption or chemical adsorption involving Van-der-Waals interactions between adsorbent and adsorbate.<sup>111</sup>

It can be seen in Fig. 5-6 (c) and (d) and Table 5-1 that before reaching equilibrium (within 90 min), both the fitting plots of the intra-particle and liquid film diffusion models exhibit good linearity, with all correlation coefficients higher than 0.97. The plots also did not pass through the origin, indicating that the rate-limiting step might not be the only one but the combination of intra-particle and liquid film diffusion.<sup>112</sup>

## RESULTS AND DISCUSSION

**Table 5-1** Adsorption kinetic parameters obtained from kinetic models fitting to the experimental data.

Adsorbents	$q_{e,exp}^a$ (mg/g)	Pseudo-first-order			Pseudo-second-order			Intra-particle diffusion			Liquid film diffusion	
		$k_1$ ( $\text{min}^{-1}$ )	$q_{e1}^b$ (mg/g)	$R^2$	$K_2$ ( $\text{g}/(\text{mg min})$ )	$q_{e2}^b$ (mg/g)	$R^2$	$K_p$ ( $\text{mg}/(\text{g min})$ )	$C$	$R^2$	$k_{fd}$	$R^2$
PMSA E- TTDD	1652.15	0.0505	1735.76	0.9453	$0.65 \times 10^{-4}$	1666.67	0.9979	212.86	37.95	0.9755	0.0406	0.9914
PMSA E- TAD	1585.25	0.0450	1711.46	0.9649	$0.49 \times 10^{-4}$	1666.67	0.9974	191.54	2.38	0.9883	0.0388	0.9793

<sup>a</sup>  $q_{e,exp}$  is experimental values

<sup>b</sup>  $q_{e1}, q_{e2}$  are calculated values

### 5.1.4 Adsorption isotherms

Adsorption isotherm studies provide information about the reaction behavior between adsorbent and adsorbate. In this study, the adsorption results were analyzed to figure out whether the adsorption processes followed the Langmuir, Freundlich or Dubinin–Radushkevich (D–R) isotherm models. The basic hypothesis of the Langmuir model is that adsorption takes place at specific homogeneous sites within the adsorbent.<sup>113, 114</sup> The Freundlich model is based on the assumption that the adsorption takes place on a heterogeneous surface.<sup>112</sup> The D-R model is applied to explore whether the nature of the adsorption mechanism is physical or chemical.<sup>115</sup> The linearized forms of these models are as follows:

Langmuir equation:

$$\frac{C_e}{q_e} = \frac{1}{q_m K_L} + \frac{C_e}{q_m} \quad (5-6)$$

Freundlich equation:

$$\ln q_e = \ln K_F + \frac{1}{n} \ln C_e \quad (5-7)$$

D–R equation:

$$\ln q_e = \ln q_m - \beta \varepsilon^2 \quad (5-8)$$

where  $C_e$  (mg/L) is the equilibrium MB concentration in solution;  $q_{\max}$  (mg/g), the maximum adsorption capacity of the adsorbent;  $K_L$  (L/mg), the Langmuir constant;  $K_F$  (l/g), the Freundlich constant;  $1/n$  gives information of the isotherm type: irreversible ( $1/n < 0$ ), desirable ( $0 < 1/n < 1$ ), undesirable ( $1/n > 1$ );  $\beta$  ( $\text{mol}^2/\text{kJ}^2$ ), a constant related to the mean free energy of adsorption;  $\varepsilon$ , the Polanyi potential, which is equal to  $RT \ln(1 + (1/C_e))$  ( $R$  ( $\text{kJ mol}^{-1} \text{K}^{-1}$ ) is the gas constant,  $T$  (K) is the temperature).

In addition,

## RESULTS AND DISCUSSION

---

$$R_L = \frac{1}{1 + K_L C_1} \quad (5-9)$$

Based on the Langmuir model,  $R_L$  is the separation factor and provides information of the adsorption process: unfavorable ( $R_L > 1$ ), favorable ( $R_L < 1$ ), linear ( $R_L = 1$ ), or irreversible ( $R_L = 0$ ).  $C_1$  (mg/L) is the highest initial MB concentration.

$$E = \frac{1}{\sqrt{2\beta}} \quad (5-10)$$

Based on the D-R model,  $E$  (kJ/mol) is the free energy of transfer of 1 mol adsorbate from solution to adsorbent surface. It provides information about the adsorption type: physical ( $E < 8$  kJ/mol) or chemical ( $8$  kJ/mol  $< E < 16$  kJ/mol).

**Table 5-2** Adsorption isotherm parameters obtained from isotherm models fitting to the experimental data.

	PMSAE-TTDD	PMSAE-TAD
Langmuir		
$q_m$ (mg/g)	2000	2000
$K_L$ (L/mg)	0.0066	0.0052
$R_L$	0.1316	0.1613
$R^2$	0.9745	0.9873
Freundlich		
$K_F$ (1/g)	23.0255	13.1090
$1/n$	0.6873	0.7663
$R^2$	0.8168	0.8236
D-R		
$q_m$ (mg/g)	1601.19	1518.84
$\beta$	2150.20	2921.30
$E$ (kJ/mol)	0.0152	0.0131
$R^2$	0.9939	0.9981

## RESULTS AND DISCUSSION

---

It can be seen from Table 5-2 that for both the adsorption isotherm of MB on PMSAE-TTDD and PMSAE-TAD, the D-R model fits the experimental data best in terms of the highest correlation coefficient  $R^2$ , while the Langmuir model fits second best.

For the D-R model, the values of  $E$  are lower than 8 kJ/mol, which means that the adsorption process corresponds best with a physisorption, as expected. The calculated maximum adsorption capacity of 1601 mg/g for PMSAE-TTDD and 1519 mg/g for PMSAE-TAD, respectively, corresponded well with the experimental data in Fig. 5-6 (a) of 1652 mg/g for PMSAE-TTDD and 1585 for PMSAE-TAD, respectively.

For the Langmuir model, the values of  $R_L < 1$  indicate that the adsorption process is favorable and that a monolayer adsorption on a homogeneous adsorbent takes place.

### 5.1.5 Reusability of the adsorbents

For commercial feasibility, reusability is a vitally important factor. As the adsorption process corresponds with a physisorption process, studies regarding a recyclability of the adsorbents were conducted. For such recyclability experiments, fibrous adsorbents were added into a MB solution. After shaking for 4 h, the adsorbents were removed from the MB solution, transferred into a NaOH solution and shaken for 30 minutes to elute the adsorbed dye. Subsequently, the adsorbents were washed with deionized water and ethanol several times until the washing solutions became neutral. Then the fibers were dried in a vacuum oven at 40 °C overnight for the next adsorption process. These adsorption-desorption processes were carried out 5 times.

It can be seen from Fig. 5-7 that for the first three recycling steps, the adsorption capacity showed a significant decline. This might be due to the remaining adsorbed MB dye stuck in the network of the fibrous adsorbents. For the last 2 recycling steps, no obvious decline was observed anymore. After 5 recycling steps, the adsorption capacity was still above 900 mg/g for PMSAE-TTDD and 700 mg/g for PMSAE-TAD, respectively. This means the fibrous

## RESULTS AND DISCUSSION

adsorbents can be reused, even though they tend to lose some of their adsorbent capacity in the first cycles.

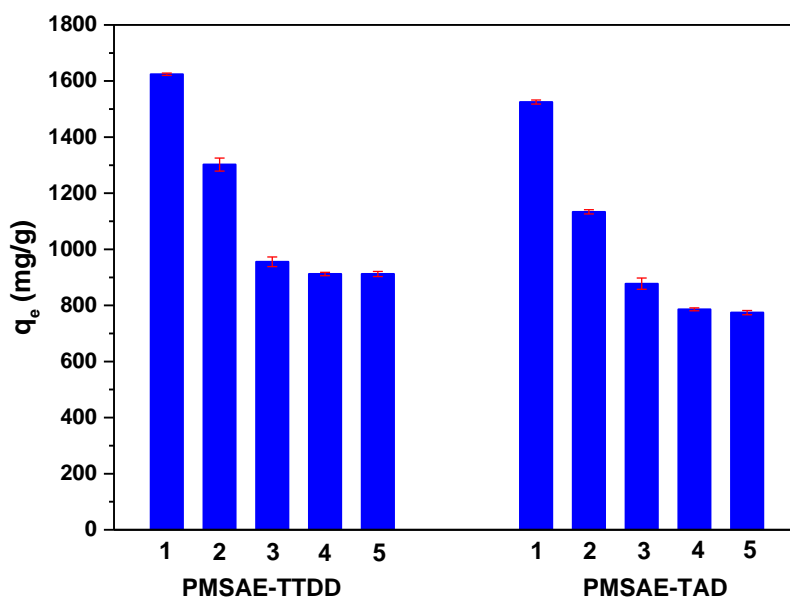


Fig. 5-7 Recyclability of PMSAE-TTDD and PMSAE-TAD for the adsorption of MB.

### 5.1.6 Comparison with other adsorbents reported in the literature

In Table 5-3 the maximum MB adsorption capacity of the fibrous adsorbents developed in this work is compared with various other adsorbents reported in the literature. It can be seen that the maximum MB adsorption capacity of the fibrous adsorbents PMSAE-TTDD and PMSAE-TAD is significantly higher than that of most reported adsorbents. Though Elsherbiny et al. reported that Mt/IPS2 shows a super high adsorption capacity of 9.95 mmol/g (7958.01 mg/g)<sup>116</sup> and Cheng et al. reported that macroscopic yttrium oxide aerogel monoliths show an excellent adsorption capacity of 8080 mg/g<sup>117</sup> for MB, respectively, they did not mention the reusability. Further, their reported preparation procedures are complicated and reaction conditions are strict. However, in my study, simple electro-spinning is used to prepare the precursor fibers. Additionally, the employed post-modification conditions to

## RESULTS AND DISCUSSION

---

prepare the final fibrous adsorbents are mild. Yet, the achieved maximum adsorption capacity is very high and reusability is possible. Moreover, the low cost of the starting materials makes it more feasible for future industrial applications.

## RESULTS AND DISCUSSION

**Table 5-3** Comparison of adsorption capacities of MB by the adsorbents in this work with other reported adsorbents.

Adsorbents	Adsorption capacity (mg/g)	Reference
Macroscopic yttrium oxide aerogel monoliths	8080	117
Polyaspartate-montmorillonite composite with quaternary phosphonium salt (Mt/IPS2)	7958.01	116
<b>PMSAE-TTDD</b>	<b>1652.15</b>	<b>This work</b>
<b>PMSAE-TAD</b>	<b>1585.25</b>	<b>This work</b>
Y <sub>2</sub> O <sub>3</sub> functionalized palygorskite (Y <sub>2</sub> O <sub>3</sub> /Pal)	1579.06	118
Polyethylenimine modified cellulose (PMC) aerogels	1333.04	119
Cationic charged hybrid nanofibrous membranes	1290	120
Polydopamine-coated electrospun poly(vinyl alcohol)/poly(acrylic acid) membranes (PVA/PAA@PDA)	1147.60	43
Multiple hierarchical structures (MHS)	480	121
Poly(ionic liquid) of poly(3-ethyl-1-vinylimidazolium bis(trifluoromethanesulfonyl)imide) (PVI-TFSI)	476.20	122
Ammonium functionalized hollow polymer particles (HPP-NH <sub>3</sub> <sup>+</sup> )	449	123
Yolk-shell structured Si/SiC@C@TiO <sub>2</sub> nanocomposites	368	124
Graphene oxide (GO)	357.14	125
Boron nitride (BN) fibrous nanonets	327.80	126
β-cyclodextrin/poly(acrylic acid)/graphene oxide nanocomposites	247.99	127
Magnetite/carbon adsorbents	< 200	128
Mussel-inspired materials (Fe <sub>3</sub> O <sub>4</sub> @PDA/PEI)	170	129
Konjacglucomannan/graphene oxide hydrogel (KGM/GO)	92.30	130
Surface fluorinated ZnO	48.54	131
Porous hollow g-Al <sub>2</sub> O <sub>3</sub> nanofibers	23.10	132
Amino functionalized corn stalk (CS) cellulose membrane (ACM)	8.75	133

### 5.1.7 Mechanism exploration

For PMSAE-TTDD, abundant primary amine and ether groups exist on the surface of the fibrous adsorbent. In particular, the electron lone pair of nitrogen of the primary amine group can easily be positively charged under acidic conditions, resulting in ammonium groups. As a consequence, the anionic dye MB can be adsorbed to the fibrous adsorbent via electrostatic attraction. Moreover, the morphology of the adsorbent is based on fibers with a diameter of 1-2  $\mu\text{m}$  and a high porosity, which significantly increases the specific surface area of the adsorbent. This can explain the extremely high adsorption capacity for the anionic dye MB. Under alkaline conditions, the surface of the fibrous adsorbent is neutral to negatively charged, resulting in a desorption due to the electrostatic repulsion between the anionic dye MB and the fibrous adsorbent. A similar adsorption-desorption mechanism was proposed for PMSAE-TAD. The difference in the case of PMSAE-TAD is that the functional and effective groups are primary and secondary amines.

This mechanism also explains why the increase of the pH of the anionic dye MB solution resulted in a decreased adsorption capacity. With the increase of the pH of the MB solution from 3 to 9, the positively charged surface of the fibrous adsorbent gradually became negatively charged and the electrostatic repulsion between the anionic dye MB and the neutral to negatively charged fibrous adsorbent caused the decrease of the adsorption capacity. This further indicates that the adsorption process of MB onto the fibrous adsorbents is the result of electrostatic interactions, which is in agreement with the small  $E$  value obtained for the adsorption isotherms (Section 5.1.4) indicating that it is physisorption. As physisorption processes are usually reversible, the fibrous adsorbents showed a good recyclability.

### 5.1.8 Conclusions

In conclusion, two new fibrous adsorbents PMSAE-TTDD and PMSAE-TAD which are based on polymeric salicyl active ester were developed by employing the electrospinning technique and via post-modification. The newly developed fibrous adsorbents showed an extremely high adsorption capacity toward MB (PMSAE-TTDD: 1652 mg/g; PMSAE-TAD: 1585 mg/g), a good selective adsorption capacity of anionic dyes from cationic dyes and they can be recycled at least 5 times. The adsorption mechanism of the fibrous adsorbents towards organic dyes is based on electrostatic interactions between the surface of the fibrous adsorbents and organic dyes. The simple and mild synthesis process, the excellent performance, and cost-efficiency, further, the good recyclability indicates that the newly developed fibrous adsorbents are promising for application in water treatment as they outperform many other adsorbents.

### **5.2 Preparation, characterization and adsorption performance study of PMAM-based fibrous adsorbents**

This chapter is partially adapted from a submitted study.<sup>134</sup>

In the above chapter 5.1, I presented the fibrous adsorbents, which combined the advantages of polymer-based adsorbents, post-polymerization modification, polymeric active esters and electro-spun fibers. And the developed low cost fibrous adsorbents showed excellent dye adsorption performance and selective adsorption of anionic dye from the mixture of cationic dye and anionic dye. However, the necessary chemicals used for post-modification should provide the desirable groups for adsorption and should act as crosslinker in order to preserve the fiber morphology as well. Such requirements limit the versatile application of electro-spun fibrous membrane precursors.

In this chapter, the diversity of the post-modification process was increased by using polymer blends instead of the homogeneous polymer PMSAE for electrospinning. Polymer blends are composed of a hydrophobic poly(methyl methacrylate) (PMMA) with good mechanical properties, the photo-crosslinker poly(4-acryloyloxybenzophenone) (PABP) and PMSAE. PMMA was chosen because of the following outstanding properties: (a) the ability to keep its stability under UV-irradiation;<sup>135</sup> (b) being easily dissolvable in dimethyl formamide (DMF) and tetrahydrofuran (THF) both of which were used as the electrospinning solvents in this work;<sup>135</sup> (c) having a good stability in ethanol<sup>135</sup> which was used as the post-modification solvent in this work; (d) PMMA with high molecular weight improves the morphology of electro-spun fibers;<sup>136</sup> (e) PMMA is commercially available. PABP was chosen because of the higher chemoselectivity compared to other photo-reactive groups as mentioned in section 3.5.

The polymer blends (PMSAE, PABP, PMMA) can result in the new fibrous membranes PMAM via electrospinning. After a simple post-modification procedure under mild reaction

## RESULTS AND DISCUSSION

---

conditions, two different types of fibrous adsorbents can be obtained. Their adsorption performance for various anionic and cationic dyes, the selective adsorption property and the effect of the solution pH on the adsorption capacity is then investigated. Also adsorption kinetics and isotherms are studied to explore the adsorption mechanisms.

### **5.2.1 Characterizations of the fibrous membrane precursor PMAM and of the fibrous adsorbents**

Building on the above work in chapter 5.1 which combining the advantages of polymer-based adsorbents, active esters and electro-spun fibers, the current study targets a simplification by blending polymers to obtain reactive polymeric adsorbents by taking advantage of PMMA and the photo crosslinker PABP. For this, PMSAE, PABP and PMMA have been electro-spun to the fibrous membranes PMAM. The fibrous membranes PMAM were further post-modified with TTDD or ( $\pm$ )-3-amino-1,2-propanediol (APD) under simple and mild reaction conditions, yet maintaining the fiber morphology. The final products were two different types of fibrous adsorbents: PMAM-TTDD and PMAM-APD.

The morphologies of the original fibrous membrane precursor PMAM and the fibrous adsorbents PMAM-TTDD and PMAM-APD are shown in Fig. 5-8 (a-c). It can be seen that they have similar morphologies: the surfaces are smooth, uniform and most of the fiber diameters remain between 1-2  $\mu\text{m}$ . There is one difference, however, namely that PMAM-APD fibers are bent and not straight like those of PMAM-TTDD.

FTIR spectra were used to determine the conversion of the post-modification process. Fig. 5-8 (d) shows the FTIR results of the original fibrous membrane PMAM before post-modification and of the fibrous adsorbents PMAM-TTDD and PMAM-APD after post-modification. For the original fibrous membrane PMAM, the bands at  $1754\text{ cm}^{-1}$  and  $1722\text{ cm}^{-1}$  correspond to the C=O stretch of methyl salicylate ester and the C=O stretch of methyl ester, respectively.<sup>1</sup> The bands at  $1599\text{ cm}^{-1}$  and  $1657\text{ cm}^{-1}$  are attributed to the C=C resonance vibrations in the aromatic ring of the methyl salicylate group and of the

## RESULTS AND DISCUSSION

benzophenones, respectively. The disappearance of the characteristic bands at  $1754\text{ cm}^{-1}$  and  $1722\text{ cm}^{-1}$ , and the appearance of the new bands at  $1643\text{ cm}^{-1}$  (C=O stretching) and  $1540\text{ cm}^{-1}$  (C-N bending) as well as the broad band at around  $3284\text{ cm}^{-1}$  (N-H stretching of amide) confirm the successful post-modification of the fibrous membrane PMAM with TTDD and APD via aminolysis. The broad band at  $3284\text{ cm}^{-1}$  of PMAM-APD is stronger than that of PMAM-TTDD due to the OH stretch of APD.

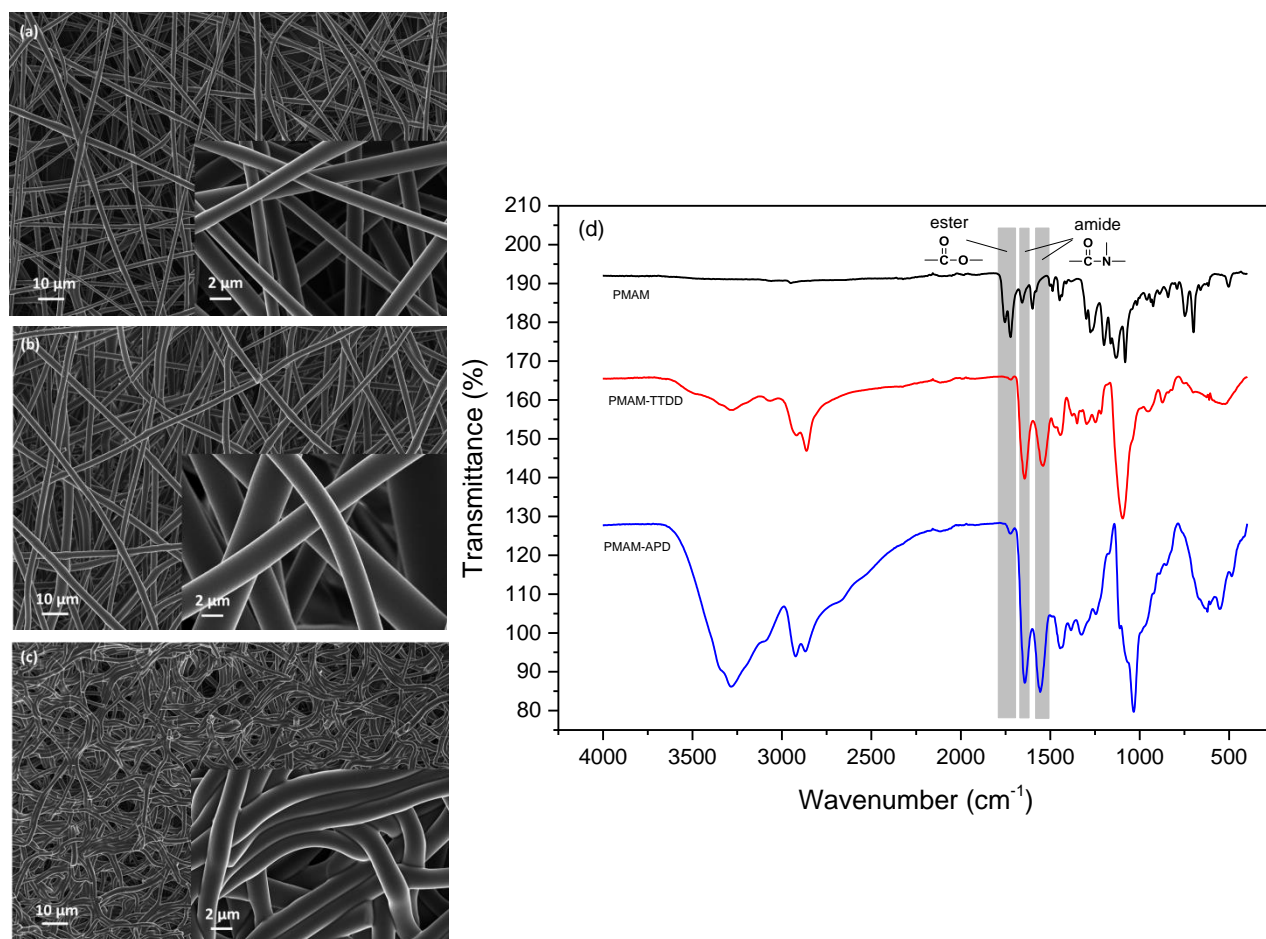


**Fig. 5-8** SEM images of (a) the original fibrous membrane PMAM, (b) the fibrous adsorbent PMAM-TTDD and (c) the fibrous adsorbent PMAM-APD. The inserts show the high resolution SEM images. (d) IR spectra of PMAM before and after post-modification with TTDD and APD.

### 5.2.2 Adsorption performance of the fibrous adsorbents for different dyes

The adsorption capacities of the fibrous adsorbents PMAM-TTDD and PMAM-APD toward organic dyes were tested with five different dyes (Fig. 5-2): two cationic dyes (MeB and CV) and three anionic dyes (AR, OG and MB). For PMAM-TTDD, 10 mg of the adsorbents were dipped into 40 mL 1 mg/mL dye solutions. For PMAM-APD, 10 mg of the adsorbents were dipped into 10 mL 1 mg/mL dye solutions. After shaking at 240 RPM at ambient temperature for 4 h, the concentrations of dye solutions after adsorption were measured and the adsorption capacities were calculated.

The corresponding results are shown in Fig. 5-9. It can be seen that PMAM-TTDD features high adsorption capacities for anionic dyes in general and for MB in particular (as high as 1545 mg/g). But for cationic dyes, the adsorption capacities were less than 160 mg/g. Compared with the results in the above section 5.1.2, where the adsorption capacity of PMSAE-TTDD (TTDD modified homogeneous fibrous membrane PMSAE) towards MB was 1652 mg/g, PMAM-TTDD shows only a slight decrease of the adsorption capacity, resulting from the addition of PMMA and the photo-crosslinker PABP to the fibrous membrane precursor.

In contrast, PMAM-APD shows the opposite trend: it has a high adsorption capacity for cationic dyes (above 340 mg/g) but no adsorption of anionic dyes could be observed. Especially for the cationic dye CV, the adsorption capacity was 577 mg/g, which is much higher than any reported value in the literature.<sup>137-139</sup> The results indicate that the newly developed fibrous membrane precursors can be post-modified with functional groups that bear the specific functional groups without the necessity of a crosslinker. Consequently, the diversity of the post-modification process could be increased.

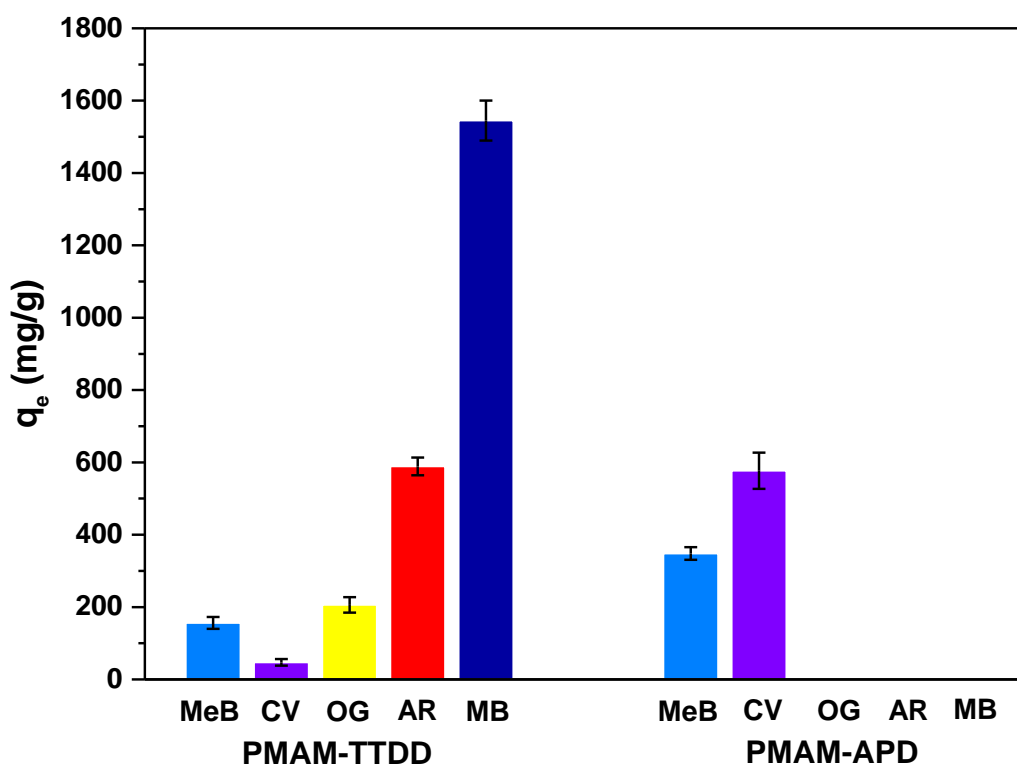


**Fig. 5-9** Adsorption capacity of different dyes on the fibrous adsorbents PMAM-TTDD and PMSAE-APD.

Dye concentration: 1000 mg/L, adsorbent dosage: 10 mg.

### 5.2.3 Selective adsorption performance of the fibrous adsorbents

Based on the result of the above section 5.2.2, a hypothesis was put forward: the fibrous adsorbent PMAM-TTDD could selectively adsorb anionic dyes and the fibrous adsorbent PMAM-APD could selectively adsorb cationic dyes. This hypothesis is verified by the following experiments.

To verify whether PMAM-TTDD is able to selectively adsorb anionic dyes, mixed anionic and cationic dye solutions of OG + CV, OG + MeB and AR + MeB with a mass ratio of 5:1 were prepared. The fibrous adsorbents PMAM-TTDD were dipped into each mixture. After shaking at room temperature for 4 h, the adsorbents were pulled out as free-standing membranes. UV-Vis spectra were measured of each mixed dye solution before and after adsorption. The corresponding results are shown in Fig. 5-10 (a-f). It can already be seen from

## RESULTS AND DISCUSSION

---

the optical photographs of Fig. 5-10 (a-c) that the anionic dyes OG and AR were selectively adsorbed from the mixed dye solutions. The corresponding UV-Vis spectra of the solutions in Fig. 5-10 (d-f) further verified the selective anionic dye adsorption ability of PMAM-TTDD. The characteristic peaks of the anionic dye OG between 470-500 nm and of the anionic dye AR at 515 nm disappeared after the adsorption process. And the characteristic peaks of the cationic dye CV at 590 nm and of the cationic dye MeB between 660-665 nm remained. In Fig. 5-10 (e) and (f) the characteristic peak of the dye MeB before adsorption was lower than after adsorption, which might be due to the interaction between the cationic dye with the anionic dye in the mixed solution.

To verify whether PMAM-APD is able to selectively adsorb cationic dyes, mixed anionic and cationic dye solutions of OG+CV, AR+CV and AR+MeB with a mass ratio of 1:1 were prepared. The subsequent procedure was the same as for PMAM-TTDD above. The corresponding results shown in Fig. 5-10 (g-l) indicated that PMAM-APD can selectively adsorb cationic dyes from a solution of mixed dyes.

## RESULTS AND DISCUSSION

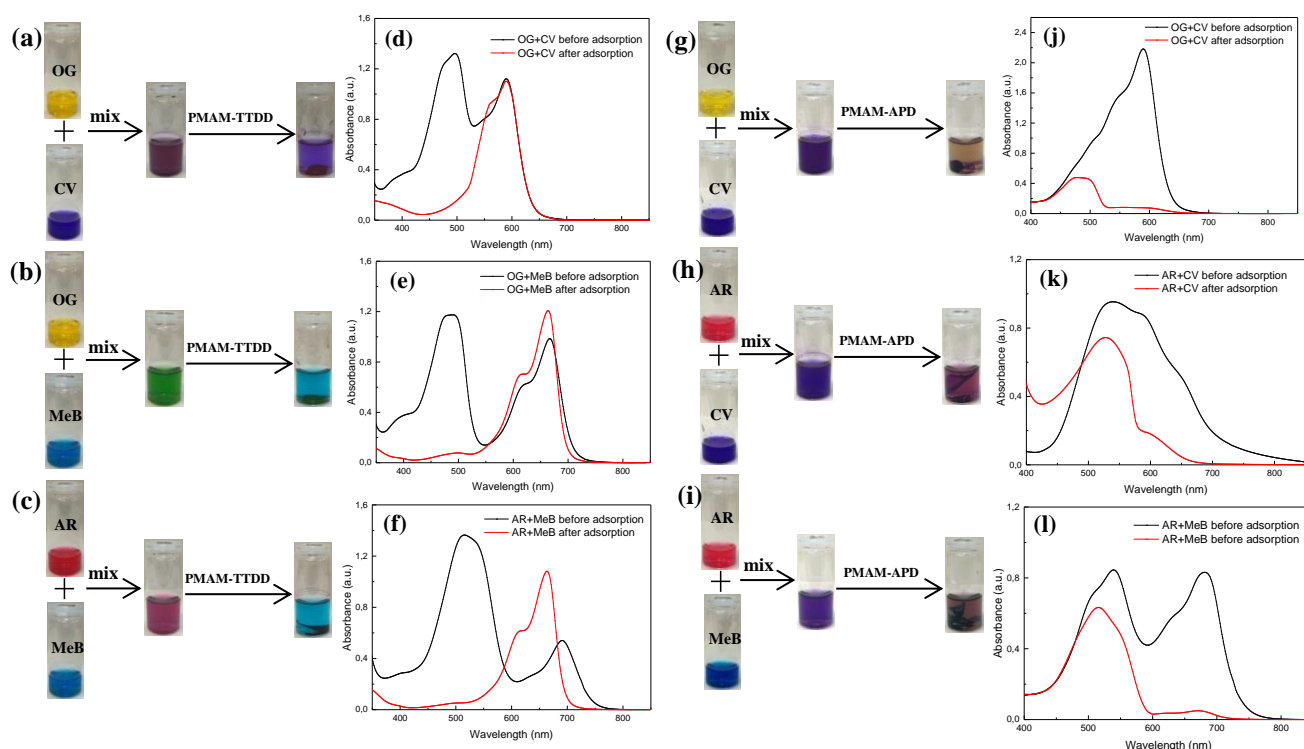


**Fig. 5-10** Optical photograph of the selective adsorption performance of PMAM-TTDD (a) of the mixture OG+CV (b) of the mixture OG+MeB (c) of the mixture AR+MeB; UV-Vis spectra (d) of the mixture OG+CV (e) of the mixture OG+MeB (f) of the mixture AR+MeB before and after adsorption of PMAM-TTDD; digital image of the selective adsorption performance of PMAM-APD (g) of the mixture OG+CV (h) of the mixture AR+CV (i) of the mixture AR+MeB; UV-Vis spectra (j) of the mixture OG+CV (k) of the mixture AR+CV (l) of the mixture AR+MeB before and after adsorption of PMAM-APD.

### 5.2.4 The effect of pH on the adsorption performance of the fibrous adsorbents

The surface charges of the fibrous adsorbents PMAM-TTDD and PMAM-APD can be significantly affected by the pH of the dye solutions. The reason for that were abundant amines, amides, ether (for PMAM-TTDD) and hydroxyl (for PMAM-APD) functional groups on the surface of the fibrous adsorbents. The following experiments were carried out to investigate these effects.

For PMAM-TTDD, 40 mL 1 mg/mL of MB solutions with different pH (3, 4, 6, 8, 9) were prepared. 10 mg of the adsorbents were dipped into each solution. After shaking at room

## RESULTS AND DISCUSSION

---

temperature for 4 h, the concentration of the dye solutions was measured by an UV-Vis spectrophotometer. For PMAM-APD, 10 mL 1 mg/mL of CV solutions with different pH (3, 4, 6, 8, 9) were prepared. The subsequent procedure was the same as for PMAM-TTDD. Considering that the highest adsorption capacity of PMAM-TTDD and PMAM-APD was observed for the anionic dye MB and the cationic dye CV, respectively, MB and CV were chosen as model dyes for these experiments and also for the following sections, 5.2.5 “Adsorption kinetics” and 5.2.6 “Adsorption isotherm”, to investigate the adsorption mechanisms.

The corresponding results are shown in Fig. 5-11. It can be seen that for PMAM-TTDD, the adsorption capacity increased significantly in the range from pH 3 to pH 4. The adsorption capacity reached its maximum at pH 4 and decreased with a further increase of pH. For PMAM-APD, the adsorption capacity increased with the increase of pH from 3 to 6. During the range from pH 3 to pH 4, a significant increase of the adsorption capacity was observed. At pH 6, the adsorption capacity reached its maximum. Then afterwards, a slight decrease of the adsorption capacity was observed with further increasing the pH.

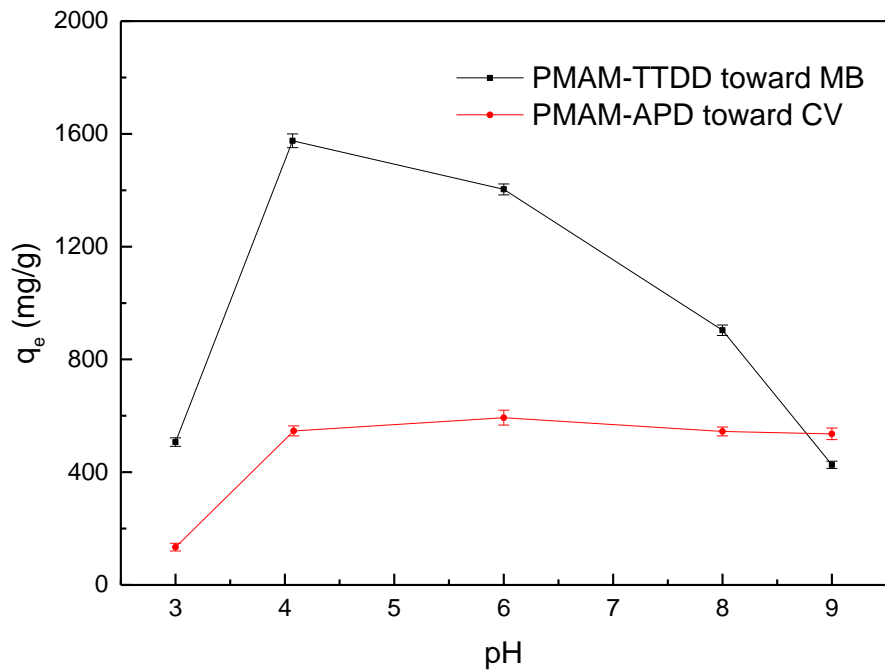


**Fig. 5-11** The effect of the solution pH on the adsorption capacity of the fibrous adsorbent PMAM-TTDD toward MB and of PMAM-APD toward CV.

### 5.2.5 Adsorption kinetics

The study of adsorption kinetics provides information on the adsorption rate and allows further exploration of the adsorption mechanism.<sup>111</sup> The corresponding experimental data was analyzed with the pseudo-first-order, pseudo-second-order, intra-particle and liquid film diffusion models. The detailed introduction of the models can be found in above section 5.1.3. The corresponding experimental data and fitting results are shown in Fig. 5-12 and Table 5-4.

## RESULTS AND DISCUSSION

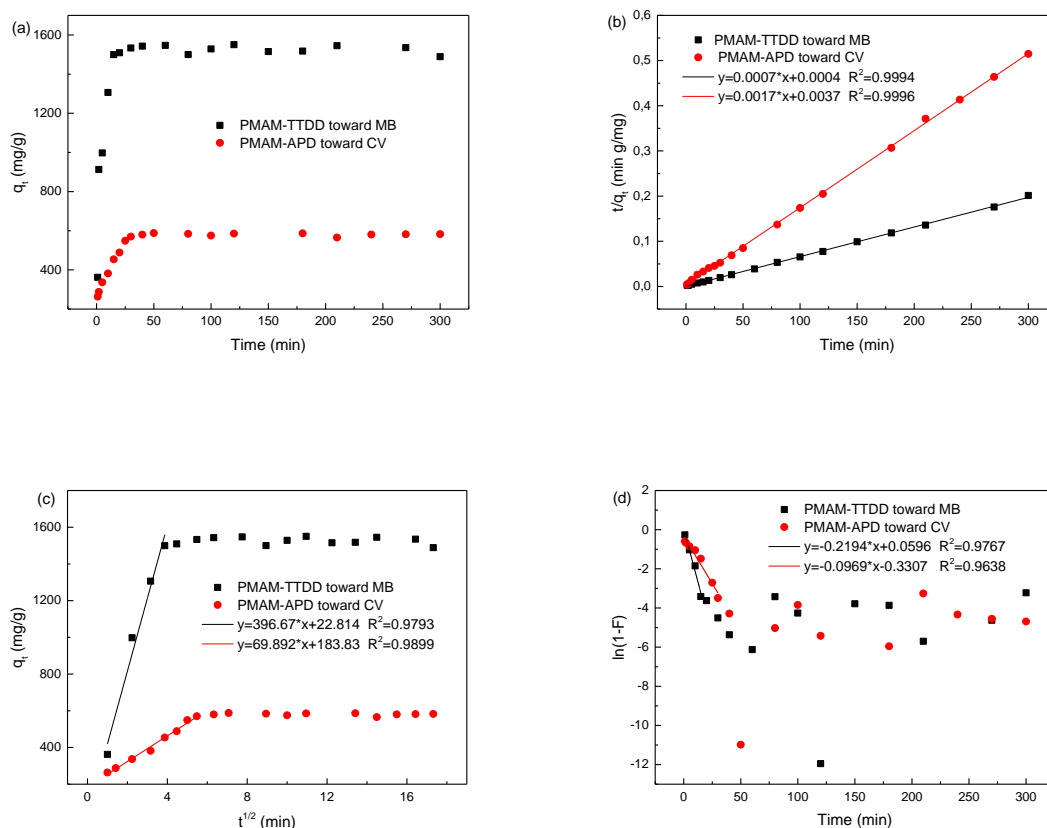


**Fig. 5-12** (a) Effect of contact time on MB adsorption by PMAM-TTDD and on CV adsorption by PMAM-APD. Linear fitting of (b) pseudo-second-order kinetics for the whole adsorption process, (c) Intra-particle diffusion before reaching equilibrium and (d) Liquid film diffusion kinetics before reaching equilibrium for adsorption of MB on PMAM-TTDD and CV on PMAM-APD.

From Fig. 5-12 (a) we can see that for PMAM-TTDD toward MB adsorption, the adsorption capacity increased fast and reached an equilibrium within 30 min. For PMAM-APD toward CV adsorption, the adsorption capacity increased relatively fast during the first 15 min, then slowed down and finally reached equilibrium after 40 min.

Fig. 5-12 (b) shows that the linear fitting plots agree with the pseudo-second-order kinetics for both PMAM-TTDD toward MB and PMAM-APD toward CV adsorption during the whole adsorption process. Moreover, in Table 5-4, the values of  $R^2$  of the pseudo-second-order kinetics were higher than 0.99 but of the pseudo-first-order kinetics they were lower

## RESULTS AND DISCUSSION

---

than 0.2. Additionally, the calculated  $q_e$  of both adsorbents of the pseudo-second-order kinetics corresponded well with the experimental  $q_e$ . These results indicate that the adsorption process of both PMAM-TTDD and PMAM-APD follows a pseudo-second-order kinetic model. This means that chemical adsorption or chemical adsorption involving Van-der-Waals interactions might take place between adsorbent and adsorbate.<sup>111</sup>

Fig. 5-12 (c) and (d) show the linear fitting of the experimental data before reaching equilibrium for adsorption of MB on PMAM-TTDD (within 15 min) and CV on PMAM-APD (within 30 min) using the intra-particle diffusion and liquid film diffusion kinetic models. The corresponding values of  $R^2$  in Table 5-4 are above 0.96, which indicates a good fitting. This means that during the adsorption process, the transfer of solute MB or CV was the result of the combination of surface adsorption and intra-fiber diffusion.<sup>112</sup> It can be seen in Fig. 5-12 (c) that the plots did not pass through the origin, meaning that the intra-fiber diffusion was not the rate-limiting step. Although the plots in Fig. 5-12 (d) did not exactly pass through the origin, the intercepts were small, indicating that surface adsorption might be the rate-limiting step during the adsorption process.

## RESULTS AND DISCUSSION

**Table 5-4** Adsorption kinetic parameters obtained from kinetic models fitting to the experimental data.

Adsorbents	$q_{e,exp}^a$ (mg/g)	Pseudo-first-order			Pseudo-second-order			Intra-particle diffusion			Liquid film diffusion	
		$k_1$ ( $\text{min}^{-1}$ )	$q_{e1}^b$ (mg/g)	$R^2$	$K_2$ (g/(mg min))	$q_{e2}^b$ (mg/g)	$R^2$	$K_p$ (mg/(g min))	$C$	$R^2$	$k_{fd}$	$R^2$
PMA M- TTDD	1550.38	-	-	0.1028	$1.23 \times 10^{-3}$	1428.57	0.9994	396.67	22.81	0.9793	0.2194	0.9767
PMA M- APD	588.15	-	-	0.1539	$7.81 \times 10^{-4}$	588.24	0.9996	69.89	183.83	0.9899	0.0969	0.9638

<sup>a</sup>  $q_{e,exp}$  is experimental values

<sup>b</sup>  $q_{e1}, q_{e2}$  are calculated values

### 5.2.6 Adsorption isotherms

The adsorption isotherms studies provide information about the reaction behavior between adsorbent and adsorbate. For PMAM-TTDD, batch adsorption isotherm experiments were recorded using 50 mL conical flasks containing 40 mL MB dyes with different concentrations (200, 400, 600, 800 and 1000 mg L<sup>-1</sup>) and 10 mg adsorbents. After shaking at 240 RPM at ambient temperature for 4 h (predetermined) equilibrium was reached. The concentration of dyes solution after adsorption was measured and the adsorption capacities of the adsorbents were calculated. For PMAM-APD, batch adsorption isotherm experiments were carried out in 20 mL vials containing 10 mL CV dyes with different concentrations (200, 400, 600, 800 and 1000 mg L<sup>-1</sup>) and 10 mg adsorbents. The subsequent procedure was the same as for PMAM-TTDD.

The corresponding experimental data were analyzed with the Langmuir, Freundlich and Dubinin–Radushkevich (D–R) isotherm models. The detailed introduction of these models can be found in the above section 5.1.4. The corresponding fitting results are shown in Table 5-5.

## RESULTS AND DISCUSSION

**Table 5-5** Adsorption isotherm parameters obtained from isotherm models fitting to the experimental data

	PMAM-TTDD	PMAM-APD
Langmuir		
$q_m$ (mg/g)	1566.67	-
$K_L$ (L/mg)	0.0490	-
$R_L$	0.0200	-
$R^2$	0.9996	0.8301
Freundlich		
$K_F$ (1/g)	772.63	0.0880
$1/n$	0.1136	1.5778
$R^2$	0.8852	0.9813
D-R		
$q_m$ (mg/g)	1542.56	732.16
$\beta$	239.93	3807.70
E (kJ/mol)	0.0460	0.0110
$R^2$	0.9755	0.9338

It can be seen in Table 5-5 that for the adsorption isotherm of PMAM-TTDD toward MB, the Langmuir model fitted the experimental data best considering the highest correlation coefficient  $R^2$  while the D-R model fitted second best. The Freundlich model did not fit the experimental data as  $R^2$  was lower than 0.9. The adsorption process followed the Langmuir model indicating the monolayer adsorption for MB on the fibrous adsorbent. In addition, the value of  $R_L < 1$  indicated that the adsorption process is favorable. For the D-R model, the calculated maximum adsorption capacity of 1542.56 mg/g corresponded well with the experimental data from the section 5.2.5 with a value of 1545 mg/g. And the value of E was lower than 8 kJ/mol, indicating that the adsorption process is driven by physisorption.

For the adsorption isotherm of PMAM-APD toward CV, the Freundlich model fitted the experimental data best and the D-R model fitted second best considering the values of the

## RESULTS AND DISCUSSION

---

correlation coefficient  $R^2$ . The Langmuir model did not fit the experimental data as  $R^2$  is lower than 0.84. The Freundlich isotherm describes the adsorption process taking place on a heterogeneous surface through a multilayer adsorption mechanism. It can be seen in Table 5-5 that  $1/n > 1$ , which indicates that the adsorption isotherm was undesirable. For the D-R model, the value of  $E$  was lower than 8 kJ/mol indicating that the adsorption process might be physisorption.

### 5.2.7 Investigation of the Mechanism

Various adsorption mechanisms were reported including electrostatic attractions, hydrogen bonding interaction, hydrophobic reaction,  $\pi$ - $\pi$  stacking interaction, rapid diffusion ion exchange, chemical surface complexation, Van-der-Waals forces, and Lewis acid-Lewis base interaction.<sup>140-143</sup>

The adsorption mechanism for PMAM-TTDD toward the adsorption of the anionic dye MB is similar to that of PMSAE-TTDD presented in the above section 5.1.7 as they occupy the same functional groups primary amine and ether groups. The difference is the addition of PMMA and the photo-crosslinker PABP which resulted in a decrease of the efficient functional groups. Therefore, the maximum adsorption capacity (1545 mg/g) is slightly lower as compared to the previous work (1652 mg/g). However, the advantages of adding PMMA and PABP far outweigh the disadvantages. Their addition has a twofold advantage. On the one hand, the adsorption equilibrium time significantly decreased from 90 min in the above chapter 5.1 to just 30 min in this study (Fig. 5-12 (a)). On the other hand, the addition of PMMA and PABP resulted in a higher diversity of the post-modification process. In this study it was for example possible to post-modify the fibrous membrane using APD in this study. Otherwise, the fibrous membrane would not be able to keep the perfect morphology of fibers after post-modification.

## RESULTS AND DISCUSSION

---

For PMAM-APD toward the adsorption of the cationic dye CV, abundant amides, hydroxyl, ester and carbonyl groups are on the surface of the fibrous adsorbent. Under acidic conditions, amides, ester and carbonyl groups are favorable for cationic dye adsorption due to the existence of the electron lone pair of oxygen atoms or nitrogen atoms. However, hydroxyl groups are easily protonised due to the existence of the electron lone pair of oxygen atoms which is adverse to the cationic dye adsorption. But with the increase of pH, the protonation decreases. This reduces the electrostatic repel, which in turn increases the adsorption capacity of cationic dye. This can well explain the increase of the adsorption capacity of the cationic dye CV with the increase of pH from 3 to 6 as shown in Fig. 5-11. Upon further increase of pH, the surface of the fibrous adsorbent is electronegative. The cationic dye can be adsorbed by electrostatic interaction with the adsorbent. However, the fact that the adsorption capacity of PMAM-APD towards CV is much lower than that of PMAM-TTDD towards MB might be due to the change of the morphology after post-modification. Fig. 5-8 (c) shows that the fibers are bent and have the preference to stick together, thus decreasing the porosity of the fibrous adsorbent. This caused a decrease of the specific surface area, which consequently resulted in a decrease of active adsorption sites. In addition, the surface of PMAM-APD is more hydrophilic than PMAM-TTDD because of the existence of hydroxyl groups. This could also be attributed to the lower adsorption capacity. As the adsorption mechanism of the fibrous adsorbents towards organic dyes is based on electrostatic interactions between the surface of the fibrous adsorbents and the organic dyes, the adsorption process is physisorption. This corresponds well with the result in above section 5.2.6 that the adsorption isotherm data fitted D-R model.

### 5.2.8 Conclusions

The addition of PMMA and PABP to the homogeneous fibrous membrane precursor PMSAE improves the diversity of the post-modification process and can therefore result in various functional fibrous adsorbents. The newly developed fibrous adsorbent PMAM-TTDD shows a high adsorption capacity of 1545 mg/g towards MB and a good selective adsorption capacity of anionic dyes from cationic dyes. PMAM-APD shows a good adsorption capacity of 577 mg/g towards CV and a good selective adsorption capacity of cationic dyes from anionic dyes. The adsorption mechanism of the fibrous adsorbents towards organic dyes is based on electrostatic interactions between the surface of the fibrous adsorbents and the organic dyes. Considering their simple and cost-efficient development process and their excellent performance, the fibrous adsorbents should be further investigated and have the promising potential for a versatile application in the field of water treatment.



### **5.3 A universal surface post-modification method based on active ester functional benzophenone**

In this section, I present a versatile post-functionalization method for surface modification that combines the advantages of an active ester and a photo-reactive group. Numerous studies have been published regarding the combination of active ester polymers with photo-reactive polymers, but to the best of our knowledge, combining a small molecule active ester with a photo-reactive group and the application of this compound for the modification of material surfaces has never been investigated. In this study, the active ester PFP is combined with the photo-reactive group benzophenone, resulting in benzoic acid, 4-benzoyl-,2,3,4,5,6-pentafluorophenyl ester (BBPE). Its application on various substrates especially on inert polyolefins, creating chemical patterns in different scales and the changing of surface properties are investigated. The unique advantage of the small molecule modification compound is explored.

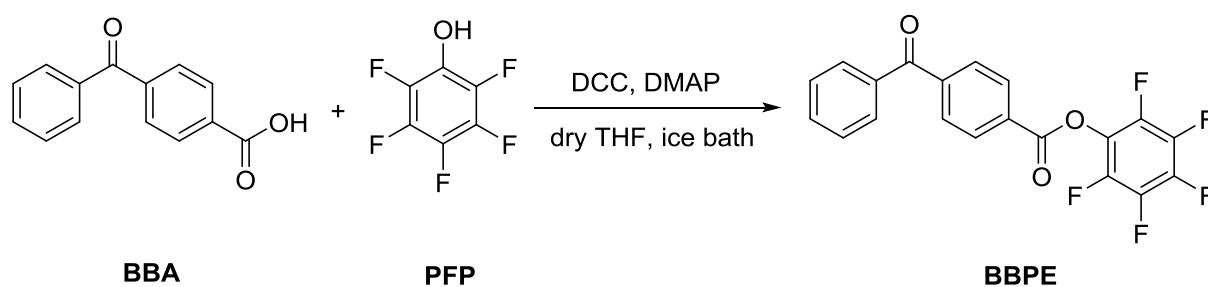
#### **5.3.1 Synthesis and characterization of active ester BBPE**

BBPE was synthesized for the first time via Steglich esterification reaction. Vooturi and coworkers reported the synthesis of a similar compound using pentafluorophenyl trifluoroacetate as one of the reactants.<sup>144</sup> In this study, PFP is used instead. This method has two advantages: 1) the reactant PFP is much cheaper (as provided by Sigma-Aldrich, the price of pentafluorophenyl trifluoroacetate is 59.90 € per 5 g, that of PFP is 25.80 € per 5 g); 2) the reaction conditions are mild.

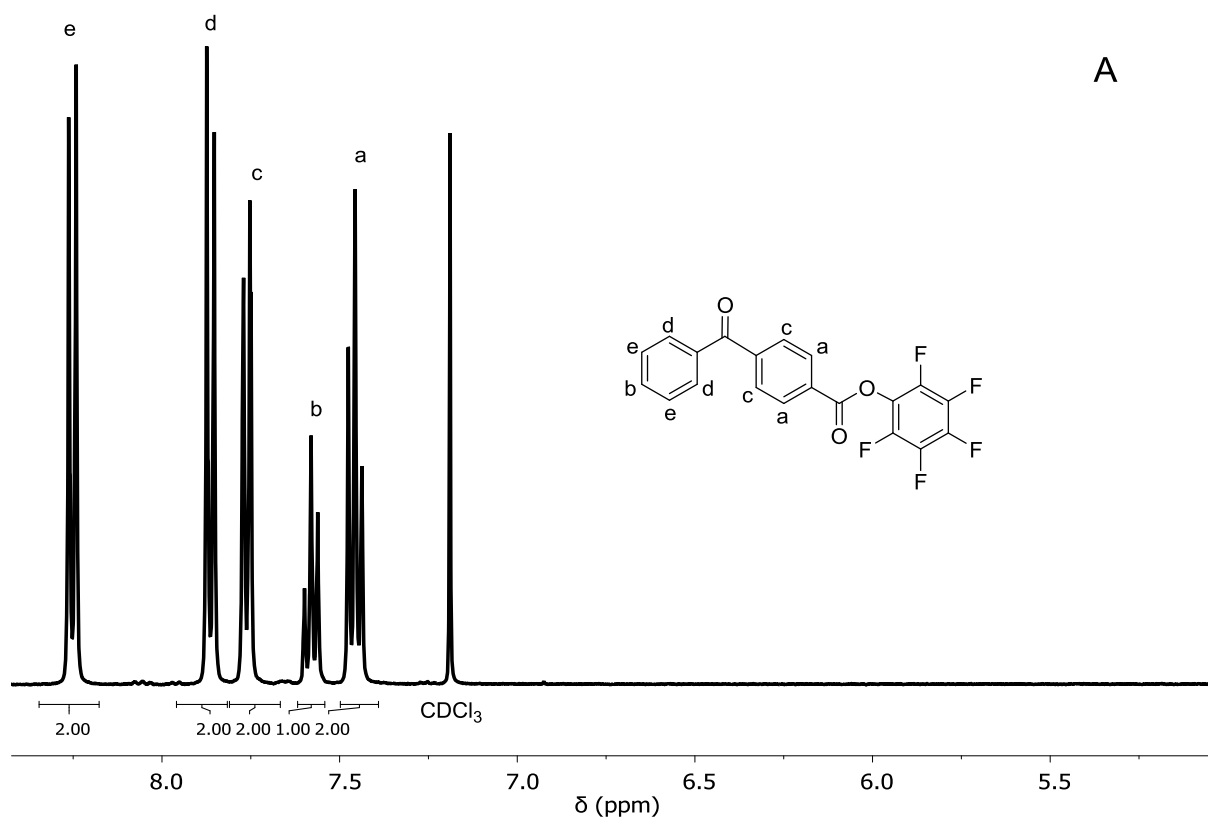
The synthesis is shown in Scheme 5-2. The detailed synthesis procedure can be found in Chapter 7 experimental part. NMR and FTIR spectra were used to confirm the successful synthesis of BBPE and the characterization result is shown in Fig. 5-13. It can be seen in Fig. 5-13 (A) that the <sup>1</sup>H NMR spectra of BBPE correspond well with the molecule structure. Fig.

## RESULTS AND DISCUSSION

5-13 (B) shows the FTIR results. The bands at  $1757\text{ cm}^{-1}$  and  $1728\text{ cm}^{-1}$  correspond to the C=O stretch of ester. The band at  $1659\text{ cm}^{-1}$  corresponds to the C=O stretch of benzophenone group. The band at  $1515\text{ cm}^{-1}$  corresponds to the benzene ring of pentafluorophenyl group. The  $^{13}\text{C}$  NMR and  $^{19}\text{F}$  NMR spectra of BBPE can be found in the supporting information in Chapter 9.



**Scheme 5-2** Synthesis of active ester BBPE via the Steglich esterification reaction.



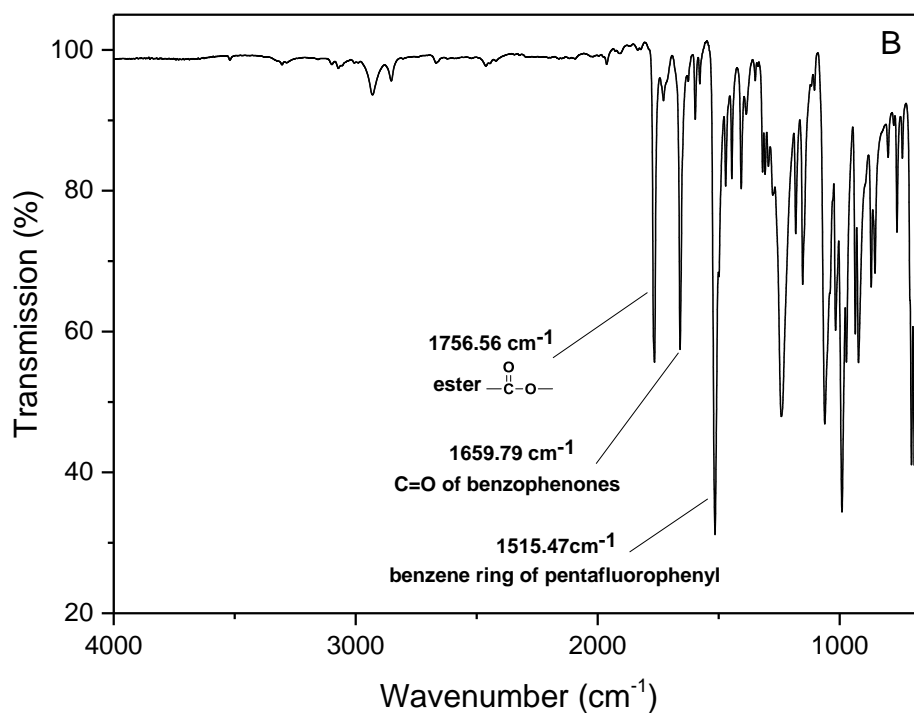
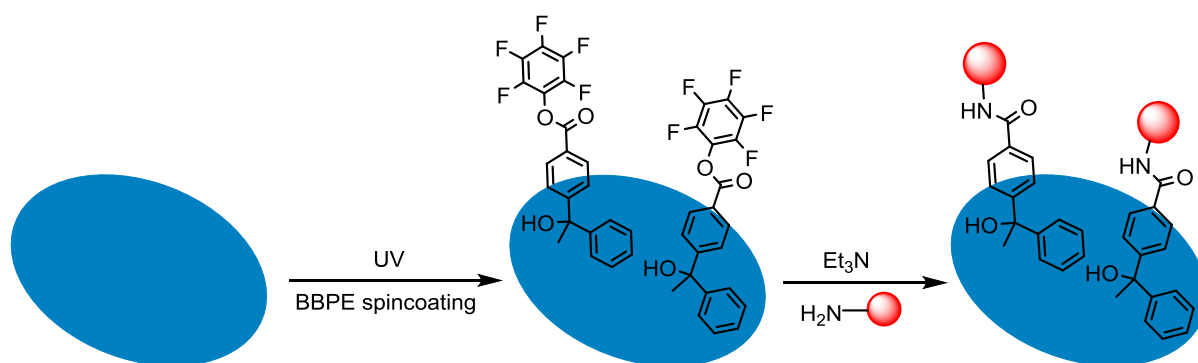


Fig. 5-13 (A) <sup>1</sup>H NMR spectra of BBPE in CDCl<sub>3</sub>. (B) IR spectra of BBPE.

### 5.3.2 Application of this surface modification method

The modification procedure of substrates with the active ester BBPE is shown in Scheme 5-3. The active esters BBPE were dissolved in DCM and covered on a substrate by spin coating (2000 r/min). After ultraviolet (UV) irradiation (lamp 18 W, 320-420 nm), an  $n-\pi^*$  or  $\pi-\pi^*$  transition within benzophenone groups would take place to form a biradical.<sup>145</sup> Subsequently, the biradical would react with nearby aliphatic CH groups to form a C-C bond through a H-abstraction/recombination mechanism.<sup>145</sup> Thus, the coating of the active ester BBPE was attached to the substrate. The unattached active esters could be washed away with DCM. Afterwards, desired functional groups could be attached through further surface-analogous reaction in simple and mild reaction.



**Scheme 5-3** Illustration of modification procedure of organic surfaces with the active ester BBPE.

### 5.3.2.1 Modification of chemically inert polyolefins surfaces

Polyolefins are known for their outstanding chemical resistance and broad-ranging mechanical properties. They have various applications including food packaging, rubbish disposal bags, ultra-high strength fibers and automobile bumpers.<sup>146</sup> However, containing only  $sp^3$  hybridized carbons in their structure, they are hard to be functionalized. Thus, chemical conversion of these plastics into value-added materials is severely limited.<sup>146</sup> Nevertheless, the surface modification method in this work is an efficient tool to modify chemically inert polyolefins.

Polyethylene (PE) and polypropylene (PP) are the most familiar and commercially produced polyolefins.<sup>146</sup> In this work, PE and PP films from Nowofol and a porous PP membrane lithium battery separator are modified. Detailed information on these three substrates is shown in Table 5-6. For the experiment they are cut into circle samples with a diameter of 16 mm.

## RESULTS AND DISCUSSION

**Table 5-6** Substrates used for modification with the active ester BBPE.

Name	Thickness ( $\mu\text{m}$ )	Porosity (%)	Company
Nowocast HD PE	100	-	Nowofol <sup>®</sup> Kunststoffprodukte GmbH & Co. KG
Nowocast HM PP	100	-	Nowofol <sup>®</sup> Kunststoffprodukte GmbH & Co. KG
Celgard <sup>®</sup> 2400 lithium battery separator	25	41	Celgard

At first, these three substrates were grafted with the active esters BBPE. As these three substrates are hydrophobic, in the next post-modification step, the hydrophilic chemical ethanolamine (ETA) was used to check the change of the wetting property of the surfaces. FTIR spectroscopy and contact angle (CA) measurements were performed to confirm the success of these two modification steps. The FTIR results are shown in Fig. 5-14. It can be seen in Fig. 5-14 (a)-(c) that after the first modification step, there is an appearance of the characteristic bands at  $1765.10\text{ cm}^{-1}$  (corresponding to the C=O stretch of pentafluorophenyl ester) and at  $1521.34\text{ cm}^{-1}$  (corresponding to the C=C resonance vibrations in the aromatic ring of pentafluorophenyl). This confirms the successful grafting of the active ester BBPE coating to the three substrates. It is obvious that the characteristic bands in Fig. 5-14 (b) and (c) are stronger than those in Fig. 5-14 (a). This could be explained by the more active tertiary C-H bonds (*i.e.*, lower bond strength) of PP as opposed to the secondary C-H bonds of PE,<sup>146</sup> with the first ones being more favorable for the hydrogen abstraction by benzophenone radicals. It can be seen in Fig.5-14 (a)-(c) that after the second modification step with ETA, the characteristic bands at  $1765.10\text{ cm}^{-1}$  and at  $1521.34\text{ cm}^{-1}$  disappear and the new bands at  $1636.11\text{ cm}^{-1}$  (C=O stretching) and at  $1550.05\text{ cm}^{-1}$  (C-N bending) appear, indicating the successful post-modification of the three substrates with ETA via aminolysis.

## RESULTS AND DISCUSSION

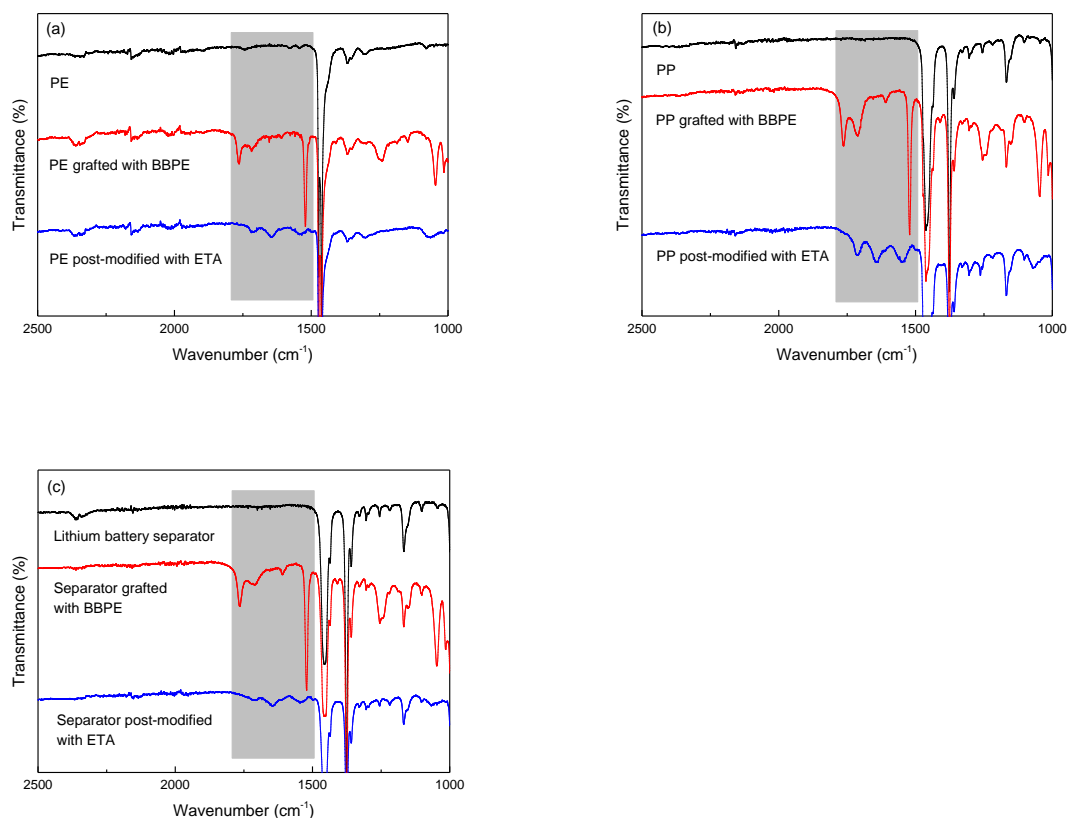


**Fig. 5-14** IR spectra of different substrates, after being grafted with BBPE and after being further post-modified with ETA. (a) PE (b) PP (c) Lithium battery separator.

Static and dynamic CA of PE and PP were measured, after being grafted with the active esters BBPE and after being further post-modified with ETA. The results are shown in Table 5-7. It can be observed that the static contact angles of both PE and PP decreased after the two-step modification. Especially after being post-modified with ETA, the hydrophobic surfaces became hydrophilic. For the dynamic CA, the CA hysteresis (the difference between the advancing angle and the receding angle) increased significantly after the modification, indicating an increase of the surface roughness. Based on Wenzel's hydrophobicity mode, an increase of the surface roughness increases the contact interface area, resulting in an increase of the CA hysteresis.<sup>147, 148</sup>

## RESULTS AND DISCUSSION

**Table 5-7** Static, advancing and receding CA of PE and PP, after being grafted with BBPE and after being further post-modified with ETA.

	Static CA (°)	Advancing CA (°)	Receding CA (°)	CA hysteresis (°)
PE	93.1±0.2	105.0±0.5	73.1±1.3	31.9
PE grafted with BBPE	81.5±0.3	85.5±1.8	21.1±2.5	64.4
PE post-modified with ETA	66.7±2.0	76.2±1.5	12.4±2.1	63.8
PP	101.4±0.8	104.7±1.0	75.1±1.5	29.6
PP grafted with BBPE	87.7±1.0	101.3±2.3	29.0±1.2	72.3
PP post-modified with ETA	73.4±1.3	76.7±2.0	14.5±0.9	62.2

The morphology of the lithium battery separator before and after each modification step is recorded by SEM. As shown in Fig. 5-15, no obvious change is observed of the morphology and porosity, indicating that the property of the separator can be changed with no effect on the morphology due to the small size of the active ester. This modification method provides a new way for battery separator modification. Compared to the traditional polymer grafting post-modification method, this method has a lower probability of a porosity block.

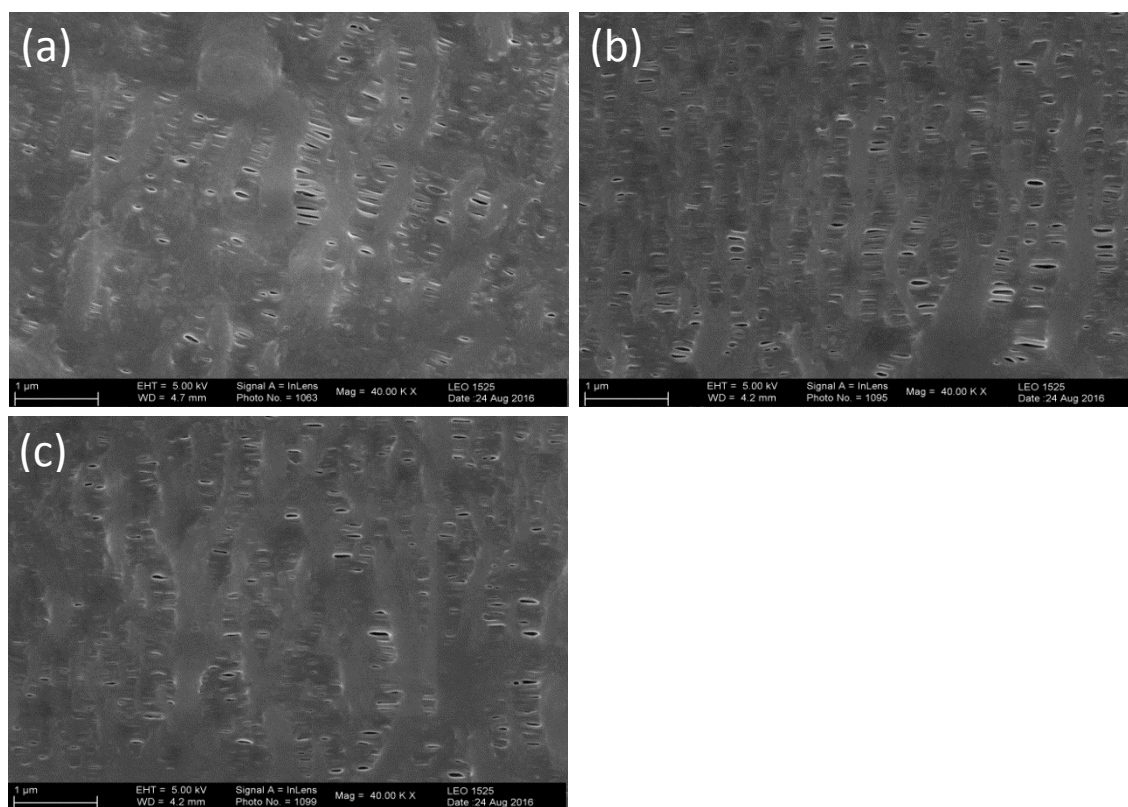


**Fig. 5-15** SEM images of (a) original lithium battery separator (b) separator being grafted with BBPE (c) separator being further post-modified with ETA.

### 5.3.2.2 Control of grafting density

The graft density of active esters BBPE on the substrates can be controlled by the coating times. The corresponding results are shown in Fig. 5-16. A PP film was chosen as the model substrate as it is much easier to be post-modified compared to PE (see the above section 5.3.2.1). IR spectra were recorded as the function of coating times. It can be seen clearly in Fig. 5-16 (a) that the characteristic bands of active ester BBPE at  $1765.10\text{ cm}^{-1}$  (corresponding to the C=O stretch of pentafluorophenyl ester) and  $1521.34\text{ cm}^{-1}$  (corresponding to the C=C resonance vibrations in the aromatic ring of pentafluorophenyl) are increasing dramatically with the increase of the coating times. The intensity of PFP groups of BBPE from IR spectra (correspond to  $1521.34\text{ cm}^{-1}$ ) is plotted as the function of BBPE coating times and is shown in Fig. 5-16 (b). It can be seen that the intensity of PFP groups is

## RESULTS AND DISCUSSION

---

increasing dramatically with the increase of the coating times. After coating 4 times, the intensity increased more than 5 times, indicating that the graft density of active esters BBPE on the substrates can be efficiently controlled by the coating times. After coating 4 times, the second post-modification with ETA was carried out. It can be seen in Fig. 5-16 (a) that the static CA decreased from  $101.4^\circ$  of the original PP film to  $25.3^\circ$  of the post-modified PP film, indicating that the surface changed from hydrophobic to hydrophilic. The surface roughness of the original PP film, the PP film after coating four times with active ester BBPE and the PP film further post-modified with ETA were recorded with atomic force microscopy (AFM) and the root mean square (RMS) roughness was calculated. It can be seen in Fig. 5-16 (c) that the RMS roughness increased from 55 nm of the original PP film to 82 nm after coating 4 times with the active ester BBPE. And a slight decrease to 77 nm after being post-modified with ETA was observed. This result is consistent with the CA hysteresis result in the above section 5.3.2.1 which showed that the CA hysteresis increased significantly after grafting with active ester BBPE, followed by a slight decrease after being post-modified with ETA. The graft density of active ester BBPE on the PP film after coating 4 times is calculated. The weight of the PP film before and after coating 4 times was recorded. The graft density is  $0.00597 \text{ mg/mm}^2$ , calculated by dividing the weight difference by the PP film area.

## RESULTS AND DISCUSSION

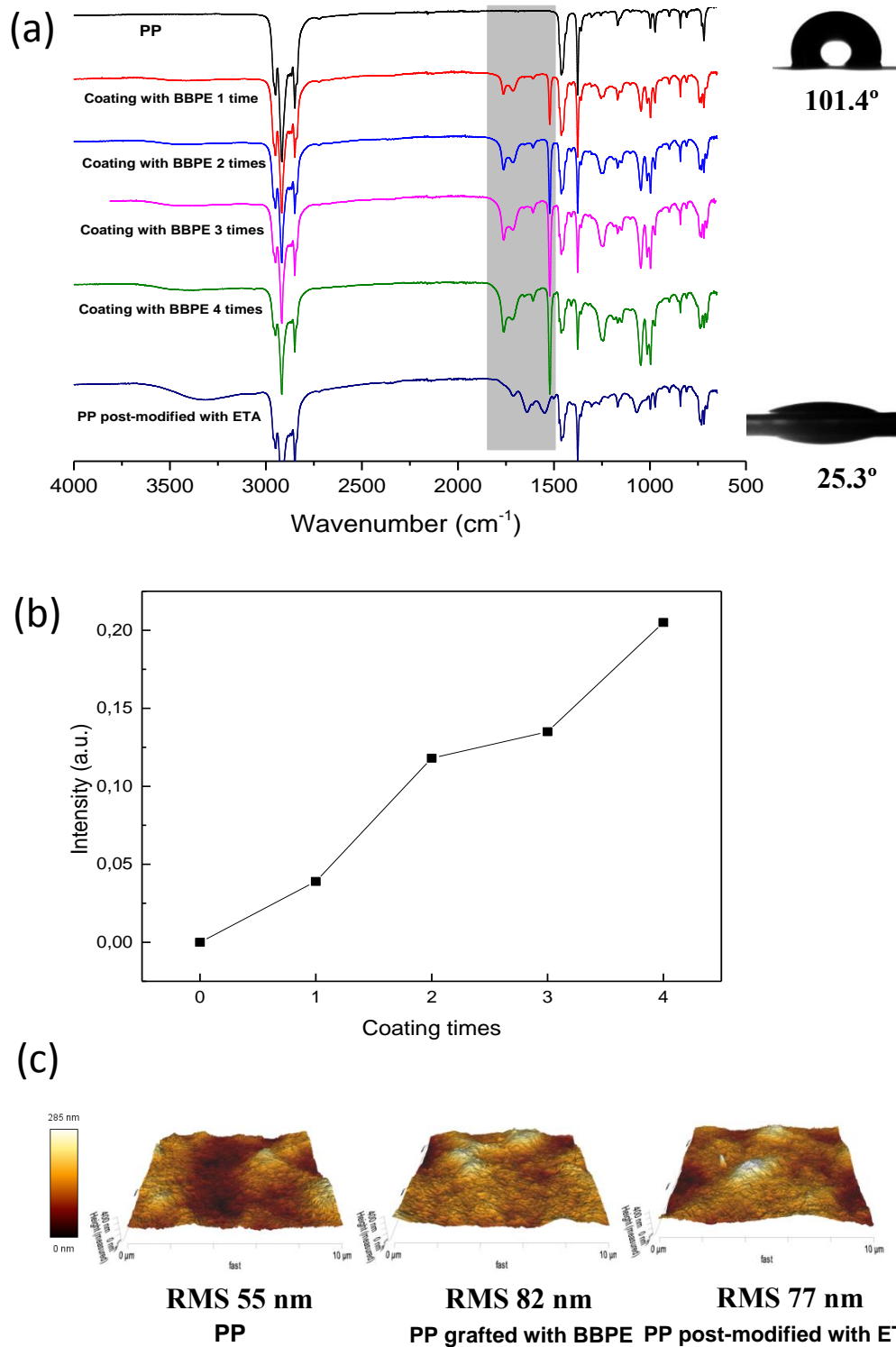
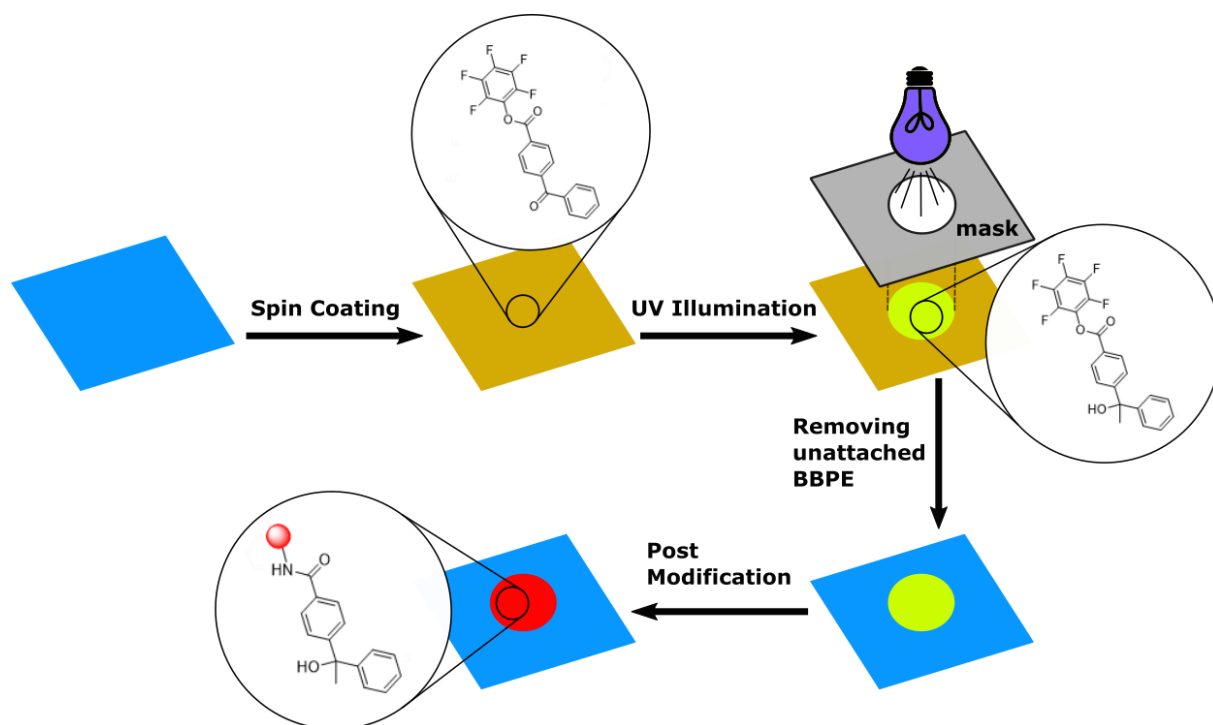


**Fig. 5-16** (a) IR spectra of PP film as the function of coating times, the change of static CA. (b) Intensity of PFP groups of BBPE from IR spectra as the function of BBPE coating times. (c) AFM images from 10 x 10  $\mu\text{m}^2$  surface sections and the measured surface roughness of original PP film, PP film being grafted with BBPE and PP film being post-modified with ETA.

## RESULTS AND DISCUSSION

### 5.3.2.3 Surface chemical patterns generation using UV-lithography

This surface post-modification method can easily fabricate patterns of various kinds and scales on the substrate surface through a simple control of the UV-irradiation area by using a photomask. The illustration of this procedure is shown in Scheme 5-4. The active esters BBPE were covered on the PP substrate homogeneously by spin coating. The patterned surface can be obtained by masking the UV-irradiation. The non-irradiated active esters can be washed away with DCM. After being further post-modified with the fluorescent dye NBD-ethylenediamine, the surface patterns can be observed under a UV-lamp (large-scale pattern) or by fluorescence optical microscopy (microscale pattern). To observe the patterns clearly, the excitation and emission spectra of the fluorescent dye NBD-ethylenediamine were measured and the result is shown in Fig. 5-17.



**Scheme 5-4** Illustration of surface chemical pattern procedure.

## RESULTS AND DISCUSSION

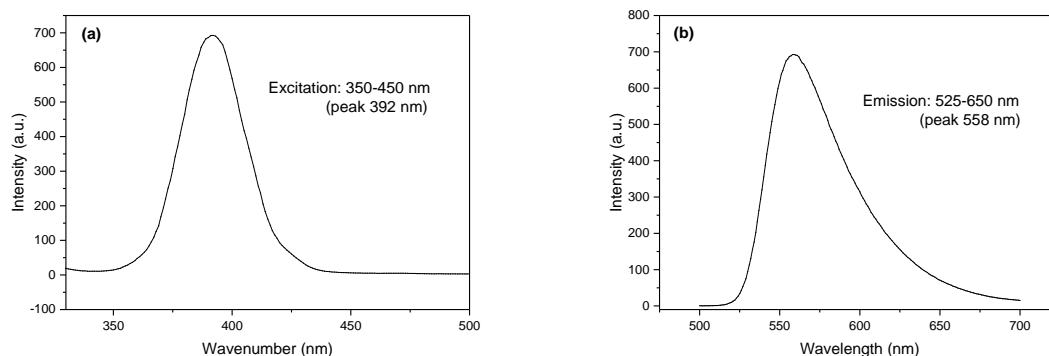


**Fig. 5-17** Fluorescence spectra of NBD-ethylenediamine (ethanol as solvent) (a) Excitation spectra. (b) Emission spectra.

This surface post-modification method can produce patterns on a large-scale surface. Fig. 5-18 (a) and (b) show two large-scale patterns with the shape of a circle and a cat. And Fig. 5-18 (c) shows a more complicated pattern of the logo of Karlsruhe Institute of Technology (KIT). The photomasks used to produce the patterns were aluminium films with the desired patterns, as they are able to stop UV-light from passing through the covered area, thus producing the shown patterns. In addition to large-scale patterns, this method is able to fabricate patterns in microscale as well. Miniaturizing patterns down to microscale is of vital importance. For example, in the field of biology, it could improve the sensitivity in biological detection or the biological diagnosis efficiency to a large extent.<sup>149-151</sup> In this study, to get a microscale pattern, we just needed to change the photomask to a micromachined one. Fig. 5-18 (d) shows a microscale pattern of University of Hamburg logo (UHH).

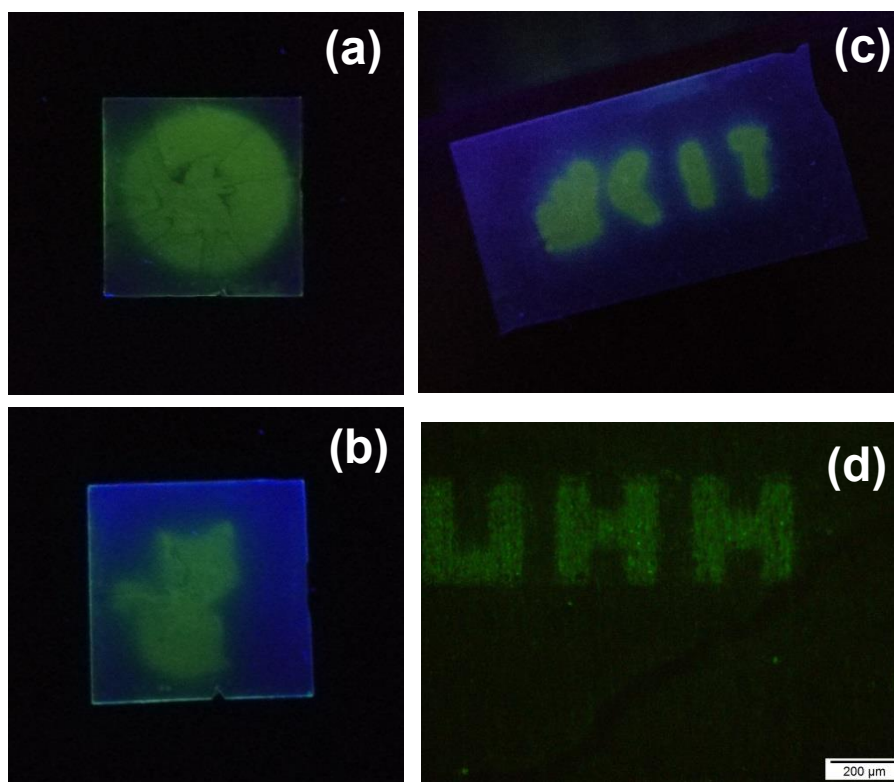


**Fig. 5-18** Fluorescence image of patterned PP film surfaces (a) Patterned circle, PP film: 2 cm x 2 cm. (b) Patterned cat, PP film: 2 cm x 2 cm. (c) Patterned “KIT”-logo, PP film: 2.5 cm x 5 cm. (d) Patterned “UHH”-logo in microscale.

#### 5.3.2.4 Other applications

This modification method can also be used on other materials such as plant leaves. As shown in Fig. 5-19, the wetting change after each step can be clearly observed. The static CA of the original leaf is  $114.1^\circ$ . After grafting with active ester BBPE, it decreased to  $77.8^\circ$ . It was further reduced to  $35.2^\circ$  after post-modifying with ETA. The leaf surface property successfully changed from hydrophobic to hydrophilic with our surface post-modification method.

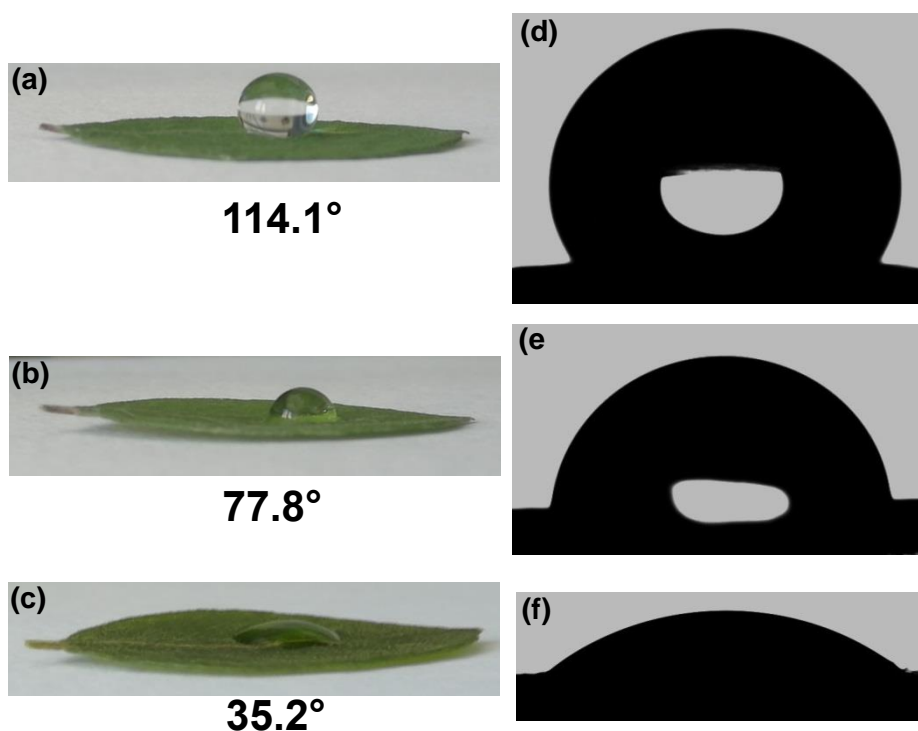


**Fig. 5-19** Optical photographs of water droplets on a leaf (a) original (b) after being grafted with active ester BBPE (c) after being post-modified with ETA. Static CA images of water droplets on a leaf (d) original (e) after being grafted with active ester BBPE (f) after being post-modified with ETA.

With this surface modification method, a chemical hydrophilic channel was obtained on the hydrophobic PP film by simply choosing a different mask than before. As shown in Fig. 5-20 (a) and (b), the PP film surface is hydrophobic, it cannot get wet when being emerged in water. However, after modification, that is to say, after being firstly grafted with active esters BBPE and subsequently post-modified with ETA, a slightly visible “人”-shaped channel appeared, as shown in Fig.5-20 (c). After being pulled out from water, a hydrophilic channel “人” was clearly visible on the hydrophobic surface as shown in Fig. 5-20 (d).

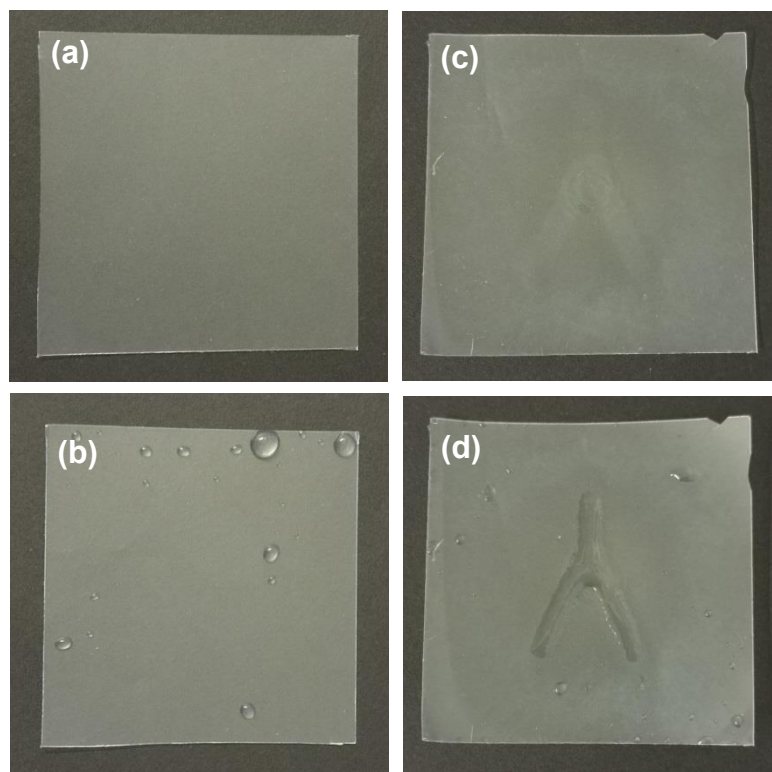


**Fig. 5-20** (a) Original PP film. (b) Original PP film after pulling out from water. (c) PP film after surface modification. (d) PP film after surface modification after pulling out from water.

### 5.3.3 Conclusions

This work provides a new and cost-efficient way to synthesize the active ester BBPE, thus resulting in a promising surface post-modification method. It provides easy and simple access to chemically attaching active coatings on any surface that contains aliphatic C-H bonds. Desired functional groups could be easily attached through a further surface-analogous reaction as PFP-based ester BBPE features an excellent reactivity towards amines under mild reaction conditions. This method is efficient to modify chemically inert polyolefins. Various chemical structures could be patterned on substrates by simply changing different photomasks to control the UV-irradiation area. The small molecule is the unique advantage of this surface modification method, which enables it to become potentially interesting for modification of porous materials, for example battery separators or filtration membranes, without changing the porosity property. Further work is necessary to enable its application in these corresponding fields.

### 6. Conclusions and Outlook

In this thesis, versatile, simple and cost-efficient modification methods for micro- and macroscopic polymeric material surfaces were developed and their corresponding applications were systematically investigated. During the development process, the advantages of active esters, electro-spun fibers, UV-irradiation and post-modification were employed. For the first time, electro-spinning of polymeric active esters into fibrous membranes and their application in the field of water purification were studied. A small molecule modification compound which combines an active ester with a photo-reactive group was synthesized in a cost-efficient way and its application was for the first time investigated.

In Chapter 5.1, the polymeric active ester PMSAE was for the first time electrospun to fibrous membranes. After post-modification via aminolysis under simple and mild reaction conditions, two fibrous adsorbents PMSAE-TTDD and PMSAE-TAD were obtained. They were used for organic dyes water purification and exhibited excellent performance. They showed an extremely high adsorption capacity towards the anionic dye MB (PMSAE-TTDD: 1652 mg/g; PMSAE-TAD: 1585 mg/g), a good selective adsorption capacity of anionic dyes from cationic dyes and they can be recycled at least 5 times. The adsorption mechanism of the fibrous adsorbents towards organic dyes is based on electrostatic interactions between the surface of fibrous adsorbents and organic dyes.

Chapter 5.2 is built on the work in Chapter 5.1, with the diversity of the post-modification process being improved by adding PMMA and the photo-crosslinker PABP to the homogeneous fibrous membrane precursor PMSAE for electrospinning. As a result, various functional fibrous adsorbents were obtained. The newly developed fibrous adsorbent PMAM-TTDD shows a high adsorption capacity of 1545 mg/g towards the anionic dye MB and a good selective adsorption capacity of anionic dyes from cationic dyes. PMAM-APD shows a good adsorption capacity of 577 mg/g towards the cationic dye CV and a good selective

## CONCLUSIONS AND OUTLOOK

---

adsorption capacity of cationic dyes from anionic dyes. The adsorption mechanism of the fibrous adsorbents towards organic dyes is based on electrostatic interactions between the surface of the fibrous adsorbents and the organic dyes.

Considering their simple and cost-efficient development process and their excellent performance, the fibrous materials should be further investigated and have promising potential for various applications in the field of water treatment. In this thesis, only the static adsorption performances of the fibrous materials were studied, but the dynamic adsorption performances can also be investigated to provide more information on their potential application in the industry. As the fibrous materials are porous, free-standing membranes, they have the potential to be used as filtration membranes. Considering that the fibrous materials showed an extremely high adsorption capacity towards anionic dyes, we anticipate that they exhibit an outstanding adsorption performance for other anionic pollutants that typically exist in contaminated water too, such as phosphates ( $\text{PO}_4^{3-}$ ), nitrates ( $\text{NO}_3^-$ ) or cyanide anions ( $\text{CN}^-$ ).

In Chapter 5.3, the small molecule compound BBPE, which combines an active ester with a photo-reactive group was synthesized in a cost-efficient way, resulting in a promising surface post-modification method. This method features the following advantages: 1) it provides an easy and simple way to chemically attach active coatings on any surface that contains aliphatic C-H bonds; desired functional groups could be easily attached through a further surface-analogous reaction; 2) the operation is simple, requires no catalyst addition, works under mild reaction conditions; 3) the scale and shape of the resulting chemical patterns can be adjusted simply by changing the photomasks used during the UV-irradiation; 4) it can also be applied to surfaces of natural substrates such as plant leaves. 5) The small molecule is the unique advantage of this surface modification method, which is potentially interesting for the modification of porous materials, such as battery separators or filtration

## CONCLUSIONS AND OUTLOOK

---

membranes, as it doesn't change the porosity degree. Further work is necessary to enable its application in these corresponding fields.



## 7. Experimental Part

### 7.1 Materials

All chemicals were commercially available and used as received unless otherwise stated. 4,7,10-trioxa-1,13-tridecanediamine (TTDD), 3,6,9-triazaundecan-1,11-diamin (TAD), triethylamine (Et<sub>3</sub>N), 4-hydroxybenzophenone, (±)-3-amino-1,2-propanediol (APD), poly(methyl methacrylate) (PMMA) ( $M_w = 350\ 000$ ), ethanolamine (ETA), 4-(dimethylamino)pyridine (DMAP), methyl blue, 1,4-dioxane, pentafluorophenol and azobisisobutyronitrile (AIBN) were obtained from Sigma Aldrich. AIBN was recrystallized from methanol prior to use. Acryloyl chloride (98%), *N,N'*-Dicyclohexylcarbodiimide (99%) (DCC), dichloromethane, tetrahydrofuran, dimethylformamide and 4-benzoylbenzoic acid (99%) (BBA) were purchased from Acros Organics. Methyl salicylate was supplied by Alfa Aesar. Azorubine was obtained from Carl Roth. Methylene blue, crystal violet, orange G, sodium hydroxide and hydrochloric acid were provided by Merck. Methanol, hexane, ethyl acetate, ethanol and acetone were purchased from VWR. NBD-ethylenediamine was supplied by our colleague Hui Zhao.<sup>15</sup>

### 7.2 Characterization

The morphology of the fibers before and after adsorption was monitored by scanning electron microscopy (SEM, Zeiss EVO-MA 10 microscope). The FTIR was obtained using the ATR unit on a Thermo Scientific Nicolet IS10 FTIR spectrometer. The concentrations of the dye solutions were calibrated and determined by a Jasco V-630 UV/Vis spectrophotometer. <sup>1</sup>H NMR spectra were examined by Bruker Advance 400-500 MHZ equipment. <sup>13</sup>C NMR and <sup>19</sup>F NMR spectra were examined by Bruker Advance III HD 600 MHZ equipment. Molecular weight and dispersity were measured via gel permeation chromatography (GPC) in tetrahydrofuran with a flow rate of 1.0 mL min<sup>-1</sup>. The change of the

## EXPERIMENTAL PART

---

wetting properties of substrates was recorded via contact angle measurements which were performed with a DataPhysics OCA 20 apparatus. The roughness of the substrates before and after the modification was measured by atomic force microscopy (AFM) on a JPK Nanowizard I instrument (intermittant contact mode, standard Silicon AFM tip, radius 10 nm, resonance frequency 300 kHz, force constant 40 N/m). The fluorescence spectra of the fluorescent dye were measured with an Agilent Cary Eclipse Fluorescence spectrophotometer with horizontal beam geometry and a Xe pulse lamp and a Czerny-Turner 0.125 m monochromator. The fluorescent patterns were observed with a fluorescence microscope (Olympus BX51 with fluorescence illuminator, X-Cite series 120 Q - EXFO).

### 7.3 Synthesis

#### Synthesis of the monomer MSAE

MSAE was synthesized according to the literature<sup>1, 110</sup> with some modification which significantly increased the yield from 77% to 92%. The details were as follows: Methyl salicylate (10.3 mL, 80 mM), Et<sub>3</sub>N (13.4 mL, 96 mM) and 45 mL dichloromethane were added to a 250 mL round-bottom flask. The resulting mixture was kept stirring for 15 min in an ice bath. Acryloyl chloride (8 mL, 96 mM) was dripped into the flask. The reaction mixture was kept stirring in the ice bath for 3 h. After the reaction, the mixture was filtrated to remove the precipitated triethylammonium salt. Then the filtrate was washed 3 times with water (40 mL) and dried over sodium sulfate. The solvent was removed by rotary evaporation. The product was isolated by silica gel column with hexane/dichloromethane (2:8 by volume) as eluent. Finally, 15.18 g (92%) MSAE was obtained as yellow oil and subsequently characterized.

<sup>1</sup>H NMR (400 MHz, CD<sub>2</sub>Cl<sub>2</sub>) δ 3.72 (s, 3H), 5.96 (dd, 1H, J = 1.3/10.4 Hz), 6.28 (dd, 1H, J = 10.4/17.3 Hz), 6.50 (dd, 1H, J = 1.3/17.3 Hz), 7.07 (dd, 1H, J = 1.2/8.1 Hz), 7.27 (td, 1H, J=1.2/7.7 Hz), 7.51 (ddd, 1H, J=1.7/7.4/8.1 Hz), 7.92 (dd, 1H, J = 1.8/7.8 Hz); <sup>13</sup>C NMR (400

## EXPERIMENTAL PART

---

MHz, CDCl<sub>3</sub>)  $\delta$  52.24; 123.33; 123.78; 126.10; 127.69; 131.83; 132.79; 133.85; 150.39; 164.62; 164.97; IR (ATR mode) 2953, 1754 (C=O methyl salicylate ester), 1722 (C=O methyl ester), 1635, 1606, 1486, 1454, 1434, 1403, 1297, 1257, 1202, 1145, 1081, 754 cm<sup>-1</sup>; ESI-MS: Cal. [M]<sup>+</sup>: 206.0579; found: [M+Na]<sup>+</sup>: 229.0487, [2M+Na]<sup>+</sup>: 435.1068.

### Synthesis of PMSAE

PMSAE was synthesized by free radical polymerization. The detailed procedure was according to the literature<sup>1</sup> but with a higher yield of 96%. <sup>1</sup>H NMR (400 MHz, CD<sub>2</sub>Cl<sub>2</sub>)  $\delta$  2.32 (t, 2H), 3.19 (s, 1H), 3.55 (m, 3H), 6.66-7.33 (m, 3H), 7.51-8.05 (m, 1H); IR (ATR mode) 2951, 1754 (C=O methyl salicylate ester), 1719 (C=O methyl ester), 1606, 1487, 1450, 1434, 1297, 1262, 1199, 1127, 1080, 749 cm<sup>-1</sup>; GPC (THF): M<sub>n</sub> = 3.80\*10<sup>4</sup> g/mol, M<sub>w</sub> = 1.32\*10<sup>5</sup> g/mol, M<sub>w</sub>/M<sub>n</sub> = 3.47.

### Synthesis of the monomer ABP

ABP was prepared according to the literature<sup>152</sup>. <sup>1</sup>H NMR spectra were measured by a Bruker 400-500 MHz Fourier NMR spectrometer to confirm the structure of the monomer ABP. <sup>1</sup>H NMR (500 MHz, CDCl<sub>3</sub>)  $\delta$  6.00 (dd, 1H, J=1.2/10.5 Hz), 6.28 (dd, 1H, J=10.4/17.3 Hz), 6.58 (dd, 1H, J=1.2/17.4 Hz), 7.17-7.24 (m, 2H), 7.42 (dd, 2H, J=7.0/8.5 Hz), 7.49-7.56 (m, 1H), 7.70-7.77 (m, 2H), 7.77-7.84 (m, 2H).

### Synthesis of PABP

The detailed procedure of free radical polymerization of PABP was as follows: ABP (10g, 100 equiv), AIBN (1 equiv) and 30 mL of 1,4-dioxane were added to a 100 mL round-bottom flask. The mixture was degassed under argon at room temperature for 30 min. Afterwards, the reaction mixture was kept stirring in a preheated oil bath at 70 °C for 19 h. The polymerization was terminated by exposure to air. Then, the mixture was diluted with THF and purified by precipitating into hexane. The reprecipitation was repeated 3 times. After

## EXPERIMENTAL PART

---

drying in a vacuum oven at 40 °C for 48 h, a white powder polymer was obtained with a yield of 8.95 g (90%).  $^1\text{H}$  NMR spectra and molecular weight were measured.

$^1\text{H}$  NMR (500 MHz,  $\text{CDCl}_3$ )  $\delta$  2.28 (d, 2H), 2.87-3.15 (m, 1H), 7.05 (t, 2H), 7.27 (t, 2H), 7.38 (q, 1H), 7.55 (t, 4H); GPC (THF):  $M_n = 1.80 \times 10^4$  g/mol,  $M_w = 3.86 \times 10^4$  g/mol,  $M_w/M_n = 2.14$ .

### Synthesis of BBPE

The detailed synthesis procedure was as follows: 4-Benzoylbenzoic acid (BBA), PFP, 4-(dimethylamino)pyridine (DMAP), *N,N'*-Dicyclohexylcarbodiimide (DCC) and 40 mL THF (mol ratio of BBA : PFP : DMAP : DCC= 1 : 2 : 4 : 2) were added to a 250 mL round-bottom flask. The reaction mixture was kept stirring in an ice bath for 10 h. Subsequently, the mixture was filtrated to remove the precipitated *N,N'*-dicyclohexylurea. Then the filtrate was washed 3 times with water (40 mL) and dried over sodium sulfate. The solvent was removed by rotary evaporation. The product was isolated by silica gel column with hexane/ethylacetate (9:1 by volume) as the eluent. Finally, 6.42 g (70%) BBPE were obtained as a white powder and subsequently characterized.

$^1\text{H}$  NMR (400 MHz,  $\text{CDCl}_3$ )  $\delta$  7.46 (dd, 2H,  $J = 7.1/8.3$  Hz), 7.53-7.63 (m, 1H), 7.72-7.80 (m, 2H), 7.83-7.90 (m, 2H), 8.21-8.29 (m, 2H);  $^{13}\text{C}$  NMR (600 MHz,  $\text{CDCl}_3$ )  $\delta$  195.58, 161.92, 142.97, 142.16, 140.47, 138.83, 137.16, 136.58, 133.27, 130.66, 130.15, 130.05, 129.80, 128.60;  $^{19}\text{F}$  NMR (600 MHz,  $\text{CDCl}_3$ )  $\delta$  -152.32, -157.37, -161.96; IR (ATR mode) 1756.56  $\text{cm}^{-1}$  (C=O of ester), 1659.79  $\text{cm}^{-1}$  (C=O of benzophenones), 1515.47  $\text{cm}^{-1}$  (benzene ring of pentafluorophenyl).

## 7.4 Preparation of electrospun fibrous membrane precursors

### Preparation of the electrospun fibrous membrane precursor PMSAE

The electrospinning solution was composed of 55 wt% polymer solution in THF/DMF (6.5:3.5, v/v). After shaking for 8 h, the electrospinning solution was transferred to a syringe

## EXPERIMENTAL PART

---

with a blunt metal needle (diameter: 0.8 mm). The electrospinning apparatus was horizontally-aligned. The fibers were collected on an aluminum foil which was attached to the grounded collector. The parameters used for the electrospinning process were as follows: the flow rate was set to 3 mL/h, the tip-to-collector distance was 20 cm, the applied voltage was 25 kV. The obtained fibrous membranes were put in a vacuum oven for 10 h to remove the remaining solvent. The morphology of the fibrous membrane PMAM was observed by SEM.

### **Preparation of the electrospun fibrous membrane precursor PMAM**

The electrospinning solution was a mixed polymer solution composed of 32 wt% PMSAE, 11 wt% PABP and 2 wt% PMMA in THF/DMF (6.5:3.5, v/v). The subsequent procedure and the parameters used for the electrospinning process were the same as for the preparation of the above fibrous membrane precursor PMSAE.

## **7.5 Post-modification of electrospun fibrous membrane precursors**

### **Post-modification of the electrospun fibrous membrane precursor PMSAE**

The electro-spun fibrous membrane precursor PMSAE was post-modified with TTDD or TAD to get two different adsorbents, named PMSAE-TTDD and PMSAE-TAD, respectively. The selection of TTDD or TAD as post-modification amine has a twofold advantage. On the one hand, they feature abundant functional groups, which are desired for the later application. On the other hand, each molecule bears two primary amines, allowing them to act as crosslinkers, which allows to maintain the fiber morphology after post-modification. The detailed post-modification procedure was as follows: TTDD (or TAD) and Et<sub>3</sub>N were dissolved in 3 mL of ethanol. After the solution has been shaken evenly, fibers were added to the solution (ratio of fibers: TTDD (or TAD): Et<sub>3</sub>N=1: 3: 3). This post-modification process was carried out at room temperature on a shaker. After a predetermined time, the fibers were taken out and washed 3 times with ethanol. Then, the fibers were dried in a vacuum oven at

## EXPERIMENTAL PART

---

40 °C for 10 h. Finally, the adsorbents were ready to use. The morphology of the fibrous adsorbents was observed by SEM.

### **Post-modification of the electrospun fibrous membrane precursor PMAM**

For post-modifying the produced fibrous membranes PMAM, TTDD and APD were used, the former bearing the desired functional groups for the adsorption of anionic dyes and the latter for cationic dyes, respectively. The detailed procedure of the post-modification was as follows: the fibrous membranes PMAM were immersed into an ethanol solution containing TTDD (or APD) and Et<sub>3</sub>N. After shaking for a predetermined time at room temperature, the fibrous membranes PMAM were pulled out and washed 3 times with ethanol. After drying in a vacuum oven for 10 h, the resulting fibrous adsorbents, named PMAM-TTDD and PMAM-APD, respectively, were ready for adsorption application. The morphology of the fibrous adsorbents was observed by SEM.

## **7.6 Adsorption experiments**

### **General adsorption experiment**

The general adsorption experiment procedure was as follows: fibrous adsorbents were added to 50 mL conical flasks with stoppers containing dye solutions. The flasks were shaken for a predetermined time of 4 h to reach equilibrium at 240 RPM at room temperature. The concentration of dye solutions after adsorption was measured by an UV-Vis spectrophotometer. The adsorption capacities of the fibrous adsorbents were calculated as follows:

$$q = \frac{(C_o - C)V}{m} \quad (7-1)$$

## EXPERIMENTAL PART

---

where  $q$  ( $\text{mg g}^{-1}$ ) is the adsorption capacity.  $C_o$  ( $\text{mg L}^{-1}$ ) and  $C$  ( $\text{mg L}^{-1}$ ) are the original concentration and solution dye concentration after adsorption, respectively.  $V$  (L) is the volume of the dye solution.  $m$  (g) is the mass of the added adsorbent.

### Adsorption isotherm experiments

Batch adsorption isotherm experiments were recorded using 50 mL conical flasks containing 40 mL of dyes with different concentrations (200, 400, 600, 800 and 1000  $\text{mg L}^{-1}$ ) and 10 mg of adsorbents. After shaking at 240 RPM at ambient temperature for 4 h (pretested) equilibrium was reached. The concentration of the dye solutions after the adsorption was measured by an UV-Vis spectrophotometer. The adsorption capacities of the adsorbents were calculated by dividing adsorbate weight by adsorbent weight:<sup>153</sup>

$$q_e = \frac{(C_o - C_e)V}{m} \quad (7-2)$$

where  $q_e$  ( $\text{mg g}^{-1}$ ) is the equilibrium adsorption capacity.  $C_o$  ( $\text{mg L}^{-1}$ ) and  $C_e$  ( $\text{mg L}^{-1}$ ) are the original concentration and equilibrium concentration of the dye solution, respectively.  $V$  (L) is the volume of the dye solution.  $m$  (g) is the mass of the added adsorbent.

### Adsorption kinetics experiments

In order to explore the adsorption kinetics, 10 mg of fibrous adsorbents were added into 40 mL 1000  $\text{mg L}^{-1}$  of dye solutions. 1 mL of solution was withdrawn at certain time intervals.

The adsorption capacities were calculated with the following equation:

$$q_t = \frac{(C_o - C_t)V}{m} \quad (7-3)$$

where  $q_t$  ( $\text{mg g}^{-1}$ ) is the adsorption capacity at time  $t$ .  $C_t$  ( $\text{mg L}^{-1}$ ) is the concentration of dye solution at time  $t$ .



## 8. References

1. He, L. R.; Szameit, K.; Zhao, H.; Hahn, U.; Theato, P., Postpolymerization Modification Using Less Cytotoxic Activated Ester Polymers for the Synthesis of Biological Active Polymers. *Biomacromolecules* **2014**, 15, (8), 3197-3205.
2. Gauthier, M. A.; Gibson, M. I.; Klok, H. A., Synthesis of Functional Polymers by Post-Polymerization Modification. *Angew. Chem., Int. Ed.* **2009**, 48, (1), 48-58.
3. Das, A.; Theato, P., Activated Ester Containing Polymers: Opportunities and Challenges for the Design of Functional Macromolecules. *Chem. Rev.* **2016**, 116, (3), 1434-1495.
4. Gaballa, H.; Lin, S. J.; Shang, J. J.; Meier, S.; Theato, P., A synthetic approach toward a pH and sugar-responsive diblock copolymer via post-polymerization modification. *Polym. Chem.* **2018**, 9, (24), 3355-3358.
5. Ferruti, P.; Fere, A.; Bettelli, A., High Polymers of Acrylic and Methacrylic Esters of N-Hydroxysuccinimide as Polyacrylamide and Polymethacrylamide Precursors. *Polymer* **1972**, 13, (10), 462-&.
6. Batz, H. G.; Franzmann, G.; Ringsdorf, H., Model Reactions for Synthesis of Pharmacologically Active Polymers by Way of Monomeric and Polymeric Reactive Esters. *Angew. Chem., Int. Ed.* **1972**, 11, (12), 1103-1104.
7. Batz, H. G.; Franzmann, G.; Ringsdorf, H., Pharmacologically Active Polymers .5. Model Reactions for Reaction of Pharmaca and Enzymes with Monomeric and Polymeric Reactive Esters. *Makromol Chem.* **1973**, 172, 27-47.
8. Yoshikawa, M.; Adachi, Y.; Yokoi, H.; Sanui, K.; Ogata, N., Synthesis of Poly(1-[(2-Methylpropenoyl)Oxy]Succinimide-Co-Acrylonitrile) and the Selective Separation of a Water-Ethanol Mixture through Its Membranes. *Macromolecules* **1986**, 19, (1), 47-50.
9. Murata, H.; Prucker, O.; Ruhe, J., Synthesis of functionalized polymer monolayers from active ester brushes. *Macromolecules* **2007**, 40, (15), 5497-5503.

## REFERENCES

---

10. Wong, S. Y.; Putnam, D., Overcoming limiting side reactions associated with an NHS-activated precursor of polymethacrylamide-based polymers. *Bioconjugate Chem.* **2007**, *18*, (3), 970-982.
11. Blazejewski, J. C.; Hofstraat, J. W.; Lequesne, C.; Wakselman, C.; Wiersum, U. E., Halogenoaryl acrylates: preparation, polymerization and optical properties. *J. Fluorine Chem.* **1999**, *97*, (1-2), 191-199.
12. Seuyep, N. D. H.; Szopinski, D.; Luinstra, G. A.; Theato, P., Post-polymerization modification of reactive polymers derived from vinylcyclopropane: a poly(vinylcyclopropane) derivative with physical gelation and UCST behaviour in ethanol-water mixtures. *Polym. Chem.* **2014**, *5*, (19), 5823-5828.
13. Zhao, H.; Gu, W. Y.; Kakuchi, R.; Sun, Z. W.; Sterner, E.; Russell, T. P.; Coughlin, E. B.; Theato, P., Photocleavable Triblock Copolymers Featuring an Activated Ester Middle Block: "One-Step" Synthesis and Application as Locally Reactive Nanoporous Thin Films. *ACS Macro. Lett.* **2013**, *2*, (11), 966-969.
14. Zhao, H.; Gu, W. Y.; Thielke, M. W.; Sterner, E.; Tsai, T. H.; Russell, T. P.; Coughlin, E. B.; Theato, P., Functionalized Nanoporous Thin Films and Fibers from Photocleavable Block Copolymers Featuring Activated Esters. *Macromolecules* **2013**, *46*, (13), 5195-5201.
15. Zhao, H.; Theato, P., Copolymers featuring pentafluorophenyl ester and photolabile amine units: synthesis and application as reactive photopatterns. *Polym. Chem.* **2013**, *4*, (4), 891-894.
16. Pedone, E.; Li, X. W.; Koseva, N.; Alpar, O.; Brocchini, S., An information rich biomedical polymer library. *J. Mater. Chem.* **2003**, *13*, (11), 2825-2837.
17. Devenish, S. R. A.; Hill, J. B.; Blunt, J. W.; Morris, J. C.; Munro, M. H. G., Dual side-reactions limit the utility of a key polymer therapeutic precursor. *Tetrahedron Lett.* **2006**, *47*, (17), 2875-2878.

## REFERENCES

---

18. Eberhardt, M.; Mruk, R.; Zentel, R.; Theato, P., Synthesis of pentafluorophenyl(meth)acrylate polymers: New precursor polymers for the synthesis of multifunctional materials. *Eur. Polym. J.* **2005**, 41, (7), 1569-1575.
19. Park, H. J.; Kim, J.; Chang, J. Y.; Theato, P., Preparation of transparent conductive multilayered films using active pentafluorophenyl ester modified multiwalled carbon nanotubes. *Langmuir* **2008**, 24, (18), 10467-10473.
20. Schattling, P.; Jochum, F. D.; Theato, P., Multi-responsive copolymers: using thermo-, light- and redox stimuli as three independent inputs towards polymeric information processing. *Chem. Commun.* **2011**, 47, (31), 8859-8861.
21. Gaballa, H.; Theato, P., Glucose-Responsive Polymeric Micelles via Boronic Acid-Diol Complexation for Insulin Delivery at Neutral pH. *Biomacromolecules* **2019**, 20, (2), 871-881.
22. Nilles, K.; Theato, P., Synthesis and polymerization of active ester monomers based on 4-vinylbenzoic acid. *Eur. Polym. J.* **2007**, 43, (7), 2901-2912.
23. Boudreaux, C. J.; Bunyard, W. C.; McCormick, C. L., Controlled activity polymers .10. Synthetically tailored monomers and copolymers with hydrolytically-labile pendent esters of allelopathic phenols. *J. Control Release* **1997**, 44, (2-3), 171-183.
24. Suja, P. S.; Reshmi, C. R.; Sagitha, P.; Sujith, A., Electrospun Nanofibrous Membranes for Water Purification. *Polym. Rev.* **2017**, 57, (3), 467-504.
25. Huang, Y. S.; Li, J. X.; Chen, X. P.; Wang, X. K., Applications of conjugated polymer based composites in wastewater purification. *RSC Adv.* **2014**, 4, (107), 62160-62178.
26. Bai, B. Y.; Mi, X.; Xiang, X.; Heiden, P. A.; Heldt, C. L., Non-enveloped virus reduction with quaternized chitosan nanofibers containing graphene. *Carbohydr. Res.* **2013**, 380, 137-142.
27. Ahmed, F. E.; Lalia, B. S.; Hashaikeh, R., A review on electrospinning for membrane fabrication: Challenges and applications. *Desalination* **2015**, 356, 15-30.

## REFERENCES

---

28. Robinson, T.; McMullan, G.; Marchant, R.; Nigam, P., Remediation of dyes in textile effluent: a critical review on current treatment technologies with a proposed alternative. *Bioresource Technol.* **2001**, 77, (3), 247-255.
29. Bailey, S. E.; Olin, T. J.; Bricka, R. M.; Adrian, D. D., A review of potentially low-cost sorbents for heavy metals. *Water Res.* **1999**, 33, (11), 2469-2479.
30. Reddy, D. H. K.; Vijayaraghavan, K.; Kim, J. A.; Yun, Y. S., Valorisation of post-sorption materials: Opportunities, strategies, and challenges. *Adv. Colloid Interfac.* **2017**, 242, 35-58.
31. Ghamsari, M.; Madrakian, T., Highly Fast and Efficient Removal of some Cationic Dyes from Aqueous Solutions Using Sulfonated-oxidized Activated Carbon. *Anal Bioanal Chem. Re.* **2019**, 6, (1), 157-169.
32. Liu, Z. Y.; Adewuyi, Y. G.; Shi, S.; Chen, H.; Li, Y.; Liu, D. J.; Liu, Y. X., Removal of gaseous Hg-0 using novel seaweed biomass-based activated carbon. *Chem. Eng. J.* **2019**, 366, 41-49.
33. Xu, J. C.; Xin, P. H.; Han, Y. B.; Wang, P. F.; Jin, H. X.; Jin, D. F.; Peng, X. L.; Hong, B.; Li, J.; Ge, H. L.; Zhu, Z. W.; Wang, X. Q., Magnetic response and adsorptive properties for methylene blue of CoFe<sub>2</sub>O<sub>4</sub>/CoxFey/activated carbon magnetic composites. *J. Alloy Compd.* **2014**, 617, 622-626.
34. Huang, T. T.; Yan, M.; He, K.; Huang, Z. Z.; Zeng, G. M.; Chen, A. W.; Peng, M.; Li, H.; Yuan, L.; Chen, G. Q., Efficient removal of methylene blue from aqueous solutions using magnetic graphene oxide modified zeolite. *J. Colloid Interf. Sci.* **2019**, 543, 43-51.
35. Caliskan, Y.; Harbeck, S.; Bektas, N., Adsorptive Removal of Basic Yellow Dye Using Bigadic Zeolites: FTIR Analysis, Kinetics, and Isotherms Modeling. *Environ. Prog. Sustain.* **2019**, 38, S185-S195.

## REFERENCES

---

36. Joseph, A.; Vellayan, K.; Gonzalez, B.; Vicente, M. A.; Gil, A., Effective degradation of methylene blue in aqueous solution using Pd-supported Cu-doped Ti-pillared montmorillonite catalyst. *Appl. Clay Sci.* **2019**, 168, 7-10.
37. Gier, S.; Johns, W. D., Heavy metal-adsorption on micas and clay minerals studied by X-ray photoelectron spectroscopy. *Appl. Clay Sci.* **2000**, 16, (5-6), 289-299.
38. Shanmugarajah, B.; Chew, I. M.; Mubarak, N. M.; Choong, T. S.; Yoo, C.; Tan, K., Valorization of palm oil agro-waste into cellulose biosorbents for highly effective textile effluent remediation. *J. Clean Prod.* **2019**, 210, 697-709.
39. Monteiro, M. S.; de Farias, R. F.; Chaves, J. A. P.; Santana, S. A.; Silva, H. A. S.; Bezerra, C. W. B., Wood (*Bagassa guianensis* Aubl) and green coconut mesocarp (*cocos nucifera*) residues as textile dye removers (Remazol Red and Remazol Brilliant Violet). *J. Environ. Manage.* **2017**, 204, 23-30.
40. Samiey, B.; Cheng, C. H.; Wu, J. N., Organic-Inorganic Hybrid Polymers as Adsorbents for Removal of Heavy Metal Ions from Solutions: A Review. *Materials* **2014**, 7, (2), 673-726.
41. Wang, B. B.; Zhang, Q.; Xiong, G.; Ding, F.; He, Y. K.; Ren, B. Y.; You, L. X.; Fan, X. L.; Hardacre, C.; Sun, Y. G., Bakelite-type anionic microporous organic polymers with high capacity for selective adsorption of cationic dyes from water. *Chem. Eng. J.* **2019**, 366, 404-414.
42. Wei, W.; Lu, R. J.; Xie, H. J.; Zhang, Y. F.; Bai, X.; Gu, L.; Da, R.; Liu, X. Y., Selective adsorption and separation of dyes from an aqueous solution on organic-inorganic hybrid cyclomatrix polyphosphazene submicro-spheres. *J. Mater. Chem. A* **2015**, 3, (8), 4314-4322.
43. Yan, J. J.; Huang, Y. P.; Miao, Y. E.; Tjiu, W. W.; Liu, T. X., Polydopamine-coated electrospun poly(vinyl alcohol)/poly(acrylic acid) membranes as efficient dye adsorbent with good recyclability. *J. Hazard Mater.* **2015**, 283, 730-739.
44. Reneker, D. H.; Chun, I., Nanometre diameter fibres of polymer, produced by electrospinning. *Nanotechnology* **1996**, 7, (3), 216-223.

## REFERENCES

---

45. Tucker, N.; Stanger, J. J.; Staiger, M. P.; Razzaq, H.; Hofman, K., The History of the Science and Technology of Electrospinning from 1600 to 1995. *J. Eng. Fiber Fabr.* **2012**, *7*, 63-73.
46. Huang, Z. M.; Zhang, Y. Z.; Kotaki, M.; Ramakrishna, S., A review on polymer nanofibers by electrospinning and their applications in nanocomposites. *Compos. Sci. Technol.* **2003**, *63*, (15), 2223-2253.
47. Thielke, M. W.; Secker, C.; Schlaad, H.; Theato, P., Electrospinning of Crystallizable Polypeptoid Fibers. *Macromol. Rapid Comm.* **2016**, *37*, (1), 100-104.
48. Taylor, G., Electrically Driven Jets. *Proc R Soc Lon Ser-A* **1969**, *313*, (1515), 453-&.
49. Stranger, J.; Tucker, N.; Staiger, M., Staiger, Electrospinning, Smithers Rapra, Shrewsbury, Shropshire, GBR. **2009**.
50. Suzuki, A.; Arino, K., Polypropylene nanofiber sheets prepared by CO<sub>2</sub> laser supersonic multi-drawing. *Eur. Polym. J.* **2012**, *48*, (7), 1169-1176.
51. Feng, L.; Li, S. H.; Zhai, J.; Song, Y. L.; Jiang, L.; Zhu, D. B., Template based synthesis of aligned polyacrylonitrile nanofibers using a novel extrusion method. *Synthetic Met.* **2003**, *135*, (1-3), 817-818.
52. Che, G.; Lakshmi, B. B.; Martin, C. R.; Fisher, E. R.; Ruoff, R. S., Chemical vapor deposition based synthesis of carbon nanotubes and nanofibers using a template method. *Chem. Mater.* **1998**, *10*, (1), 260-267.
53. Ma, P. X.; Zhang, R. Y., Synthetic nano-scale fibrous extracellular matrix. *J. Biomed. Mater. Res.* **1999**, *46*, (1), 60-72.
54. Frenot, A.; Chronakis, I. S., Polymer nanofibers assembled by electrospinning. *Curr. Opin. Colloid In.* **2003**, *8*, (1), 64-75.
55. Loccufier, E.; Geltmeyer, J.; Daelemans, L.; D'hooge, D. R.; De Buysser, K.; De Clerck, K., Silica Nanofibrous Membranes for the Separation of Heterogeneous Azeotropes. *Adv. Funct. Mater.* **2018**, *28*, (44).

## REFERENCES

---

56. Kampalanonwat, P.; Supaphol, P., Preparation and Adsorption Behavior of Aminated Electrospun Polyacrylonitrile Nanofiber Mats for Heavy Metal Ion Removal. *ACS Appl. Mater. Inter.* **2010**, 2, (12), 3619-3627.
57. Zhao, R.; Li, X.; Sun, B. L.; Shen, M. Q.; Tan, X. C.; Ding, Y.; Jiang, Z. Q.; Wang, C., Preparation of phosphorylated polyacrylonitrile-based nanofiber mat and its application for heavy metal ion removal. *Chem. Eng. J.* **2015**, 268, 290-299.
58. Mei, Y.; Yao, C.; Fan, K.; Li, X. S., Surface modification of polyacrylonitrile nanofibrous membranes with superior antibacterial and easy-cleaning properties through hydrophilic flexible spacers. *J. Membrane Sci.* **2012**, 417, 20-27.
59. Homaeigohar, S.; Koll, J.; Lilleodden, E. T.; Elbahri, M., The solvent induced interfiber adhesion and its influence on the mechanical and filtration properties of polyethersulfone electrospun nanofibrous microfiltration membranes. *Sep. Purif. Technol.* **2012**, 98, 456-463.
60. Homaeigohar, S. S.; Elbahri, M., Novel compaction resistant and ductile nanocomposite nanofibrous microfiltration membranes. *J. Colloid Interf. Sci.* **2012**, 372, 6-15.
61. Huang, L. W.; Arena, J. T.; Manickam, S. S.; Jiang, X. Q.; Willis, B. G.; McCutcheon, J. R., Improved mechanical properties and hydrophilicity of electrospun nanofiber membranes for filtration applications by dopamine modification. *J. Membrane Sci.* **2014**, 460, 241-249.
62. Arribas, P.; Khayet, M.; Garcia-Payo, M. C.; Gil, L., Self-sustained electro-spun polysulfone nano-fibrous membranes and their surface modification by interfacial polymerization for micro- and ultra-filtration. *Sep. Purif. Technol.* **2014**, 138, 118-129.
63. Kang, G. D.; Cao, Y. M., Application and modification of poly(vinylidene fluoride) (PVDF) membranes - A review. *J. Membrane Sci.* **2014**, 463, 145-165.
64. Ahmed, F. E.; Lalia, B. S.; Hilal, N.; Hashaikeh, R., Underwater superoleophobic cellulose/electrospun PVDF-HFP membranes for efficient oil/water separation. *Desalination* **2014**, 344, 48-54.

## REFERENCES

---

65. He, T.; Zhou, W. Y.; Bahi, A.; Yang, H.; Ko, F., High permeability of ultrafiltration membranes based on electrospun PVDF modified by nanosized zeolite hybrid membrane scaffolds under low pressure. *Chem. Eng. J.* **2014**, 252, 327-336.
66. Lee, J. W.; Jung, J.; Cho, Y. H.; Yadav, S. K.; Baek, K. Y.; Park, H. B.; Hong, S. M.; Koo, C. M., Fouling-Tolerant Nanofibrous Polymer Membranes for Water Treatment. *ACS Appl. Mater. Inter.* **2014**, 6, (16), 14600-14607.
67. Pant, H. R.; Kim, H. J.; Joshi, M. K.; Pant, B.; Park, C. H.; Kim, J. I.; Hui, K. S.; Kim, C. S., One-step fabrication of multifunctional composite polyurethane spider-web-like nanofibrous membrane for water purification. *J. Hazard Mater.* **2014**, 264, 25-33.
68. Tijing, L. D.; Ruelo, M. T. G.; Amarjargal, A.; Pant, H. R.; Park, C. H.; Kim, D. W.; Kim, C. S., Antibacterial and superhydrophilic electrospun polyurethane nanocomposite fibers containing tourmaline nanoparticles. *Chem. Eng. J.* **2012**, 197, 41-48.
69. Suriyaraj, S. P.; Bhattacharyya, A.; Selvakumar, R., Hybrid Al<sub>2</sub>O<sub>3</sub>/bio-TiO<sub>2</sub> nanocomposite impregnated thermoplastic polyurethane (TPU) nanofibrous membrane for fluoride removal from aqueous solutions. *RSC Adv.* **2015**, 5, (34), 26905-26912.
70. Xu, G. R.; Wang, J. N.; Li, C. J., Preparation of hierarchically nanofibrous membrane and its high adaptability in hexavalent chromium removal from water. *Chem. Eng. J.* **2012**, 198, 310-317.
71. Kayaci, F.; Aytac, Z.; Uyar, T., Surface modification of electrospun polyester nanofibers with cyclodextrin polymer for the removal of phenanthrene from aqueous solution. *J. Hazard Mater.* **2013**, 261, 286-294.
72. Stephen, M.; Catherine, N.; Brenda, M.; Andrew, K.; Leslie, P.; Corrine, G., Oxolane-2,5-dione modified electrospun cellulose nanofibers for heavy metals adsorption. *J. Hazard Mater.* **2011**, 192, (2), 922-927.

## REFERENCES

---

73. Celebioglu, A.; Demirci, S.; Uyar, T., Cyclodextrin-grafted electrospun cellulose acetate nanofibers via "Click" reaction for removal of phenanthrene. *Appl. Surf. Sci.* **2014**, 305, 581-588.
74. Sarioglu, O. F.; Yasa, O.; Celebioglu, A.; Uyar, T.; Tekinay, T., Efficient ammonium removal from aquatic environments by *Acinetobacter calcoaceticus* STB1 immobilized on an electrospun cellulose acetate nanofibrous web. *Green Chem.* **2013**, 15, (9), 2566-2572.
75. Hallaji, H.; Keshtkar, A. R.; Moosavian, M. A., A novel electrospun PVA/ZnO nanofiber adsorbent for U(VI), Cu(II) and Ni(II) removal from aqueous solution. *J. Taiwan Inst. Chem. E* **2015**, 46, 109-118.
76. Mahanta, N.; Valiyaveettil, S., Surface modified electrospun poly(vinyl alcohol) membranes for extracting nanoparticles from water. *Nanoscale* **2011**, 3, (11), 4625-4631.
77. Padil, V. V. T.; Cernik, M., Poly (vinyl alcohol)/gum karaya electrospun plasma treated membrane for the removal of nanoparticles (Au, Ag, Pt, CuO and Fe<sub>3</sub>O<sub>4</sub>) from aqueous solutions. *J. Hazard Mater.* **2015**, 287, 102-110.
78. Najafabadi, H. H.; Irani, M.; Rad, L. R.; Haratameh, A. H.; Haririan, I., Removal of Cu<sup>2+</sup>, Pb<sup>2+</sup> and Cr<sup>6+</sup> from aqueous solutions using a chitosan/graphene oxide composite nanofibrous adsorbent. *RSC Adv.* **2015**, 5, (21), 16532-16539.
79. Li, L.; Li, Y. X.; Yang, C. F., Chemical filtration of Cr (VI) with electrospun chitosan nanofiber membranes. *Carbohydr. Polym.* **2016**, 140, 299-307.
80. Li, Z. Y.; Li, T. T.; An, L. B.; Liu, H.; Gu, L. N.; Zhang, Z. M., Preparation of chitosan/polycaprolactam nanofibrous filter paper and its greatly enhanced chromium(VI) adsorption. *Colloid Surface A* **2016**, 494, 65-73.
81. Ma, F. F.; Zhang, D.; Zhang, N.; Huang, T.; Wang, Y., Polydopamine-assisted deposition of polypyrrole on electrospun poly (vinylidene fluoride) nanofibers for bidirectional removal of cation and anion dyes. *Chem. Eng. J.* **2018**, 354, 432-444.

## REFERENCES

---

82. Sharma, R.; Singh, N.; Gupta, A.; Tiwari, S.; Tiwari, S. K.; Dhakate, S. R., Electrospun chitosan-polyvinyl alcohol composite nanofibers loaded with cerium for efficient removal of arsenic from contaminated water. *J. Mater. Chem. A* **2014**, *2*, (39), 16669-16677.
83. Roller, S.; Covill, N., The antifungal properties of chitosan in laboratory media and apple juice. *Int. J. Food Microbiol.* **1999**, *47*, (1-2), 67-77.
84. Manukumar, H. M.; Umesha, S., Photocrosslinker technology: An antimicrobial efficacy of cinnamaldehyde cross-linked low-density polyethylene (Cin-C-LDPE) as a novel food wrapper. *Food Res. Int.* **2017**, *102*, 144-155.
85. Kleiner, P.; Heydenreuter, W.; Stahl, M.; Korotkov, V. S.; Sieber, S. A., A Whole Proteome Inventory of Background Photocrosslinker Binding. *Angew. Chem., Int. Ed.* **2017**, *56*, (5), 1396-1401.
86. Sakurai, K.; Ozawa, S.; Yamada, R.; Yasui, T.; Mizuno, S., Comparison of the Reactivity of Carbohydrate Photoaffinity Probes with Different Photoreactive Groups. *Chembiochem.* **2014**, *15*, (10), 1399-1403.
87. Böhm, A.; Gattermayer, M.; Trieb, C.; Schabel, S.; Fiedler, D.; Miletzky, F.; Biesalski, M., Photo-attaching functional polymers to cellulose fibers for the design of chemically modified paper. *Cellulose* **2013**, *20*, (1), 467-483.
88. Rizk, M. S.; Shi, X. F.; Platz, M. S., Lifetimes and reactivities of some 1,2-didehydroazepines commonly used in photoaffinity labeling experiments in aqueous solutions. *Biochemistry* **2006**, *45*, (2), 543-551.
89. Blencowe, A.; Hayes, W., Development and application of diazirines in biological and synthetic macromolecular systems. *Soft Matter* **2005**, *1*, (3), 178-205.
90. Hashimoto, M.; Hatanaka, Y., Recent progress in diazirine-based photoaffinity labeling. *Eur. J. Org. Chem.* **2008**, (15), 2513-2523.
91. Das, J., Aliphatic Diazirines as Photoaffinity Probes for Proteins: Recent Developments. *Chem. Rev.* **2011**, *111*, (8), 4405-4417.

## REFERENCES

---

92. Dorman, G.; Prestwich, G. D., Benzophenone Photophores in Biochemistry. *Biochemistry* **1994**, 33, (19), 5661-5673.
93. Cho, J. D.; Kim, S. G.; Hong, J. W., Surface modification of polypropylene sheets by UV-radiation grafting polymerization. *J. Appl. Polym. Sci.* **2006**, 99, (4), 1446-1461.
94. Li, X.; Ballerini, D. R.; Shen, W., A perspective on paper-based microfluidics: Current status and future trends. *Biomicrofluidics* **2012**, 6, (1).
95. Regev, C.; Belfer, S.; Hohenberg, M.; Fainstein, R.; Parola, A. H.; Kasher, R., Fabrication of poly(ethylene glycol) particles with a micro-spherical morphology on polymeric fibers and its application in high flux water filtration. *Sep. Purif. Technol.* **2019**, 210, 729-736.
96. Kaneda, M.; Lu, X. L.; Cheng, W.; Zhou, X. C.; Bernstein, R.; Zhang, W.; Kimura, K.; Elimelech, M., Photografting Graphene Oxide to Inert Membrane Materials to Impart Antibacterial Activity. *Environ. Sci. Tech. Let.* **2019**, 6, (3), 141-147.
97. Dong, L.; Liu, X. D.; Xiong, Z. R.; Sheng, D. K.; Lin, C. H.; Zhou, Y.; Yang, Y. M., Preparation and characterization of functional poly(vinylidene fluoride) (PVDF) membranes with ultraviolet-absorbing property. *Appl. Surf. Sci.* **2018**, 444, 497-504.
98. Rahimpour, A., Preparation and modification of nano-porous polyimide (PI) membranes by UV photo-grafting process: Ultrafiltration and nanofiltration performance. *Korean J. Chem. Eng.* **2011**, 28, (1), 261-266.
99. Chen, S. G.; Zhang, S. B.; Galluzzi, M.; Li, F.; Zhang, X. C.; Yang, X. H.; Liu, X. Y.; Cai, X. H.; Zhu, X. L.; Du, B.; Li, J. N.; Huang, P., Insight into multifunctional polyester fabrics finished by one-step eco-friendly strategy. *Chem. Eng. J.* **2019**, 358, 634-642.
100. Krebs, F. C., Fabrication and processing of polymer solar cells: A review of printing and coating techniques. *Sol. Energ. Mat. Sol. C* **2009**, 93, (4), 394-412.
101. Norrman, K.; Ghanbari-Siahkali, A.; Larsen, N. B., 6 Studies of spin-coated polymer films. *Annual Reports Section "C" (Physical Chemistry)* **2005**, 101, 174.

## REFERENCES

---

102. Teichler, A.; Perelaer, J.; Schubert, U. S., Inkjet printing of organic electronics - comparison of deposition techniques and state-of-the-art developments. *J. Mater. Chem. C* **2013**, 1, (10), 1910-1925.
103. Hall, D. B.; Underhill, P.; Torkelson, J. M., Spin coating of thin and ultrathin polymer films. *Polym. Eng. Sci.* **1998**, 38, (12), 2039-2045.
104. Chang, J. F.; Sun, B. Q.; Breiby, D. W.; Nielsen, M. M.; Solling, T. I.; Giles, M.; McCulloch, I.; Sirringhaus, H., Enhanced mobility of poly(3-hexylthiophene) transistors by spin-coating from high-boiling-point solvents. *Chem. Mater.* **2004**, 16, (23), 4772-4776.
105. Sonker, R. K.; Yadav, B. C.; Gupta, V.; Tomar, M., Fabrication and characterization of ZnO-TiO<sub>2</sub>-PANI (ZTP) micro/nanoballs for the detection of flammable and toxic gases. *J. Hazard Mater.* **2019**, 370, 126-137.
106. Chang, D.; Yoon, D.; Ro, M. D.; Hwang, I.; Park, I.; Shin, D., Synthesis and characteristics of protective coating on thin cover layer for high density-digital versatile disc. *Jpn. J. Appl. Phys. I* **2003**, 42, (2b), 754-758.
107. Walheim, S.; Schaffer, E.; Mlynek, J.; Steiner, U., Nanophase-separated polymer films as high-performance antireflection coatings. *Science* **1999**, 283, (5401), 520-522.
108. Yan, X. H.; Liu, G. J.; Dickey, M.; Willson, C. G., Preparation of porous polymer membranes using nano- or micro-pillar arrays as templates. *Polymer* **2004**, 45, (25), 8469-8474.
109. Zhang, X. X.; Li, Z. W.; Lin, S. J.; Théato, P., Fibrous materials based on polymeric salicyl active esters as efficient adsorbents for selective removal of anionic dye *Submitted* **2019**.
110. Barbosa, T. P.; Sousa, S. C. O.; Amorim, F. M.; Rodrigues, Y. K. S.; de Assis, P. A. C.; Caldas, J. P. A.; Oliveira, M. R.; Vasconcelos, M. L. A. A., Design, synthesis and antileishmanial in vitro activity of new series of chalcones-like compounds: A molecular hybridization approach. *Bioorgan. Med. Chem.* **2011**, 19, (14), 4250-4256.

## REFERENCES

---

111. Ho, Y. S.; McKay, G., Pseudo-second order model for sorption processes. *Process Biochem.* **1999**, 34, (5), 451-465.
112. Zhou, Y. Y.; Liu, X. C.; Tang, L.; Zhang, F. F.; Zeng, G. M.; Peng, X. Q.; Luo, L.; Deng, Y. C.; Pang, Y.; Zhang, J. C., Insight into highly efficient co-removal of p-nitrophenol and lead by nitrogen-functionalized magnetic ordered mesoporous carbon: Performance and modelling. *J. Hazard Mater.* **2017**, 333, 80-87.
113. Gunay, A.; Arslankaya, E.; Tosun, I., Lead removal from aqueous solution by natural and pretreated clinoptilolite: adsorption equilibrium and kinetics. *J. Hazard Mater.* **2007**, 146, (1-2), 362-71.
114. Atas, M. S.; Dursun, S.; Akyildiz, H.; Citir, M.; Yavuz, C. T.; Yavuz, M. S., Selective removal of cationic micro-pollutants using disulfide-linked network structures. *RSC Adv.* **2017**, 7, (42), 25969-25977.
115. Zhou, Y. Y.; Liu, X. C.; Xiang, Y. J.; Wang, P.; Zhang, J. C.; Zhang, F. F.; Wei, J. H.; Luo, L.; Lei, M.; Tang, L., Modification of biochar derived from sawdust and its application in removal of tetracycline and copper from aqueous solution: Adsorption mechanism and modelling. *Bioresour. Technol.* **2017**, 245, 266-273.
116. Elsherbiny, A. S.; El-Hefnawy, M. E.; Gemeay, A. H., Linker impact on the adsorption capacity of polyaspartate/montmorillonite composites towards methyl blue removal. *Chem. Eng. J.* **2017**, 315, 142-151.
117. Cheng, W.; Rechberger, F.; Niederberger, M., Three-Dimensional Assembly of Yttrium Oxide Nanosheets into Luminescent Aerogel Monoliths with Outstanding Adsorption Properties. *ACS Nano.* **2016**, 10, (2), 2467-2475.
118. He, X.; Wang, J. J.; Shu, Z.; Tang, A. D.; Yang, H. M., Y<sub>2</sub>O<sub>3</sub> functionalized natural palygorskite as an adsorbent for methyl blue removal. *RSC Adv.* **2016**, 6, (48), 41765-41771.

## REFERENCES

---

119. Guo, D. M.; An, Q. D.; Li, R.; Xiao, Z. Y.; Zhai, S. R., Ultrahigh selective and efficient removal of anionic dyes by recyclable polyethylenimine-modified cellulose aerogels in batch and fixed-bed systems. *Colloid Surface A* **2018**, 555, 150-160.
120. Zhu, Z. G.; Wu, P.; Liu, G. J.; He, X. F.; Qi, B. Y.; Zeng, G. F.; Wang, W.; Sun, Y. H.; Cui, F. Y., Ultrahigh adsorption capacity of anionic dyes with sharp selectivity through the cationic charged hybrid nanofibrous membranes. *Chem. Eng. J.* **2017**, 313, 957-966.
121. Wang, Z. X.; Ji, S. Q.; Zhang, J.; He, F.; Xu, Z. D.; Peng, S. Q.; Li, Y. X., Dual functional membrane with multiple hierarchical structures (MHS) for simultaneous and high-efficiency removal of dye and nano-sized oil droplets in water under high flux. *J. Membrane Sci.* **2018**, 564, 317-327.
122. Mi, H.; Jiang, Z. G.; Kong, J., Hydrophobic Poly(ionic liquid) for Highly Effective Separation of Methyl Blue and Chromium Ions from Water. *Polymers* **2013**, 5, (4), 1203-1214.
123. Qin, Y.; Wang, L.; Zhao, C. W.; Chen, D.; Ma, Y. H.; Yang, W. T., Ammonium-Functionalized Hollow Polymer Particles As a pH-Responsive Adsorbent for Selective Removal of Acid Dye. *ACS Appl. Mater. Inter.* **2016**, 8, (26), 16690-16698.
124. Liu, M. P.; Su, T. T.; Sun, L.; Du, H. B., Facile preparation of yolk-shell structured Si/SiC@C@TiO<sub>2</sub> nanocomposites as highly efficient photocatalysts for degrading organic dye in wastewater. *RSC Adv.* **2016**, 6, (5), 4063-4069.
125. Abd-Elhamid, A. I.; Aly, H. F.; Soliman, H. A. M.; El-Shanshory, A. A., Graphene oxide: Follow the oxidation mechanism and its application in water treatment. *J. Mol. Liq.* **2018**, 265, 226-237.
126. Lian, G.; Zhang, X.; Si, H. B.; Wang, J.; Cui, D. L.; Wang, Q. L., Boron Nitride Ultrathin Fibrous Nanonets: One-Step Synthesis and Applications for Ultrafast Adsorption for Water Treatment and Selective Filtration of Nanoparticles. *ACS Appl. Mater. Inter.* **2013**, 5, (24), 12773-12778.

## REFERENCES

---

127. Liu, J. S.; Liu, G. N.; Liu, W. X., Preparation of water-soluble beta-cyclodextrin/poly(acrylic acid)/graphene oxide nanocomposites as new adsorbents to remove cationic dyes from aqueous solutions. *Chem. Eng. J.* **2014**, *257*, 299-308.
128. Ma, J.; Sun, S. S.; Chen, K. Z., Facile and scalable synthesis of magnetite/carbon adsorbents by recycling discarded fruit peels and their potential usage in water treatment. *Bioresource Technol.* **2017**, *233*, 110-115.
129. Wang, Z. X.; Guo, J.; Ma, J.; Shao, L., Highly regenerable alkali-resistant magnetic nanoparticles inspired by mussels for rapid selective dye removal offer high-efficiency environmental remediation. *J. Mater. Chem. A* **2015**, *3*, (39), 19960-19968.
130. Gan, L.; Shang, S. M.; Hu, E. L.; Wah, C.; Yuen, M.; Jiang, S. X., Konjac glucomannan/graphene oxide hydrogel with enhanced dyes adsorption capability for methyl blue and methyl orange. *Appl. Surf. Sci.* **2015**, *357*, 866-872.
131. Mirzaei, A.; Chen, Z.; Haghghat, F.; Yerushalmi, L., Enhanced adsorption of anionic dyes by surface fluorination of zinc oxide: A straightforward method for numerical solving of the ideal adsorbed solution theory (IAST). *Chem. Eng. J.* **2017**, *330*, 407-418.
132. Peng, C.; Zhang, J. L.; Xiong, Z. G.; Zha, B. H.; Liu, P. C., Fabrication of porous hollow gamma-Al<sub>2</sub>O<sub>3</sub> nanofibers by facile electrospinning and its application for water remediation. *Micropor Mesopor Mat.* **2015**, *215*, 133-142.
133. Wu, L. S.; Sun, J. F.; Wu, M. T., Modified cellulose membrane prepared from corn stalk for adsorption of methyl blue. *Cellulose* **2017**, *24*, (12), 5625-5638.
134. Zhang, X. X.; Théato, P., Free-standing fibrous membranes based on polymeric salicyl active esters for highly efficient and selective adsorption of anionic or cationic dyes from water. *Submitted* **2019**.
135. Ali, U.; Karim, K. J. B. A.; Buang, N. A., A Review of the Properties and Applications of Poly (Methyl Methacrylate) (PMMA). *Polym. Rev.* **2015**, *55*, (4), 678-705.

## REFERENCES

---

136. Thielke, M.; Bultema, L.; Brauer, D.; Richter, B.; Fischer, M.; Theato, P., Rapid Mercury(II) Removal by Electrospun Sulfur Copolymers. *Polymers* **2016**, 8, (7), 266.
137. Liu, H. L.; Sun, R. X.; Feng, S. Y.; Wang, D. X.; Liu, H. Z., Rapid synthesis of a silsesquioxane-based disulfide-linked polymer for selective removal of cationic dyes from aqueous solutions. *Chem. Eng. J.* **2019**, 359, 436-445.
138. Gabal, M. A.; Al-Harthy, E. A.; Al Angari, Y. M.; Salam, M. A., MWCNTs decorated with Mn<sub>0.8</sub>Zn<sub>0.2</sub>Fe<sub>2</sub>O<sub>4</sub> nanoparticles for removal of crystal-violet dye from aqueous solutions. *Chem. Eng. J.* **2014**, 255, 156-164.
139. Chen, Y. F.; He, F. B.; Ren, Y.; Peng, H.; Huang, K. X., Fabrication of chitosan/PAA multilayer onto magnetic microspheres by LbL method for removal of dyes. *Chem. Eng. J.* **2014**, 249, 79-92.
140. Azha, S. F.; Sellaoui, L.; Shamsudin, M. S.; Ismail, S.; Bonilla-Petriciolet, A.; Ben Lamine, A.; Erto, A., Synthesis and characterization of a novel amphoteric adsorbent coating for anionic and cationic dyes adsorption: Experimental investigation and statistical physics modelling. *Chem. Eng. J.* **2018**, 351, 221-229.
141. Yu, S. J.; Wang, X. X.; Chen, Z. S.; Wang, J.; Wang, S. H.; Hayat, T.; Wang, X. K., Layered double hydroxide intercalated with aromatic acid anions for the efficient capture of aniline from aqueous solution. *J. Hazard Mater.* **2017**, 321, 111-120.
142. Li, X.; Liu, Y.; Zhang, C. L.; Wen, T.; Zhuang, L.; Wang, X. X.; Song, G.; Chen, D. Y.; Ai, Y. J.; Hayat, T.; Wang, X. K., Porous Fe<sub>2</sub>O<sub>3</sub> microcubes derived from metal organic frameworks for efficient elimination of organic pollutants and heavy metal ions. *Chem. Eng. J.* **2018**, 336, 241-252.
143. Yu, S. J.; Wang, X. X.; Yao, W.; Wang, J.; Ji, Y. F.; Ai, Y. J.; Alsaedi, A.; Hayat, T.; Wang, X. K., Macroscopic, Spectroscopic, and Theoretical Investigation for the Interaction of Phenol and Naphthol on Reduced Graphene Oxide. *Environ. Sci. Technol.* **2017**, 51, (6), 3278-3286.

## REFERENCES

---

144. Vooturi, S. K.; Cheung, C. M.; Rybak, M. J.; Firestine, S. M., Design, synthesis, and structure-activity relationships of benzophenone-based tetraamides as novel antibacterial agents. *J. Med. Chem.* **2009**, 52, (16), 5020-31.
145. Schenderlein, H.; Voss, A.; Stark, R. W.; Biesalski, M., Preparation and Characterization of Light-Switchable Polymer Networks Attached to Solid Substrates. *Langmuir* **2013**, 29, (14), 4525-4534.
146. Boanen, N. K.; Hillmyer, M. A., Post-polymerization functionalization of polyolefins. *Chem. Soc. Rev.* **2005**, 34, (3), 267-275.
147. Wenzel, R. N., Surface Roughness and Contact Angle. *J. Phys. Colloid Chem.* **1949**, 53, (9), 1466-1467.
148. Jo, H.; Haberkorn, N.; Pan, J. A.; Vakili, M.; Nielsch, K.; Theato, P., Fabrication of Chemically Tunable, Hierarchically Branched Polymeric Nanostructures by Multi-branched Anodic Aluminum Oxide Templates. *Langmuir* **2016**, 32, (25), 6437-6444.
149. Wang, Q. B.; Meng, Q. A.; Wang, P. W.; Liu, H.; Jiang, L., Bio-Inspired Direct Patterning Functional Nanorod Microlines: Controllable Liquid Transfer. *ACS Nano*. **2015**, 9, (4), 4362-4370.
150. Hu, W. H.; Liu, Y. S.; Yang, H. B.; Zhou, X. Q.; Li, C. M., ZnO nanorods-enhanced fluorescence for sensitive microarray detection of cancers in serum without additional reporter-amplification. *Biosens. Bioelectron.* **2011**, 26, (8), 3683-3687.
151. Tabakman, S. M.; Lau, L.; Robinson, J. T.; Price, J.; Sherlock, S. P.; Wang, H. L.; Zhang, B.; Chen, Z.; Tangsombatvisit, S.; Jarrell, J. A.; Utz, P. J.; Dai, H. J., Plasmonic substrates for multiplexed protein microarrays with femtomolar sensitivity and broad dynamic range. *Nat. Commun.* **2011**, 2.
152. Stoychev, G.; Puretskiy, N.; Ionov, L., Self-folding all-polymer thermoresponsive microcapsules. *Soft Matter* **2011**, 7, (7), 3277.

## REFERENCES

---

153. van Kuringen, H. P. C.; Eikelboom, G. M.; Shishmanova, I. K.; Broer, D. J.; Schenning, A. P. H. J., Responsive Nanoporous Smectic Liquid Crystal Polymer Networks as Efficient and Selective Adsorbents. *Adv. Funct. Mater.* **2014**, 24, (32), 5045-5051.

## APPENDIX

### 9. Appendix

#### A. List of chemicals

The Information of the substances were taken from <http://www.sigmaldrich.com>

Chemicals (CAS number)	Hazard symbol	H-Phrases	P-Phrases
Acetone (67-64-1)	 GHS02 GHS07	H225-H319- H336	P210-P280-P304 + P340 + P312-P305 + P351 + P338-P337 + P313-P403 + P235
Acryloyl chloride (814-68-6)	 GHS02 GHS05 GHS06 GHS09	H225-H290- H302 + H312- H314-H330	P210-P280-P304 + P340 + P310-P305 + P351 + P338-P370 + P378-P403 + P235
(±)-3-Amino-1,2- propanediol (616-30-8)	 GHS05	H314	P280- P305+P351+P338-P310
Azobisisobutyronitrile (78-67-1)	 GHS02 GHS07	H242-H302 + H332-H412	P210-P220-P234-P261- P280-P370 + P378
Azorubine (3567-69-9)	-	-	-
4-Benzoylbenzoic acid (611-95-0)	-	-	-
Crystal violet (548-62-9)	 GHS08 GHS05 GHS07 GHS09	H302-H318- H350-H410	P201-P273-P280- P305+P351+P338- P308+P313-P501

## APPENDIX

Dichloromethane (75-09-2)	  GHS07 GHS08	H315-H319- H335-H336- H351-H371	P260-P280-P305 + P351 + P338
N,N'- Dicyclohexylcarbodiimide (538-75-0)	  GHS06 GHS05	H302-H311- H317-H318	P280- P301+P312+P330- P302+P352+P312- P305+P351+P338+P310
4- (Dimethylamino)pyridine (1122-58-3)	 GHS06	H301-H310- H315-H319- H335	P280-P301 + P310 + P330-P302 + P352 + P310-P304 + P340 + P312-P305 + P351 + P338-P337 + P313
Dimethylformamide (68-12-2)	  GHS02 GHS07  GHS08	H226- H312- H319- H332- H360	P201-P280-P305 + P351 + P338-P308 + P313
1,4-Dioxane (123-91-1)	  GHS02 GHS07  GHS08	H225-H351- H319-H335	P210-P280-P305 + P351 + P338-P370 + P378-P403 + P235
Ethanol (64-17-5)	  GHS02 GHS07	H225-H319	P210-P280- P305+P351+P338- P337+P313-P403+P235
Ethanolamine (141-43-5)	  GHS05 GHS07	H302 + H312 + H332-H314- H335-H412	P261-P273-P301 + P312 + P330-P303 + P361 + P353-P304 + P340 + P310-P305 + P351 + P338
Ethyl acetate (141-78-6)	  GHS02 GHS07	H225-H319- H336	P210-P233-P261-P280- P303+P361+P353- P370+P378

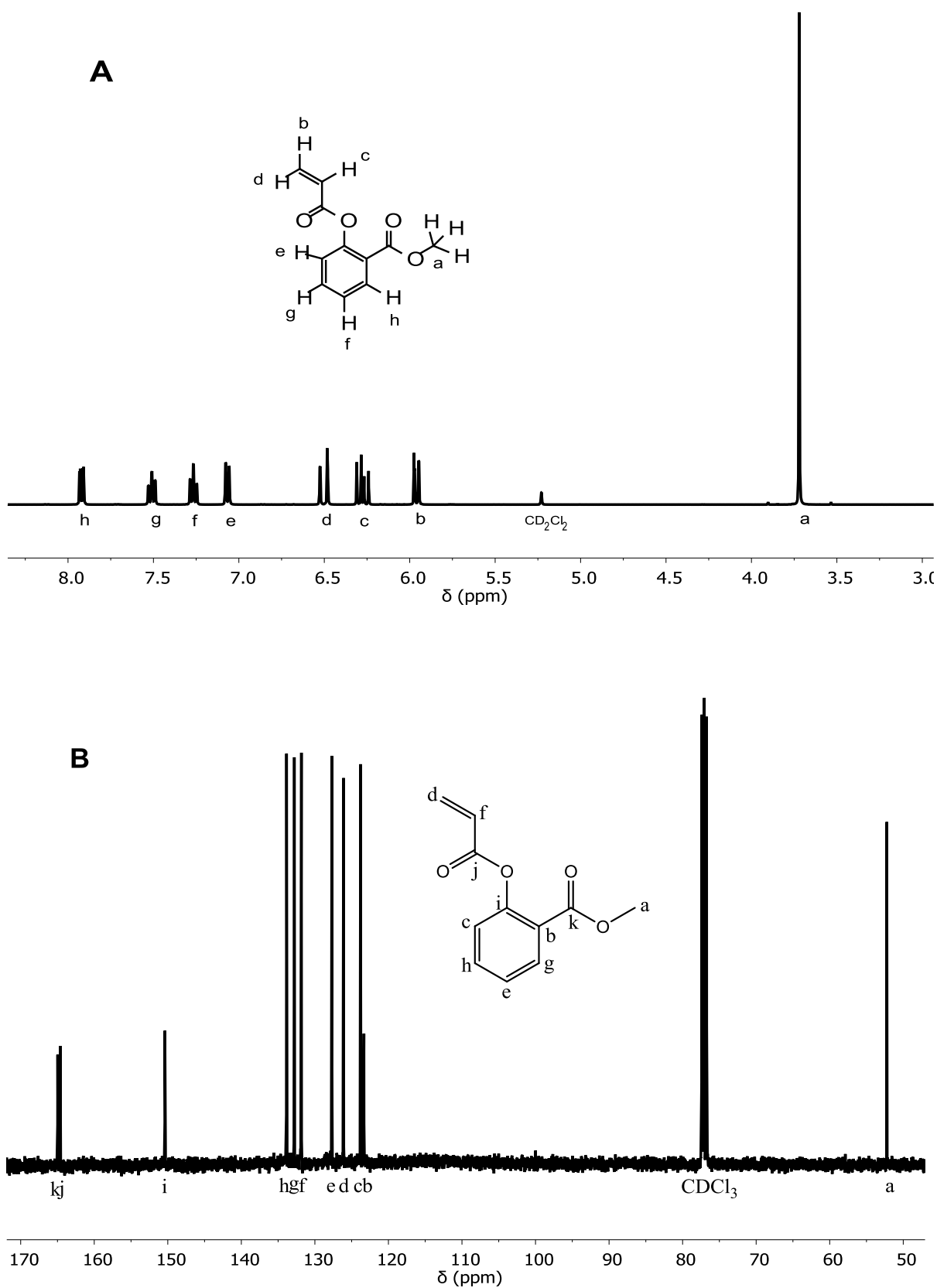
## APPENDIX

Hexane (110-54-3)	  GHS02 GHS07   GHS08 GHS09	H225-H304- H315-H336- H361f-H373- H411	P201-P210-P273-P301 + P310-P308 + P313- P331
Hydrochloric acid (7647-01-0)	  GHS05 GHS07	H290-H314- H335	P261-P280-P301 + P330 + P331-P303 + P361 + P353-P304 + P340 + P310-P305 + P351 + P338 + P310
4-Hydroxybenzophenone (1137-42-4)	 GHS07	H315-H319-H 335	P261-P264-P271-P280- P302+P352- P304+P340- P305+P351+P338- P312-P321-P332+P313- P337+P313-P362, P403+P233-P405-P501
Methanol (67-56-1)	  GHS02 GHS06  GHS08	H225-H301 + H311 + H331- H370	P210-P280-P302 + P352 + P312-P304 + P340 + P312- P370 + P378-P403 + P235
Methyl blue (28983-56-4)	 GHS07	H302-H315- H319-H335	P261-P305+P351+P338
Methylene blue (61-73-4)	 GHS07	H302	P301+P312+P330
Methyl salicylate (119-36-8)	 GHS07	H302	P301+P312+P330
Orange G (1936-15-8)	-	-	-
Pentafluorophenol (14533-84-7)	  GHS02 GHS07	H226-H315- H319-H335	P261-P305 + P351 + P338

## APPENDIX

Poly(methyl methacrylate) (9011-14-7)	-	-	-
Sodium hydroxide (1310-73-2)	 GHS05	H290-H314	P280-P303 + P361 + P353-P304 + P340 + P310-P305 + P351 + P338
Tetrahydrofuran (109-99-9)	 GHS02  GHS07  GHS08	H225-H302- H319-H335- H351	P210-P280-P301 + P312 + P330-P305 + P351 + P338-P370 + P378-P403 + P235
3,6,9-Triazaundecan-1,11-diamin (112-57-2)	 GHS05  GHS07  GHS09	H302-H312- H314-H317- H411	P273-P280- P305+P351+P338-P310
Triethylamine (121-44-8)	 GHS02  GHS05  GHS06	H225-H302- H311 + H331- H314-H335	P210-P261- P280-P303 + P361 + P353-P305 + P351 + P338-P370 + P378
4,7,10-Trioxa-1,13-tridecanediamine (4246-51-9)	 GHS05	H314	P280- P305+P351+P338-P310

## B. Supporting information

**Fig. S-1** NMR spectra of MSAE (A)  $^1\text{H}$  NMR in  $\text{CD}_2\text{Cl}_2$  (B)  $^{13}\text{C}$  NMR in  $\text{CDCl}_3$ .

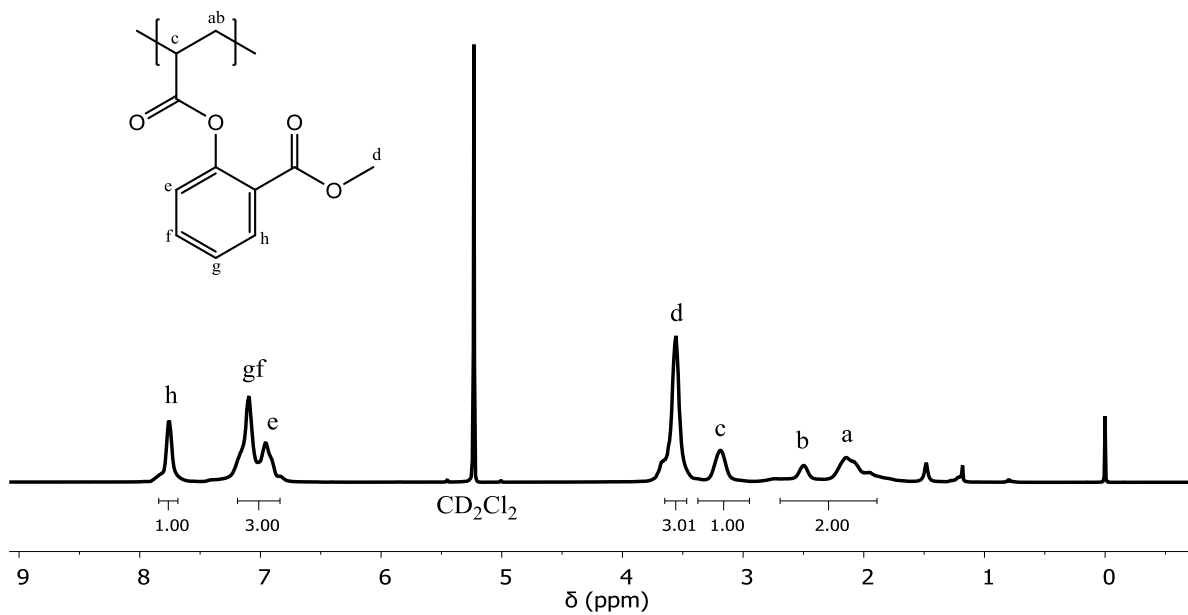


**Fig. S-2**  $^1\text{H}$  NMR spectra of PMSAE in  $\text{CD}_2\text{Cl}_2$ .

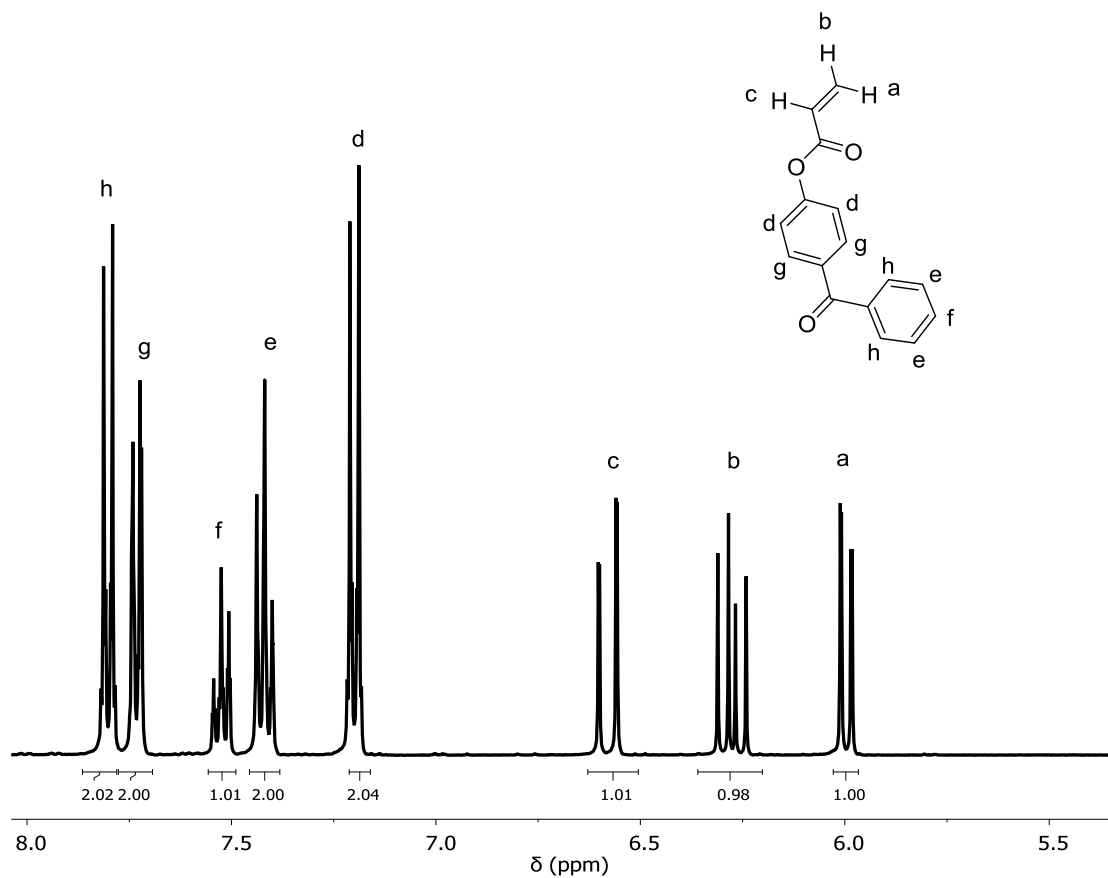


**Fig. S-3**  $^1\text{H}$  NMR spectra of ABP in  $\text{CDCl}_3$ .

# APPENDIX

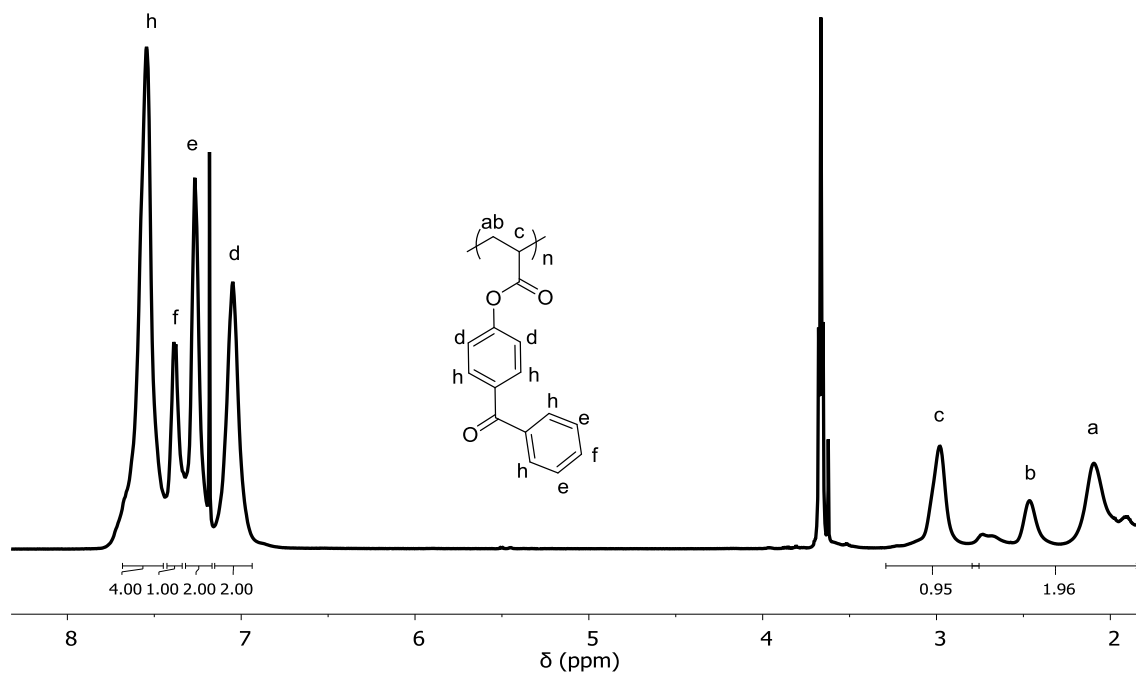


**Fig. S-4**  $^1\text{H}$  NMR spectra of PABP in  $\text{CDCl}_3$ .

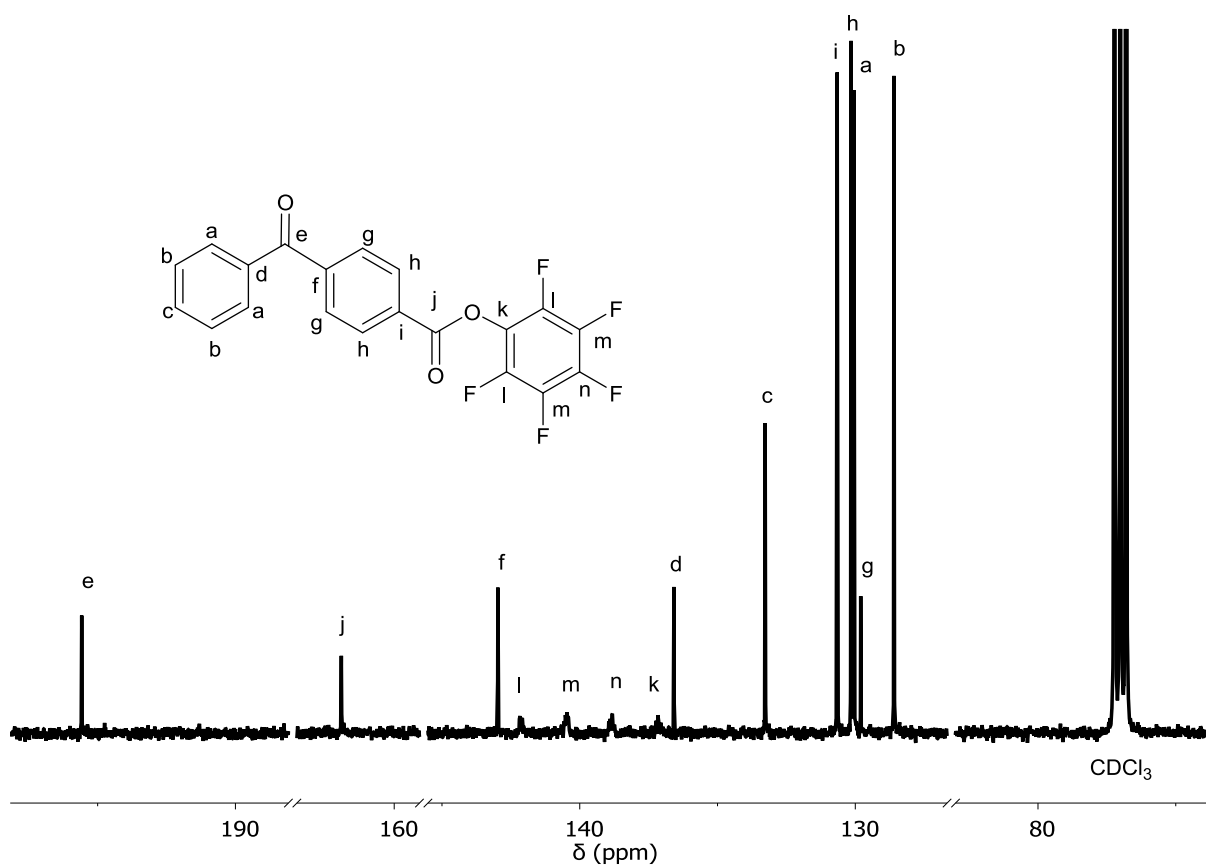


**Fig. S-5**  $^{13}\text{C}$  NMR spectra of BBPE in  $\text{CDCl}_3$ .

# APPENDIX

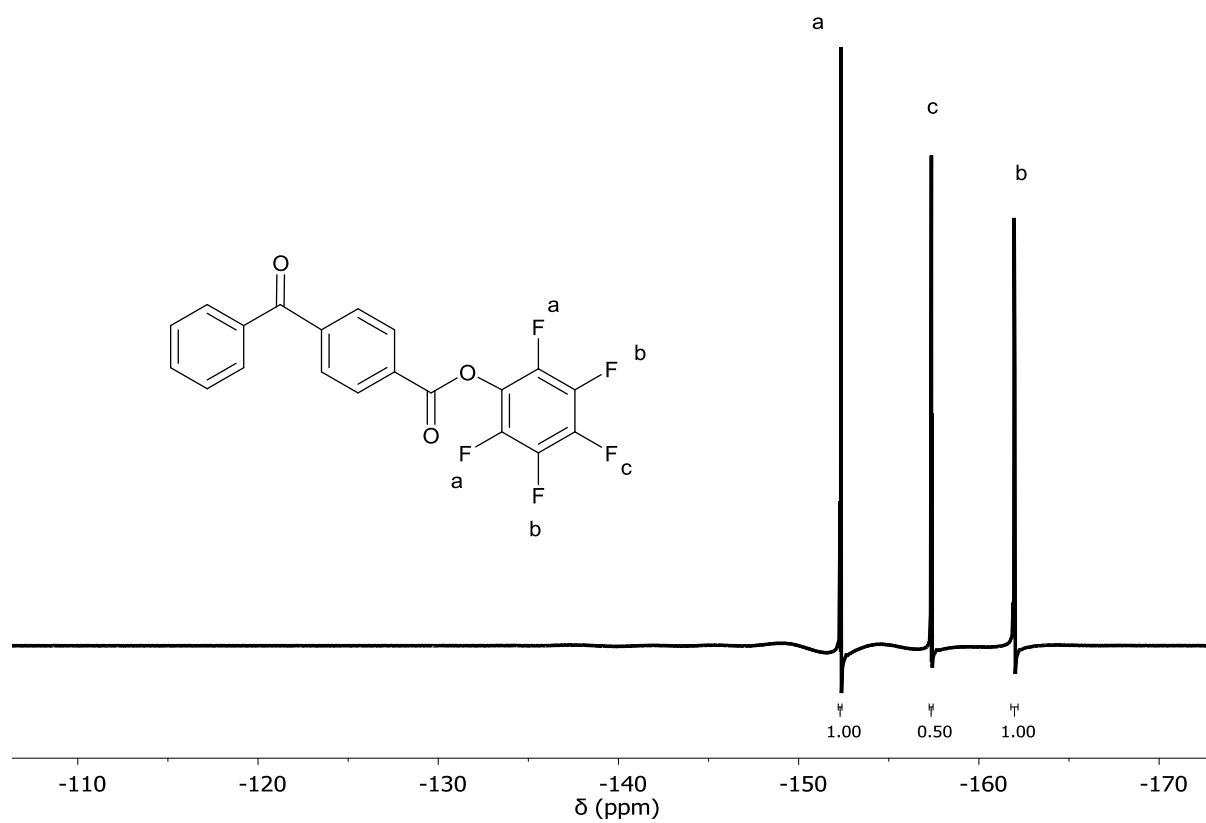


**Fig. S-6**  $^{19}\text{F}$  NMR spectra of BBPE in  $\text{CDCl}_3$ .

### 10. Acknowledgement

Herein, I would like to sincerely thank those who have given direct or indirect support to my doctoral studies. Without you, the presented work would not have been possible.

First, I would like to thank my supervisor Prof. Patrick Théato for providing me the opportunity to start the doctoral study in Hamburg and suggesting me this interesting research topic. He is a knowledgeable, humorous and nice professor. During the doctoral study, he properly guided me and gave me many valuable suggestions. He also supported me to attend international conferences in the relevant fields in order to communicate with peers and broaden my horizon. It helped me a lot with my research at hand and my long-term professional goals.

Big thanks go to Mrs. Christina Khenkhar. She is a friendly and patient lady. She polished my manuscripts by correcting the language although it was not part of her job duties. She always made clear and detailed revisions and provided patient explanations.

Special thanks go to Dr. Shaojian Lin and Mr. Zengwen Li for their constructive contribution to my research plan and lab work. Dr. Lin is the first group member I met in Hamburg. He showed me around the polymer lab and introduced some equipment for characterization in TMC and the chemistry department. He helped to design one of my research projects and attended some data analysis. Mr. Li gave valuable suggestions for the setup of some reactions and helped with some difficult data analysis.

Sincere thanks go to the current group members Dr. Heba Gabala and Ms. Julia Steicke in Hamburg. We had a great time together. I could always talk to them when I felt stressed, which was a huge relief for me and helped a lot. Dr. Gabala gave me many valuable tips for Merit scholarships application. Ms. Steicke gave me powerful support in the lab and helped translate German documents.

## ACKNOWLEDGEMENT

---

I would also like to thank all the former group members who already graduated or moved to Karlsruhe together with Prof. Théato: Dr. Denis Seuyep, Dr. Alexander Hoefling, Dr. Michael Thielke, Dr. Tim Krappitz, Dr. Hanju Jo, Dr. Jiaojiao Shang, Dr. Anindita Das, Ms. Fenja Moldenhauer, Mr. Sven Petersen, Ms. Lindsey Bultema, Ms. Wenwen Xue, Ms. Xia Huang, Ms. Xiaohui Li. We have had great times together and share lots good memories. The friendly, warm and cosy atmosphere in the group impressed me when I joined it. Dr. Alexander Hoefling gave me the safety training of the lab. Dr. Michael Thielke gave me many valuable advices about the electrospinning technique. Ms. Fenja Moldenhauer gave me a lot of useful tips on different kinds of analysis software. Dr. Hanju Jo gave me useful suggestions for contact angle measurement. Ms. Wenwen Xue helped me with the applications for the student dorm and German courses and introduced me to PIASTA. Mr. Sven Petersen helped me with the ordering process for glassware and chemicals.

I also deeply appreciate and thank all the scientific and technical staff who assisted me in the analytical measurements. Many thanks to Ms. Renate Walter (SEM), Dr. Andreas Meyer (AFM), Mr. Michael Gröger (GPC), Dr. Felix Scheliga (GPC), Dr. Inokentijis Josts (Fluorescence spectrophotometer), Dr. Christian Strelow and Mr. Marten Rittner (fluorescent microscope and photomask), Prof. Mathias Ulbricht and Mr. Qirong Ke from University of Duisburg-Essen (Surface Zeta Potential) as well as the whole NMR facility.

I gratefully acknowledge the financial support from the China Scholarship Council and the Department of International Affairs of University of Hamburg.

I would also like to thank Prof. Gerrit A. Luinstra for taking care of me after Prof. Patrick Théato had to move to Karlsruhe.

In addition to the academic environment, very warm thanks go to my family, my friends and my boyfriend Philip for their unconditional support, encouragement and love. Thank Philip for bringing dinner to the office, helping with the language correction of my manuscripts and encouraging me when I felt down. Without them, I could not have made it.

### **11. Declaration on oath**

I hereby declare on oath that I have written the present dissertation myself and have not used other than the acknowledged resources and aids. The submitted written version corresponds to the version on the electronic storage medium. I hereby declare that I have not previously applied or pursued for a doctorate (Ph.D. studies).

Hamburg, May 30, 2019

Hiermit versichere ich an Eides statt, die vorliegende Dissertation selbst verfasst und keine anderen als die angegebenen Hilfsmittel benutzt zu haben. Die eingereichte schriftliche Fassung entspricht der auf dem elektronischen Speichermedium. Ich versichere, dass diese Dissertation nicht in einem früheren Promotionsverfahren eingereicht wurde.

Hamburg, May 30, 2019